Determination of Oxygen Functionality on Highly Oriented Pyrolytic Graphite (HOPG)

Dissertation zur Erlangung des akademischen Grades des Doktors der Naturwissenschaften (Dr. rer. nat.)

eingereicht im Fachbereich Biologie, Chemie, Pharmazie der Freien Universität Berlin

vorgelegt von

Henan Li
aus China

Berlin, 2012

1. Gutachter: Prof. Dr. Robert Schlögl

2. Gutachter: Prof. Dr. Thomas Risse

Disputation am 12.12.2012

Zusammenfassung

Kohlenstoff kann als Alternative zu metallbasierten Katalysatoren für die oxidative Dehydrierungsreaktionen (ODH) von aromatischen Kohlenwasserstoffen, Alkanen oder Alkenen verwendet werden. Die aktiven Zentren des Katalysators sind noch unbekannt, aber es sollte eine oder mehrere der Sauerstoffgruppen sein. Andererseits werden Kohlenstoffe als Trägermaterialien für Metall-Katalysatoren verwendet. Die Sauerstoff-Gruppen auf den Trägermaterialien sind Verankerungsstellen für die Metallpartikel. Des Weiteren finden Wechselwirkungen zwischen den Metallpartikeln und Sauerstoffgruppen statt, dadurch wird die katalytische Aktivität und Selektivität verbessert. In diesem Zusammenhang ist es sehr wichtig zu wissen, welche Arten von Sauerstoffgruppen es auf dem Kohlenstoff gibt. Bis jetzt ist über diese Sauerstoffgruppen immer noch sehr wenig bekannt.

Highly oriented pyrolytic Graphite (HOPG) ist ein sehr gut definiertes Modellmaterial ohne Metallverunreinigungen und Poren. Deshalb wurden Sauerstoffgruppen auf HOPG funktionalisiert und mittels einer Kombination von temperatur- programmierter Desorption (TPD) und Röntgen Photoelektronen-Spektroskopie (XPS) untersucht. UV-Photoelektronen-Spektroskopie (UPS) wurde verwendet, um die elektronische Struktur und die Beschädigung der Oberflächen zu überwachen. Die Untersuchung der HOPG-Morphologie erfolgte mittels Rasterelektron-Mikroskopie (SEM) und Rastertunnel-Mikroskopie (STM).

Da die Dissoziationsrate von Sauerstoff auf defektfreiem HOPG praktisch null ist, wurden Defekte durch Sputtern auf HOPG erzeugt. Zwei Wege wurden hier beschritten: Sputtern mit Argon in einer Sauerstoff- oder Wassergasatmosphäre und das Sputtern mit Argon und Sauerstoff selbst. Unsere Untersuchung zeigt, Sputtern mit Sauerstoff erzeugt hauptsächlich Sauerstoff-Spezies in der HOPG-Matrix. Sputtern mit Ar in Sauerstoff-Gasatmosphäre erzeugt hauptsächlich Sauerstoff-Spezies in kleiner Menge auf der HOPG-Oberfläche. Diese Sputter-Methode wird als Standard-Funktionalisierungsmethode verwendet, um Sauerstoffgruppen auf HOPG zu erzeugen.

Obwohl HOPG ein gut definiertes Modellmaterial ist, gibt es Konstruktionsdefekte in der HOPG-Matrix. Unsere Untersuchung zeigt, dass diese minimalen Strukturunterschiede mit Ar-TPD-Spektren detektiert werden können. Dadurch kann die HOPG Qualität beurteilt werden.

Sauerstoff auf HOPG wird hauptsächlich mit XPS bestimmt. In XPS-Spektren kommen verschiedenen O1s-Signale nur in einem engen Bereich von 2,5 eV vor und überlappen sich. Somit ist es sehr schwierig einzelne Sauerstoff-Komponenten zu identifizieren und zuzuordnen. In der Literatur wurden O1s-Signale mit zwei bis sieben Sauerstoff-Komponenten gefittet, allerdings ohne zu erklären, warum eine gewisse Anzahl von Komponenten verwendet wird. Unsere Untersuchung zeigt deutlich, dass mindestens fünf Sauerstoff-Komponenten notwendig sind, um die O1s-XPS-Spektren zu fitten. Anhand der Thermostabilität und Oxidierbarkeit der Sauerstoffgruppen werden die Eigenschaften der funktionellen Gruppen diskutiert.

Abstract

Carbon can be used as an alternative to metal based catalysts for oxidative dehydrogenation reaction (ODH) of aromatic hydrocarbons, alkanes or alkenes. The active sites of the catalyst are still unknown, but it should be either one or more of the oxygen functional groups. On the other hand, carbon materials are used as catalytic supports for metal particles. The oxygen groups on the support material are the anchoring sites to immobilize the metal particles. The interaction between oxygen groups and metal particles improves the catalytic activity and selectivity of the catalyst. Therefore, functionalization of carbon materials is a very important method, furthermore it is important to know how many different oxygen groups exist on the carbon surface. There is still a big lack of information about the kind of oxygen groups on carbon.

Highly oriented pyrolytic graphite (HOPG) is a well-defined model system without any metal impurities and pores. Therefore, the oxygen functionalities on HOPG were studied. To study the nature of the induced oxygen groups, combined Temperature Programmed Desorption (TPD) and X-Ray Photoelectron Spectroscopy (XPS) were used. UV photoelectron spectroscopy (UPS) was applied to monitor the electronic structure and the damage of the HOPG surfaces. The surface morphology was characterized by Scanning Electron Microscopy (SEM) and Scanning Tunneling Microscopy (STM).

Since the dissociation rate of oxygen on defect-free HOPG is practically zero, defects were introduced on HOPG by sputtering. Two paths were used: Sputtering with argon in an oxygen- or water-gas atmosphere and sputtering with argon and oxygen itself. Our investigation shows that sputtering with oxygen produces mainly oxygen species in the HOPG matrix. In contrast, sputtering with Ar in oxygen gas atmosphere produces mainly oxygen species in a small amount and these oxygen species are situated on the HOPG surface. The second sputter method is used as the standard method for functionalization of HOPG, with the goal of generating oxygen groups on it.

Even though HOPG is a well-defined material, there are various construction defects in the HOPG matrix. Our investigation shows that these minimal differences of the original HOPG structure can be determined with Ar-TPD spectra. Furthermore, this method can be used to assess the HOPG quality.

In XPS spectra, various oxygen 1s signals occur only in a narrow range of 2.5 eV and overlap in this range. Thus, it is very difficult to identify single oxygen peaks and assign them clearly. In the literature, O1s peaks are fitted with different numbers of O1s components, but without mentioning why a certain number of oxygen groups is used for O1s-XPS fitting. Our investigation shows clearly, at least five O1s components are necessary to fit the O1s XPS spectra properly. The thermal stability and oxidizability of the oxygen components is used to discuss the character of the oxygen components.

Index

1. Application of carbon material ……..1

2. Structure of Highly Oriented Pyrolytic Graphite ……5

2.1 Lattice Structure ……5

2.2 Construction defects and surface defects ……...5

3. Process of graphite oxidation ……..……..7

3.1 Proposed oxidation processes ……..7

3.1.1 Adsorption ……....8

3.1.2 Defects generation and demonstration ……8

3.1.3 O_2 splitting ……10

3.1.4 Formation of functional groups and the identification methods ……...11

3.2 Theory of oxidation processes ……....14

3.2.1 Graphite oxidation at point defects ……..14

3.2.2 Unzipping oxidation process of graphite ……..15

4. Scope of this investigation ……..19

4.1 Material selection ……..20

4.2 Functionalization of HOPG ……...21

4.3 Characterization ……...22

5. Surface treatment and characterization methods ……...27

5.1 Ultra-high vacuum (UHV) ……27

5.2 Sputtering ……....28

5.3 Thermal Programmed Desorption (TPD) ……28

5.4 Photoelectron spectroscopy ……32

5.4.1 X-Ray Photoelectron Spectroscopy (XPS) ……32

5.4.2 Ultra violet Photoelectron Spectroscopy (UPS) ……38

5.5 Scanning Tunneling Microscopy (STM) ……41

6. Results and discussion ……45

6.1 Sample preparation ……45

6.2 A new concept for assessing the structure quality of Highly Oriented Pyrolytic Graphite ……47

6.3 Combined XPS and TDS study of oxygen groups on Highly Oriented Pyrolytic Graphite functionalized by two sputter procedures ……61

6.4 A systematic characterization of oxygen functional groups on Highly Oriented Pyrolytic Graphite ……73

7. Conclusion ……107

8. Acknowledgement ……113

Curriculum Vitae ……115

1. Application of carbon material

In recent years carbon material has become more and more important in various fields. One of the most important discoveries in the field of carbon material is that carbon can be used as a metal free catalyst[1;2]. The catalytic character of carbon was found in the generation of carbon deposits on the surface of the metal catalyst after he dehydrogenation of ethylbenzene[1]. By now carbon material has proven to be an attractive alternative to conventional metal-based catalysts for the oxidative dehydrogenation (ODH) of ethylbenzene[3;4], alkanes[5] or alkenes[6]. The active site of the catalyst is still unknown, but it is surmised to be one or more of the oxygen functional groups. In the literature, surface carbonyl/quinine-type oxygen functional groups have been proposed as the active sites[3;6-9]. These functional groups dissociate to CO and CO_2 at high temperatures. In the ODH reaction of ethylbenzene, the starting carbon material (onion-like carbon: OLC) without oxygen does not have any catalytic activity. Catalytic activity develops during the exposure to steam[3]. When the ODH reaction of ethylbenzene to styrene with active carbon as catalyst is finished, only the surface groups survive and decompose to CO_2 and CO in a low temperature range. This indicates that these surface groups are not the active sites for the catalysis[7].

Nevertheless, surface oxygen functional groups are not the only factor in the mechanism of the ODH reaction. In the ODH reaction of ethylbenzene, when the reaction takes a long time, the amount of coke and oxygen groups increases in the later stages of the reaction, yet the catalytic activity of the carbon decreases[7]. In all catalytic systems tested so far, disordered sp^2 and sp^3 hybridized polymeric carbon deposition (coke) was formed during the ODH reaction[9-11]. The formation of coke blocked the micro porosity of active carbon and changed the increasing catalytic reactivity towards oxidizing the catalyst[7]. Therefore, coke may be one factor for the deactivation of the carbon catalyst. In another example, carbon nanotubes (CNTs) were used as the catalyst in the ODH reaction of butene. After the ratio of the feed gases (oxygen and 1-butene) was increased from 1 to 2, the selectivity of butadiene still remained almost constant. That means, the excess of oxygen cannot increase the amount of active sites on the CNTs[6].

Apart from using carbon material itself as catalyst, different types of carbon, such as graphite, CNTs and CNFs, are often used as catalytic supports for metal particles[12-

[14]. The existence of functional groups on them is the prerequisite for their function as catalytic supports, because functional groups are the anchoring sites for immobilizing the metal particles. In addition, the functional groups interact with metal particles and thereby the catalytic activity and selectivity of the catalyst is improved.

Furthermore, functionalized graphite[15], CNTs and active carbon present excellent electrochemical properties and are widely used as electrode material in batteries. Graphite electrodes, for instance, possess a large inter layer distance, therefore the bonding between two graphene layers is weak and allows for intercalation of various compounds[16]. Thereby, the electronic structure of graphite is changed. The electron density can be increased (corresponding to chemical reduction), when a donor compound, such as alkali atoms, is incorporated in the graphene layers. Alternatively, the electron density can be decreased (corresponding to chemical oxidation), when an electron acceptor, such as oxygen atoms, is incorporated in the graphene layers. The incorporation of hydrogen or oxygen molecules is not possible, as shown in previous investigations[17;18].

Nevertheless, no consensus has been reached if this is generally the case. In order to conclusively answer, if oxygen may be incorporated in graphene layers, it is of paramount importance to understand the process of graphite oxidation. If oxygen can be incorporated in graphene layers, than the oxidation of graphite can begin not only from defects on the surface, but also from the bulk.

In addition, e.g. in lithium batteries, not only the well-graphitized part of carbon can intercalate Li-ions in order to store Li ions, but also surface oxygen is able to store Li-ions via the reaction between the functional groups and Li ions. For instance, surface C-OH groups can adsorb Li-ions through the formation of Li-salt $C\text{-}O^{-}Li^{+}$. However, the formation of different kinds of surface Li-salts could also result in the loss of reversible storage capacity and disturb the stability of the batteries. Therefore, the chemical properties of surface oxygen groups, as well as their quantity on the electrode play a very important role for the specific high charge capacity and for the cycle stability of the battery[19;20].

Reference List

[1.] M. Muhler, R. Schlögl, G. Ertl, *J.Cat.* **1992,** *138* 413-444.

[2.] W. Weiss, R. Schlögl, *Topics in Catalysis* **2000,** *13* 75-90.

[3.] Nicolas Keller, *Angewandte Chemie International Edition* **2002,** *41* 1885-1888.

[4.] D. S. Su, N. I. Maksimova, G. Mestl, V. L. Kuznetsov, V. Keller, R. Schlögl, N. Keller, *Carbon* **2007,** *45* 2145-2151.

[5.] Z. J. Sui, J. H. Zhou, Y. C. Dai, W. K. Yuan, *Catalysis Today* **2005,** *106* 90-94.

[6.] X. Liu, D. S. Su, R. Schlögl, *Carbon* **2008,** *46* 547-549.

[7.] M. F. R. Pereira, J. J. M. Orfao, J. L. Figueiredo, *Applied Catalysis A-General* **2001,** *218* 307-318.

[8.] M. F. R. Pereira, J. J. M. Orfao, J. L. Figueiredo, *Applied Catalysis A-General* **1999,** *184* 153-160.

[9.] G. Mestl, N. I. Maksimova, N. Keller, V. V. Roddatis, R. Schlögl, *Angewandte Chemie-International Edition* **2001,** *40* 2066-2068.

[10.] J. Zhang, D. S. Su, A. Zhang, D. Wang, R. Schlögl, H. Cécile, *Angewandte Chemie International Edition* **2007,** *46* 7319-7323.

[11.] M. F. R. Pereira, J. J. M. Orfao, J. L. Figueiredo, *Applied Catalysis A-General* **2000,** *196* 43-54.

[12.] K. P. De Jong, J. W. Geus, *Catalysis Reviews: Science and Engineering* **2000,** *42* 481-510.

[13.] E. Auer, A. Freund, J. Pietsch, T. Tacke, *Applied Catalysis A: General* **1998,** *173* 259-271.

[14.] P. Serp, M. Corrias, P. Kalck, *Applied Catalysis A: General* **2003,** *253* 337-358.

[15.] J. F. Evans, T. Kuwana, *Analytical Chemistry* **1977,** *49* 1632-1635.

[16.] Robert Schlögl, in *Handbook of Heterogeneous Catalysis,* Eds.: G.Ertl, H.Knözinger, F.Schüth, J.Weitkamp **2008**.

[17.] M.S.Dresselhaus and G.Dresselhaus, *Adv.Phys.* **1981,** *30* 139-326.

[18.] R. Schlögl, *Graphite - A Unique Host Lattice, Progress in Intercalation Research*, 17ed. Springer Netherlands, **1994,** pp. 83-176.

[19.] M. Endo, C. Kim, K. Nishimura, T. Fujino, K. Miyashita, *Carbon* **2000,** *38* 183-197.

[20.] E. Frackowiak, S. Gautier, H. Gaucher, S. Bonnamy, F. Beguin, *Carbon* **1999,** *37* 61-69.

2. Structure of Highly Oriented Pyrolytic Graphite

2.1 Lattice Structure

HOPG is a highly ordered form of pyrolytic graphite with an angular spread of the c axes of less than 1 degree and a relatively perfect sp^2 Graphite structure (i.e. sparse sp^3 and sp hybridization). The trigonal connectivity of the sp^2 hybrid orbital in graphite leads to a hexagonal planar structure of carbon and one electron of each carbon atom is left. These electrons (similar to the π-electrons in benzene rings) interact with each other. Very weak bonds (Van der Waals bonds 5 kJ/mol) connect the graphene layers and the inter layer distance is 0.335 nm. The π - electron density is orthogonal to the plane of the strong C-C σ bonds (0.142 nm). These electrons give graphite a good metallic electrical conductivity within the plane direction, but perpendicular to the planes graphite exhibits insulator behavior (figure 2.1). Altogether, the graphite crystal has the form of a hexagonal lattice, with a stacking order of the layers of either AB ABAB, or ABC ABCABC. The edge of a hexagonal graphite layer can consist of Zigzag and armchair edges, as has been established in STM and STS[1].

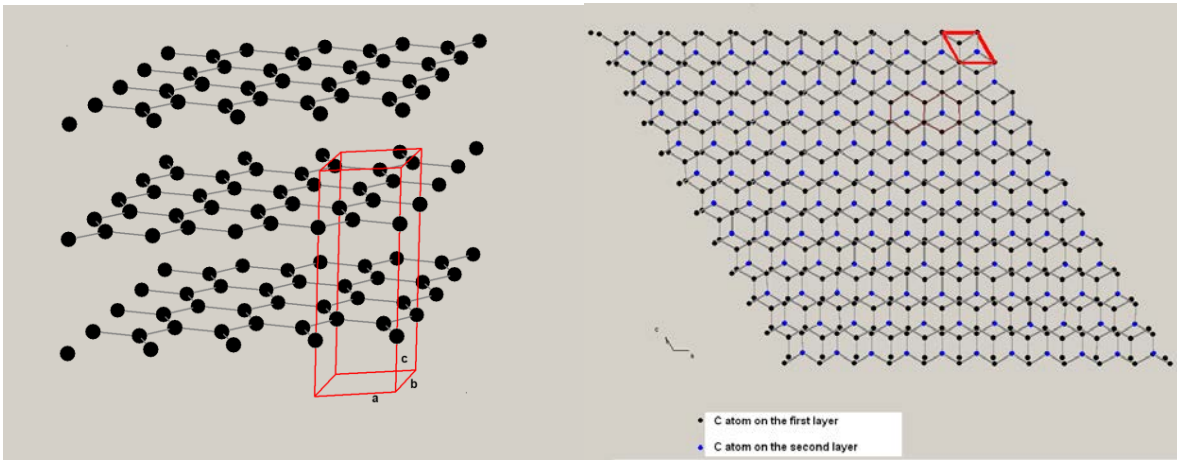

(a) (b)

Figure 2.1 Hexagonal structure of perfect graphite, the framed part is the elemental cell. Lattice constants a = b = 2.46 Å, c = 6.70 Å[2]. (a) Side view; (b) top view

2.2 Construction defects and surface defects

The perfect hexagonal structure of graphite, described in chapter 2.1, is only a model of the true structure of graphite. Both, in natural graphite and in all kinds of synthetic graphite, there are various surfaces[3] and construction defects, such as lattice vacancy, stacking fault, displacement of small graphite crystals and parallelism

deviation of the graphene layers[4]. HOPG is composed of various crystals with different lengths, but the same orientation[5].

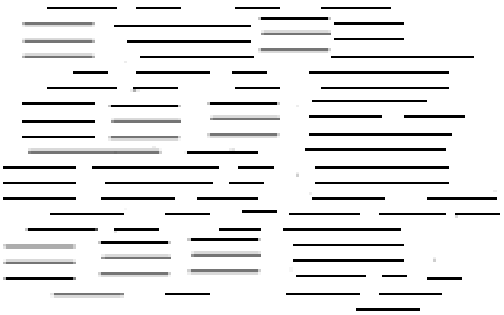

Figure 2.2

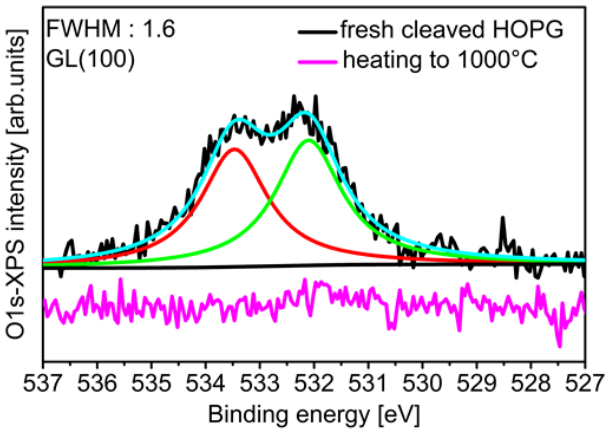

Figure 2.3

Figure 2.2 Structure of HOPG

Figure 2.3 O1s-XPS of freshly cleaved HOPG and HOPG heated to 1000 °C

Aside from the construction defects, described above, different surface defects can exist on HOPG[3]. For example, if HOPG is cleaved, oxygen can adsorb to the defect sites of HOPG's graphitic surface. The existence of oxygen on the HOPG surface can be established by XPS. XP spectra of freshly cleaved HOPG show a distinct oxygen peak, providing evidence for the existence of surface defects.

Reference List

[1.] Y. Kobayashi, K. i. Fukui, T. Enoki, K. Kusakabe, Y. Kaburagi, *Physical Review B: Condensed Matter and Materials Physics* **2005,** *71* 193406-4.

[2.] P. Trucano, R. Chen, *Nature* **1975,** *258* 136-137.

[3.] Wing-Tat Pong and Colm Durkan, *Journal of Physics D: Applied Physics* **2005,** *38* R329.

[4.] S. Wu, R. Yang, D. Shi, G. Zhang, *Nanoscale* **2012,** *4* 2005-2009.

[5.] Akira Yoshida, Yoshihiro Hishiyama Yutaka Kaburagi. Characterization of crystal grain shape and crystal axis orientation mapping on surface of HOPG using electron backscatter diffraction, **2004**, The American Carbon Society.

3. Process of graphite oxidation

3.1 Proposed oxidation processes

The following oxidation process model is proposed by Robert Schlögl[1]. Furthermore, a similar model is given by Radovic for the oxidation of graphene[2].

The reaction requires two independent, electronically different sites. One site (site ***A***) has to be electron rich to activate molecular oxygen, e.g. 5-member rings in graphite. The other site (site ***C***) has to be electron poor to react with activated oxygen atoms, e.g. 7-member rings in graphite.

Firstly, oxygen adsorbs on the electron rich defects on graphite basal planes and then diffuses on the surface.

$$O_2 + 2\boldsymbol{A} \rightarrow A\text{-}O_2\text{-}A$$

Secondly, the adsorbed oxygen molecules react with the electron rich defects ***A***, in order to dissociate the oxygen molecules.

$$A\text{-}O_2\text{-}A \rightarrow A\text{-}O_2^{2-}\text{-}A^{2+}$$
$$A\text{-}O_2^{2-}\text{-}A^{2+} \rightarrow 2O^{-}\text{-}A^{+}\ (ads)$$

Thirdly, the dissociated oxygen atoms diffuse on the surface again until they either recombine and desorb, or find a structural defect ***C,*** where they can form a covalent bond to carbon (oxygen functional groups).

$$O^{2-}(ads) + \boldsymbol{C} \rightarrow CO(ads) + 2e^{-} + \boldsymbol{A}$$
$$O^{2-}(ads) + CO(ads) \rightarrow CO_2(ads) + 2e^{-} + \boldsymbol{A}$$

Finally, oxygen functional groups decompose to CO, CO_2 or H_2O by heating and desorb. Defects are recreated at the same time and are available for the next adsorption.

$$CO(ads) \longrightarrow CO(gas) + \boldsymbol{C}$$
$$CO_2(ads) \longrightarrow CO_2(gas) + \boldsymbol{C}$$

3.1.1 Adsorption

It was established that the basal plane of HOPG (graphite) is relatively unreactive towards molecular oxygen. Exposure of this surface to up to $6*10^5$ Langmuir (1 L = 133 Pa · 10^{-6} s) of O_2 at ambient temperature did not result in any oxygen-containing surface complexes[3]. Even after exposure in O_2 ($8*10^{-8}$ mbar) at 820 ˚C for 2 hours, no oxygen was found[4]. In air, HOPG surface can be oxidized at temperatures above 650 ˚C[5;6]. In the literature, the desorption behavior of a series of gases was investigated[7]. The HOPG surfaces were exposed to up to 10 L of different gases. The TPD-spectra show that small-molecule-gases H_2O, CO, CO_2, H_2, and O_2 do not adsorb at room temperature on the HOPG surface in UHV[7]. If there are no defects on the basal plane of graphite, no oxygen chemisorption will happen at room temperature.

3.1.2 Defects generation and demonstration

(a) Methods for defect generation

Edges and defects on the surface can be oxidized more easily. The usual methods to generate defects and incorporate oxygen are: ion bombardment e.g. sputtering, plasma oxidation or electron irradiation[8]. Sputtering is established as an effective method to generate defects on the carbon surface[3;9-11]. Because oxygen can adsorb on the defects, O-containing HOPG surfaces can be obtained through the sputter method.

However, the intensity of sputtering should be monitored carefully. The effect of ion irradiation on the electronic structure of HOPG has been investigated and the results tell us: Amorphous carbons will be produced, if the sample is irradiated by a 0.5 keV Ar^+ beam with dose from $3*10^{14}$ up to $3*10^{15}$ ions/cm^2 [9]. $3*10^{14}$ ions/cm^2 correspond to 48 μA Ar^+ current flowing on the surface for one second. The process of amorphization by an ion beam is very fast.

What happens to HOPG during the sputter process? In the sputter process, carbon atoms are removed. At the beginning of sputtering, only very little carbon atoms are removed and the corresponding holes can be considered as point defects[12]. Oxygen can adsorb on these point defects and thereby oxygen functional groups are formed. Point defect formation is considered to be the initial step of the carbon oxidation process[12] (described in chapter 3.2.1 in detail).

(b) Methods for defect demonstration

Small sized point defects caused by two missing carbon atoms can be observed in TEM and STM. With high resolution transmission electron microscopy (TEM) hexagons motif of sp^2 in the graphite surface can be successfully observed with a resolution of 0.19 nm. Similarly, it was also observed in Scanning Tunneling Microscopy (STM) with a resolution of 0.2 nm[6;13]. A size benchmark of the defect is given in figure 3.1.

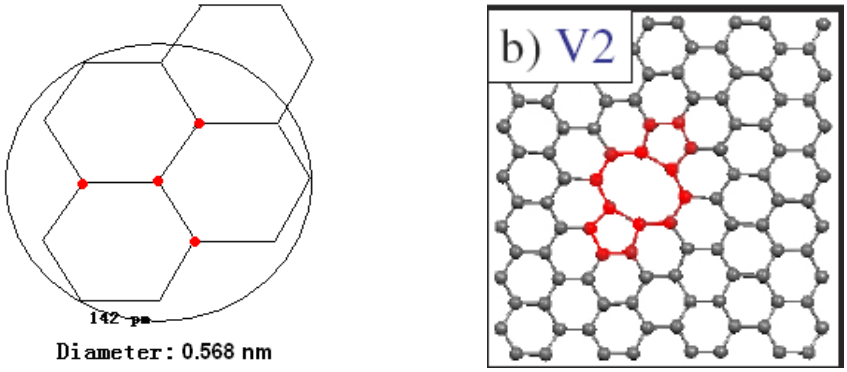

(a) (b)

Figure 3.1 (a) scale of three hexagonal carbon rings to estimate the defect size; (b) defects with two removed carbon atoms, V2: divacancy[12]

Many holes were observed in STM on the HOPG, which was oxidized in air at 650˚C, the diameter of these holes increased linearly with the reaction time[5]. This phenomenon indicates that the oxidation spread from the location of the point defect. Big hexagonal defects and line defects (corresponding to edges) can be seen in the optical microscope[14]. In the AFM image[15], the author used the image as an experimental support for the theory of "unzipping oxidation process of graphite"[16] (described in chapter 3.2.2 in detail), but in our view this is a clear evidence of graphite oxidation at step edges.

3.1.3 O_2 splitting

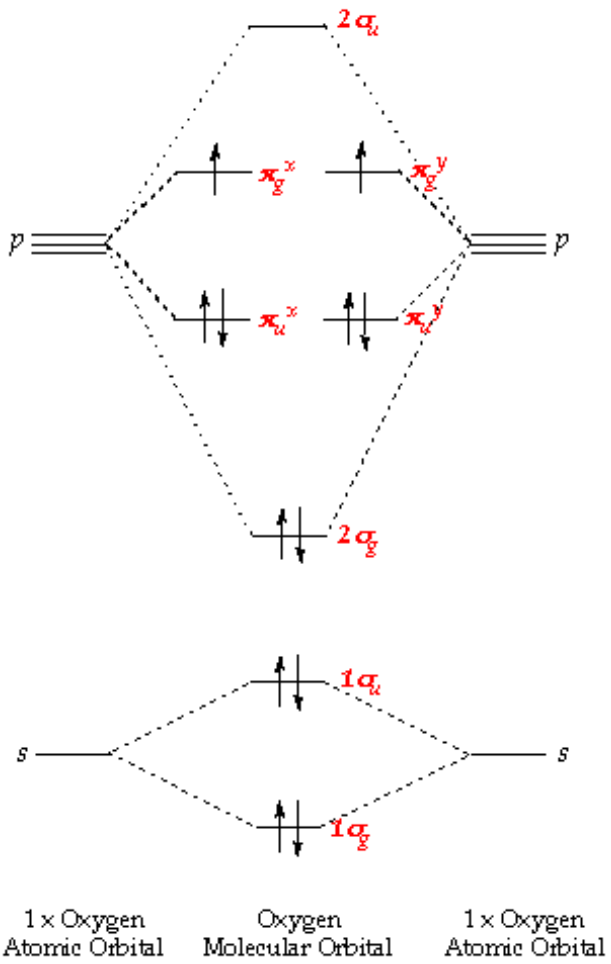

Figure 3.2 Molecular orbital schema of oxygen

The assembly of O atomic orbitals is $1s^2\ 2s^2\ 2p_x^2\ 2p_y^1\ 2p_z^1$. The bond energy of the O_2 is 117 kcal/mol[17]. In order to split the oxygen double bond in the oxygen molecule, electron rich sites (***A***) on the surface are needed.

$$O_2(ads) + \boldsymbol{A} \rightarrow O_2^{2-}(ads) + \boldsymbol{A}^{2+}$$
$$O_2^{2-}(ads) + \boldsymbol{A} \rightarrow 2O^{2-}(ads) + \boldsymbol{A}^{2+}.$$

An O ion can also be used directly to oxidize the graphite surface. An O-atom can for instance be obtained by O_2-plasma, which can attack the HOPG surface not only from the position of the defect[6]. Furthermore, N_2O can be used as well to provide one oxygen atom.

3.1.4 Formation of functional groups and the identification methods

The oxygen ions that were created in the way described in chapter 3.1.3 diffuse on the surface until they either recombine and desorb, or find a structural defect ***C*** where they can form a covalent bond to carbon (oxygen functional groups).

$$O^{2-}(ads) + \boldsymbol{C} \rightarrow CO(ads) + 2e^{-} + \boldsymbol{A}$$

$$O^{2-}(ads) + CO(ads) \rightarrow CO_2(ads) + 2e^{-} + \boldsymbol{A}$$

The most difficult part of this investigation is to identify the oxygen functional groups. In the following the different types of oxygen functional groups will be introduced. After this, the chapter will conclude with a presentation of the surface sensitive measurement methods that were used for the identification of the functional groups.

(a) Species of the functional groups and their properties

Oxygen atoms react with defects and thereby different kinds of functional groups can be formed. The thus created functional groups depend on the kind of the defects and the pressure of the oxygen[18]. The possible surface oxygen groups are shown in figure 3.3. Determination of the oxygen species is very difficult. So far different assumptions for the type of oxygen species have been put forward in the literature[3;18;21;24;25], but no proofs were given for these assumptions. Carbon with high oxygen content shows acidic character (hydrophilic) and cation exchange behavior. Carbon with low oxygen content shows basic character and anion exchange behavior[19;20]. This is established by titration. Boehm has analyzed this chemical property in detail[19;20].

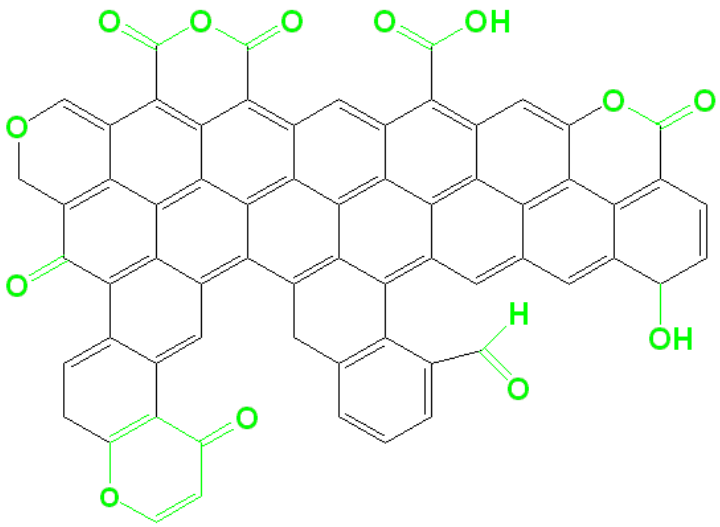

Figure 3.3 Possible structures of oxygen functional groups on graphite surface

(b) Identification of different functional groups

$$CO_n(ads) \xrightarrow{Heating} CO_n(gas) + \boldsymbol{C}$$

It has to be noted, that all the assignments here and in the entire thesis are assumptions.

The reader is referred to the reviews[19;22] for a survey of the different methods to determine oxygen functional groups. Among the most powerful of these methods in UHV are TPD, XPS and HREELS.

In classical TPD, desorption peaks correspond to decomposition of different functional groups, which sit on the different sites of the surface. With this method, the type of the oxygen functional groups on the surface can be deduced through the detected gases. However, the analysis of TPD is very complex because of many factors, for instance diffusion, re-adsorption and desorption of gases in the bulk of the sample.

XPS is a surface sensitive method, it can detect small amounts of oxygen[23]. The analyzable depth is restricted by the escape depth of the electrons. Within the initial state model, binding energy shifts are easily assigned to chemical surroundings. However, the assignment cannot be done only with the initial state model, the final effect plays also an very important role in our system. The detection of oxygen functional groups with XPS has been studied by Clark[24;25]. His study shows that different oxygen 1s-signals appear only in a narrow area (2.5 eV). Therefore, it is not possible to classify them clearly. A stepwise heating process, which was already used by Marchon et al.[21], is very helpful in this respect. Oxygen groups are removed sequentially from the surface and are subsequently characterized by TPD. This yields a series of XPS spectra. It is this combination of of TPD and XPS that allows a classification of the XPS peaks.

To identify each individual peak, High Resolution Electron Energy Loss Spectroscopy (HREELS) can be used as well. HREELS is a powerful method to differentiate the oxygen groups. The sputtered HOPG in oxygen was studied with a combination of TPD and HREELS by Nowakowski[3].

The findings from previous investigations are summarized in the following table:

Carbon	Oxidant	Desorption temperature [K] T > room temperature	E_{des} [kcal/mol]	Supposed oxygen functional group
Not oxidized HOPG[7]	CO O_2 H_2O CO_2	No adsorption, if T > R.T.		
Polycrystalline graphite[21]	O_2 H_2O	CO: 973, 1093, 1253 CO_2: 463, 573, 693, 793, 923 H_2 : 1300 Aliphatic C_xH_y: 400-900 CO and CO_2	64-83 28-60	Carbonyls Lactones Aromatic hydrocarbons
Sputtered HOPG[3]	O_2	CO: 780, 910 CO_2:400-740 H_2O (less): 300-500 C_xH_y(less): 300-500		Semiquinone Lactones Dissociation of H_2O
Active carbon[26]	HNO_3 H_2O_2	CO: 510(less), 720-1060 (a lot) CO_2: 575 (a lot), high temperature (less)		
Graphite with point defect[18]	O_2	CO: around 450, 1200 CO_2: around 350, 750		Anhydride, carbonyl Anhydride, lactones

– After the oxidation of graphite, CO, CO_2, H_2, H_2O and C_xH_y are the gases which can be detected by TPD measurement.

– Pyrographite was oxidized in one bar O_2 at 940 K in high pressure UHV chamber, and the oxidized surfaces of pyrographite brought to room temperature chamber were always covered with water. The hypotheses for the existence of water are: this water comes either as impurity from the spectrometer residual gas or is a genuine product of the oxidation[27].

– CO desorbs at high temperatures and CO_2 desorbs at low temperatures.

– There is always O-H (H_2O) at 3600 cm^{-1} in HREELS spectra on the oxidized graphite surface between room temperature and 1000 K[3], which probably result in the desorption of H_2 , aliphatic hydrocarbons and CO_x.

– After the sample was heated to 1000 K, there were O-H (in water), C-OH and C=O groups present on the surface[3]. Considering the thermal stability of various oxygen functionalities, only ether-type groups, carbonyls, hydroxyls, quinones and semiquinones can survive in this temperature range. Therefore, the peaks in HREELS[3] at 1000 K could be contributed by the presence of semiquinone, quinones, carbonyls and hydroxyls.

– Beyond 1250 K, no oxygen groups exist according to HREELS spectra[3].

– It was calculated that ether (C-O-C) and carbonyl (C=O) groups are CO releasing and have large binding energy. C-O-C group is the most stable state compared to other oxygen functional groups, as it was calculated by the Johan Carlsson and Felix Hanke[18]. The binding energy of ether is around 6 eV and of carbonyl is 3-4 eV, which correspond to a TPD desorption temperature of 873-1173 K in the Redhead equation[28]. Therefore, the carbonyl and ether groups are suggested as the major source of released CO in high temperature area[18].

3.2 Theory of oxidation processes

3.2.1 Graphite oxidation at point defects

(a) Generation of point defect – Johan M. Carlsson[12]

The results of Johan Carlsson´s DFT calculation are: The atoms ZZ shown in figure 3.4a and figure 3.4c are similar to atoms on the zigzag edge of the graphene sheet. They can be removed without any energy cost to form a larger even vacancy, as shown in figure 3.4b and figure 3.4d. That means, when defects are generated, uneven carbon atoms can be easily removed.

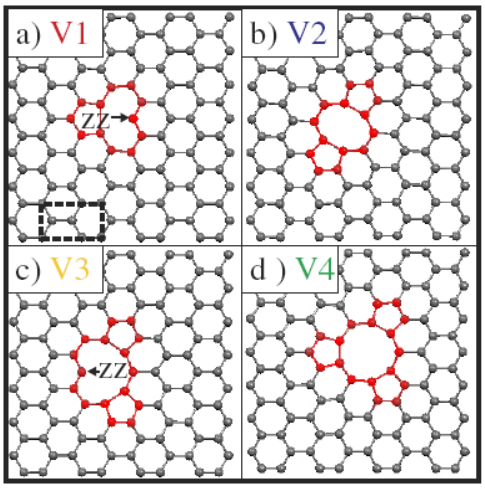

Figure 3.4 Atomic structures of various NPC motives (fully relaxed). The atoms that are part of the non-hexagonal region are colored red. Panel (a) also gives the unit cell of a graphene sheet (dashed lines). The left panels (a), (c) show defect structures with an odd number of removed atoms: (a) single vacancy (V1), and (c) trivacancy (V3). Under coordinated atoms are labeled as ‘‘ZZ’’ (zigzag atom). Panels at the right show defects with an even number of removed atoms: (b) divacancy(V2) and (d) quadrovacancy (V4)[12].

(b) Oxidation mechanism

If several carbon atoms are removed from the graphene sheet, vacancies are formed. “Vacancies are initially saturated by stable O groups, such as ether (C-O-C)

and carbonyl (C=O) groups. The etching is activated by a second step of additional O_2 adsorption at the ether groups, forming larger oxygen groups, primarily lactones (C-O-C=O), that desorb directly as CO_2 just above room temperature or that are further activated by additional O_2 dissociation forming anhydride groups (O=C-O-C=O). These groups decompose rapidly above room temperature, and the CO_2 desorption exposes new sites for O_2 dissociation, thus driving the etching reaction further"[18]. The studies show that "the partial pressure of oxygen is an important external parameter that affects the mechanisms of oxidation"[18].

3.2.2 Unzipping oxidation process of graphite

Unzipping theory is another proposed mechanism. The starting point is the fact that chains on the oxidized HOPG can be observed by an optical microscope. This led theoreticians to propose, by means of DFT calculations[18], that an unzipping mechanism is energetically favorable. Schniepp has completed this mechanism furthermore by AFM images and by DFT calculations of oxidized HOPG. The unzipping mechanism is: An oxygen atom attacks the graphene layer from the top and thereby ether groups (C-O-C) are formed. The oxidation proceeds further along linearly aligned ether groups. The reason for this is that the oxidation along the linearly aligned groups is energetically favorable compared to an oxidation in other directions. The graphene layer with linearly aligned ether groups is called an unzipped structure. The linear alignment of ether groups causes the linearly serial breaking of C-C bonds. Consequently, the oxidized graphene layer is bend up[15]. The bending effect results from the ether groups which were described in detail by Incze et al.[29].

However, the optical image[16] and the AFM image of graphene[15] are unconvincing, because the line in the image is probably caused by the oxidation of the step edges on the graphite surface, such as many other optical images show[14]. Therefore, it is not the experimental evidence for the unzipping mechanism. Sun and Fabris[30] showed that the starting point for the unzipping mechanism is an ensemble of three ether groups on one hexagonal ring for extended molecules and graphene. Since all energy barriers are in the same range, two things are crucial for the unzipping mechanism: the number of ether groups and their mobility as the slightly highest required energy barrier.

Reference List

[1.] Robert Schlögl, in *Handbook of Heterogeneous Catalysis*Eds.: G.Ertl, H.Knözinger, F.Schüth, J.Weitkamp **2008**.

[2.] Ljubisa R.Radovic, *J.Am.Chem.Soc.* **2009,** *131* 17166-17175.

[3.] M. J. Nowakowski, J. M. Vohs, D. A. Bonnell, *Surface Science* **1992,** *271* L351-L356.

[4.] Samer Aburous, *Dissertation: HOPG as a model catalyst for the oxidative dehydrogenation of ethylbenzene over carbon materials*, Free University Berlin, **2007**.

[5.] H. P. Chang, A. J. Bard, *Journal of the American Chemical Society* **1990,** *112* 4598-4599.

[6.] J. I. Paredes, A. Martinez-Alonso, *Carbon* **2000,** *386* 1183-1197.

[7.] H. Ulbricht, R. Zacharia, N. Cindir, T. Hertel, *Carbon* **2006,** *44* 2931-2942.

[8.] A. Hashimoto, K. Suenaga, A. Gloter, K. Urita, S. Iijima, *Nature* **2004,** *430* 870-873.

[9.] S. Ravesi, A. Terrasi, L. Torrisi, G. Foti, *Radiation Effects and Defects in Solids* **1993,** *127* 137-145.

[10.] J. Fournier, D. Miousse, L. Brossard, H. Ménard, *Materials Chemistry and Physics* **1995,** *42* 181-187.

[11.] C. T. Reimann, B. U. R. Sundqvist, S. Andersson, P. A. Bruhwiler, N. Martensson, *Nuclear.Instruments.and Methods in Physics Research.Section.B: Beam.Interactions.with.Materials and Atoms.* **1997,** *122* 343-346.

[12.] J. M. Carlsson, M. Scheffler, *Physical Review Letters* **2006,** *96* 046806-4.

[13.] S. I. Park, C. F. Quate, *Applied.Physics Letters* **1986,** *48* 112-114.

[14.] B. Mccarroll, D. W. McKEE, *Nature* **1970,** *225* 722-723.

[15.] H. C. Schniepp, J. L. Li, M. J. McAllister, H. Sai, M. Herrera-Alonso, D. H. Adamson, R. K. Prudhomme, R. Car, D. A. Saville, I. A. Aksay, *J.Phys.Chem.B* **2006,** *110* 8535-8539.

[16.] J. L. Li, K. N. Kudin, M. J. McAllister, R. K. Prud'homme, I. A. Aksay, R. Car, *Physical Review Letters* **2006,** *96* 176101-176104.

[17.] P. Brix, G. Herzberg, *The.Journal of Chemical Physics* **1953,** *21* 2240.

[18.] J. M. Carlsson, F. Hanke, S. Linic, M. Scheffler, *Physical Review Letters* **2009,** *102* 166104.

[19.] H. P. Boehm, *Carbon* **1994,** *32* 759-769.

[20.] H. P. Boehm, *Carbon* **2002,** *40* 145-149.

[21.] B. Marchon, J. Carrazza, H. Heinemann, G. A. Somorjai, *Carbon* **1988,** *26* 507-514.

[22.] B. Marchon, W. T. Tysoe, J. Carrazza, H. Heinemann, G. A. Somorjai, *Journal of Physical Chemistry* **1988,** *92* 5744-5749.

[23.] P. R. Norton, *Surface Science* **1975,** *47* 98-114.

[24.] D. T. Clark, H. R. Thomas, *J.Polym.Sci.Polym.Chem.Ed.* **1978,** *16* 791-820.

[25.] D. T. Clark, H. R. Thomas, *J.Polym.Sci.Polym.Chem.Ed.* **1976,** *14* 1671-1700.

[26.] S. Haydar, C. Moreno-Castilla, M. A. Ferro-Garcia, F. Carrasco-Marin, J. Rivera-Utrilla, A. Perrard, J. P. Joly, *Carbon* **2000,** *38* 1297-1308.

[27.] R. Schlögl, G. Loose, M. Wesemann, *Solid State Ionics* **1990,** *43* 183-192.

[28.] P. A. Redhead, *Vacuum* **1962,** *12* 203-211.

[29.] A. Incze, A. Pasturel, P. Peyla, *Phys.Rev.B* **2004,** *70* 212103.

[30.] T. Sun, S. Fabris, *Nano Lett.* **2011,** *12* 17-21.

4. Scope of this investigation

The knowledge of how to functionalize the carbon material and the nature of oxygen functionalities on functionalized carbon materials is very important. The quantity and type of these oxygen groups is highly dependent on the method of functionalization. It is very difficult or even not possible to differentiate the various oxygen functionalities precisely with the existing analytical techniques. Since many years, the nature of the oxygen functional groups on different carbon material has been investigated with various techniques for instance Titration[1;2], Infrared Spectroscopy (IR)[3;4], High-Resolution Electron Energy Loss Spectroscopy (HREELS)[5], X-Ray Diffraction (XRD), X-Ray Photoelectron Spectroscopy (XPS)[2-4;6-10], Temperature Programmed Desorption (TPD)[2-4;7;8] and Scanning Tunneling Microscopy (STM)[1-3]. A bulk of literature exists on this topic and gives assumptions about the possible oxygen functionalities on carbon surface. However, the existing literature does not document oxygen functionalities systematically and does not give clear evidence and reason for their assumptions. There is still a big lack of information about the oxygen groups, due to the high number and complexity of them.

The aim of our investigation is to gain information about the nature of oxygen functionalities on carbon surface. We propose to do this by introducing oxygen functionalities on carbon through different approaches, followed by the systematic characterization of the oxygen functionalities and the carbon surface with selected techniques.

Due to the complexity of the oxygen functionalities themselves, we first need to build a suitable model system, which should be as simple as possible. This is done through two approaches: (a) choose a simple carbon material, which has a simple structure with a small amount of defects and ideally no contaminations at all, in order to reduce the complexity from carbon side. (b) Choose suitable functionalization methods introducing some oxygen groups (ideally only one kind of oxygen group), in order to reduce the complexity of the oxygen functionalities. In the following, details about the selection of the carbon material, functionalization methods and the characterization techniques are described.

4.1 Material selection

After comparing various carbon materials such as HOPG, natural graphite, carbon nanotubes (CNTs) etc., we decided to use HOPG. There are two reasons for choosing HOPG.

(a) Structure

The basic building unit for HOPG is a graphene sheet and the graphene layers are connected with very weak Van der Waals bonds. Hence, HOPG is a three dimensional material, but it offers two dimensional surfaces layers. This reduces the complexity of the system compared to other carbon materials e.g. active carbon, soot or CNTs. The structure of HOPG is described in detail in chapter 2.1. The difference between graphene and graphite is: Graphene has only one sheet and does not have a subsurface layer. It is only one atom thick and colorless[4]. Hence graphene offers a big surface area (front and back side of the graphene layer). Additionally, graphene exhibits exceptional quantum effect and good electron conductivity as well as many other excellent properties[4;5]. Graphene as a perfect 2D material is a good model for the theoretical calculation of the graphite oxidation mechanism. Nevertheless, due to its instability and big challenges in the graphene production, it is not a suitable material for our experiment. Here it should be noted that the graphene is available on the commercial market mostly as multilayer graphene, which is actually the same as thin graphite.

(b) Purity

HOPG's structure does not have any metal impurities and pores in contrast to CNTs, CNFs and active carbon. As described above, information about oxygen functionalities on HOPG are needed, therefore it is very important to use a metal free carbon material such as HOPG, to ensure that the properties of the functional groups on HOPG are investigated and not the interaction between functional groups and the metal. It is known that metal is able to absorb gases not only at metal surface but also at subsurface and form a solid solution. This results in changes of the surface energy and leads to complex superstructures and reconstructions of the surface. These intermediate metal-gas layers serve as a precursor for the additional adsorption of gases. Therefore, if there are metal contaminations in the used carbon, the interpretation of the oxygen groups by XPS and TDS is hampered. Compared to HOPG, natural graphite has an even better graphitic structure with less construction

defects (described in chapter 2.2), but the amount of contaminations is too high in natural graphite. Therefore, natural graphite is not suitable for our purpose.

4.2 Functionalization of HOPG

Functionalization of HOPG is a challenge due to its inertness. It is reported in the literature, that with maximum gas exposure of 10 Langmuir (L) on pristine HOPG there is no adsorption of gases at room temperature[11]. The basal plane of HOPG is very unreactive towards molecular oxygen. In other words, small gas molecules can only adsorb on defects of HOPG. Ion bombardment (sputtering) is a very well-known method to generate defects. In the PhD thesis of Samer Aburous[2] (preliminary work of this PhD thesis), two sputter procedures (sputtering with Ar and O_2 and sputtering only with Ar following exposure to O_2) were used to functionalize HOPG for investigating the interaction between the defects and molecular oxygen[2]. The results show, when HOPG was sputtered with a mixture of Ar and O_2, oxygen was introduced in HOPG successfully and the total amount of oxygen-containing groups on HOPG depends on the sputtering time. Therefore, this sputter procedure is further used in the present work. When HOPG was sputtered only with Ar followed by exposure to molecular oxygen, no oxygen can be determined by XPS, TPD and Auger spectroscopy[2]. The reason could be that the sputtering defects are partly saturated by the rest gases in the UHV-chamber and partly restructured during the sputtering process before they are exposed to molecular oxygen. For this reason, this sputter procedure is improved. In the present work, HOPG was sputtered with Ar and exposed in molecular oxygen atmosphere while sputtering, so that the generated sputter defects can be saturated by oxygen immediately. To investigate the influence of water, HOPG was also sputtered with Ar and exposed to water atmosphere while sputtering. In comparison to my thesis Samer Aburous used the two sputter procedures described above for his work and investigated oxygen groups introduced by these two sputter procedures mainly by TPD and AES. In my thesis, a third sputter procedure was used; detailed and systematic XPS-O1s, TPD and UPS measurements are part of my work. To sum up, in my investigation two different sputter procedures were used to generate defects in order to introduce the oxygen groups: Sputtering with Ar and O_2 (procedure ‘a’) and sputtering with Ar in different gas atmospheres (O_2 / H_2O / H_2) (procedure ‘b’). With procedure ‘a’ both Ar and O_2 gas were ionized and accelerated to sputter the sample. That means the defects are

generated not only by Ar^+, but also by O_2^+/O^+. With procedure 'b' the defects were only generated by Ar^+, the O_2 / H_2O / H_2 gas atmosphere ensures that the defects are saturated by O_2 / H_2O / H_2 molecules but not by other molecules.

Accelerated ions can penetrate into the bulk of the sample. That means both surface defects and bulk defects are generated by sputtering. Sputtering procedures on carbon material were well investigated in the literature[3;6-11]. It is known that the amorphization process of graphite while sputtering is very fast[6]. Amorphous carbons will be produced, if the sample is irradiated by a 0.5 keV Ar^+ beam with doses from $3*10^{14}$ up to $3*10^{15}$ ions/cm^2 [6]. In the work of Hang and Kang[12], 40-100 eV Ar was used to irradiate graphite surface with an Ar-dose between $9*10^{11}$ and $6*10^{13}$ ions/cm^2, under this sputter condition "non-amorphous" graphite surface with small isolated vacancy-defects were generated[12]. One of our challenges is to find suitable sputter parameters to produce little amounts of small defects in order to introduce little amounts of oxygen and keep the HOPG surface graphitic after sputtering. Ideally, only point defects (described in chapter 3.2.1) are generated, so that the experimental results can be compared with theoretical calculation about oxidation at point defects on graphene surface[13;14]. Another challenge is to introduce oxygen only on HOPG surface and not in HOPG bulk, ideally to introduce only one kind of oxygen functionality. This is to simplify the oxygen-carbon model system and to enable the use of surface sensitive techniques to determine the oxygen functionalities.

Besides sputtering methods, various strong oxidants such as HNO_3, H_2O_2 and O_3 etc.[3;8;12] are widely used to functionalize carbon material. In comparison with the strong oxidants, the advantages of the sputter methods to oxidize the HOPG surface are: Firstly, the amount of the defects can be well controlled by changing the sputter dosage[13]. Secondly, sputter methods and most of the characterization methods can be carried out in the same vacuum chamber without any contact of the sample with outside of the chamber. Nevertheless, HOPGs were also functionalized in HNO_3-solution in our investigation, in order to have a comparison with the oxygen introduced by sputtering.

4.3 Characterization

Results of the Samer Aburous PHD thesis[2] show that after HOPG was successively sputtered with a mixture of Ar and O_2 for several cycles, an additional CO desorption peak appeared at high temperature (about 750 °C), but no AES-signal of this oxygen can be seen. The most probable reason for the appearance of this CO-peak is that this oxygen is bound deep in the bulk of the sample, which makes it invisible for surface sensitive techniques (in his experiments AES and XPS were used). This assumption is strongly supported by the SEM and STM images, which show large number of pits and pinholes on HOPG surface, which correspond to large defective HOPG surface[2]. From this phenomenon (work of Samer Aburous) and our investigation later, it can be concluded that the type of defects as well as the surface morphology has a strong influence on the desorption behavior of gases and on the binding energy position of the intercalated atoms such as Ar (detail in chapter 6.2). That means, to make a plausible statement about the nature of the oxygen functionalities, detailed characterization of the HOPG surface after sputtering is required. Therefore, a systematic characterization of the sputter damage and the HOPG surface morphology is absolutely necessary. To characterize the HOPG surfaces with damages, UV Photoelectron Spectroscopy (UPS), SEM, STM, XPS and TPD were used. UPS is a method, which delivers very important information about the electronic structure of the valence band of HOPG. With SEM and STM the surface damage can be observed. Surface roughness can be estimated through the STM images. With C1s-XPS direct information about intensity change of the graphitic carbon on the surface can be obtained. During the investigation it was found, that Ar-TPD spectra are very sensitive to HOPG structure and the damages. Ar-TPD deliver also very important information about gas diffusion processes, which are correlated with the desorption of oxygen-containing gases. Therefore, Ar-TPD spectra have a very important contribution for building the model of the sputtered HOPG surface structure. It has to be mentioned, in literature the characterization of oxygen groups during the heating process ignored often the influence of the surface morphology. In our systematical investigation of the oxygen-HOPG system, the influences of HOPG structure and surface defects are considered.

To research the nature of the induced oxygen groups, TPD and XPS are used. TPD can detect the desorbed gas species from HOPG, which are the products of decomposition of surface functionalities. XPS is a surface sensitive method and can

differentiate the oxygen species existing on the surface, because of their characteristic chemical shift in XPS. However, various oxygen 1s XPS signals occur in a narrow range of 2.5 eV on oxidized carbons[14;15], so that they overlap. Thus, it is very difficult to identify single oxygen peaks and to assign them clearly. To solve this problem a step wise heating process followed by TDS and XPS analysis was used. This step wise heating procedure was already reported in the literature[15;16]. Marchon's groups used this procedure first to investigate the adsorption of H_2O on graphite. The results show, that the step wise heating procedure leads to significant changes in the O1s intensity and shifts of O1s binding energy[15]. A combined analysis of O1s-XPS and desorbed gas-TPD is here very helpful. This technique was found useful in order to link the release of oxygen containing molecules from the samples at different temperatures directly with the decomposition of oxygen-functional groups present on the sample surface. Recently, Dirk Rosenthal[16] used this technique and successfully characterized the oxygen on CNFs, which were functionalized by strong oxidants. His investigation shows, that the XPS analysis of such a step wise heating process provides insights into the nature of CO_2 releasing groups[16]. Nevertheless, the change of O1s shape by step wise heating was not clear enough to distinguish different oxygen functionalities. A deconvolution model for O1-XPS spectra is needed. In literature O1s peaks are fitted with two to seven oxygen components and the assignment for the oxygen components is not consistent (details in chapter 6.4). In our investigation, at least five oxygen components on HOPG surface can be distinguished and evidently established in O1s-XPS difference spectra, thereby a new deconvolution/fitting model for O1s-XPS spectra is build.

Reference List

[1.] F. Atamny, R. Schlögl, W. J. Wirth, *Ultramicroscopy* **1992,** *426* 660-667.

[2.] Samer Aburous, *Dissertation: HOPG as a model catalyst for the oxidative dehydrogenation of ethylbenzene over carbon materials*, Free University Berlin, **2007**.

[3.] J. Fournier, D. Miousse, L. Brossard, H. Ménard, *Materials Chemistry and Physics* **1995,** *42* 181-187.

[4.] A. K. Geim, K. S. Novoselov, *Nat.Mater* **2007,** *6* 183-191.

[5.] K. S. Novoselov, A. K. Geim, S. V. Morozov, D. Jiang, M. I. Katsnelson, I. V. Grigorieva, S. V. Dubonos, A. A. Firsov, *Nature* **2005,** *438* 197-200.

[6.] S. Ravesi, A. Terrasi, L. Torrisi, G. Foti, *Radiation Effects and Defects in Solids* **1993,** *127* 137-145.

[7.] E. Asari, I. Kamioka, W. A. Lewis, T. Kawabe, K. G. Nakamura, M. Kitajima, *Nuclear Instruments and Methods in Physics Research Section B: Beam Interactions with Materials and Atoms* **1994,** *91* 545-548.

[8.] W. Choi, C. Kim, H. Kang, *Surface Science* **1993,** *281* 323-335.

[9.] S. Maurer, P. Oelhafen, P. Gantenbein, P. Kania, S. Schelz, *Helvatica Physica Acta* **1992,** *656* 860-861.

[10.] M. J. Nowakowski, J. M. Vohs, D. A. Bonnell, *Surface Science* **1992,** *271* L351-L356.

[11.] M. J. Nowakowski, J. M. Vohs, D. A. Bonnell, *Journal of the American Ceramic Society* **1993,** *76* 279-283.

[12.] J. R. Hahn, H. Kang, *Surface Science* **1996,** *357-358* 165-169.

[13.] J. M. Carlsson, F. Hanke, S. Linic, M. Scheffler, *Physical Review Letters* **2009,** *102* 166104.

[14.] J. M. Carlsson, F. Hanke, *not published* **2008**.

[15.] B. Marchon, J. Carrazza, H. Heinemann, G. A. Somorjai, *Carbon* **1988,** *26* 507-514.

[16.] D. Rosenthal, M. Ruta, R. Schlögl, L. Kiwi-Minsker, *Carbon* **2010,** *48* 1835-1843.

5. Surface treatment and characterization methods

5.1 Ultra-high Vacuum (UHV)

The investigation was carried out in an UHV chamber. The reasons for using an UHV chamber are twofold. On the one hand, the surface of the sample can be kept clean in UHV, otherwise the sample will be covered by foreign gas molecules very quickly (even at very low Pressure). On the other hand, various methods for analyzing the surface (UPS, XPS, LEED, AES, LEIS) and methods for cleaning or modifying the surface (such as sputtering) are based on the unrestricted spread of the electrons, ions or neutral particles. These methods must be carried out in UHV. Otherwise, the electron beam can never reach the sample, because it is already absorbed on the way to the sample by different gas molecules.

The UHV system used for preparing and characterizing the HOPG surface is illustrated in figure5.1.

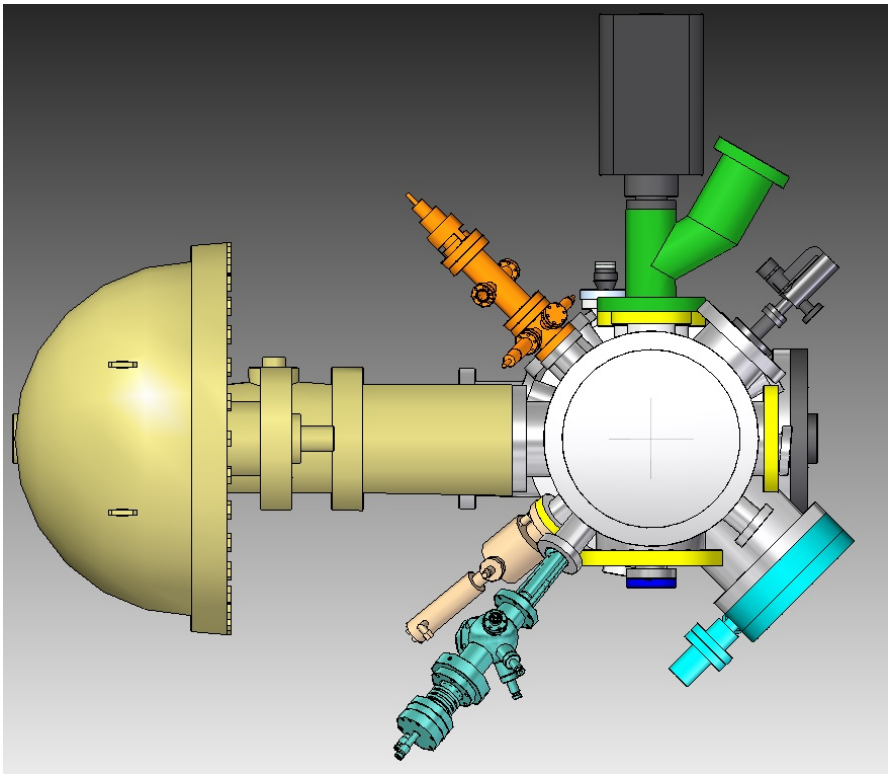

Figure 5.1 Top view of the UHV chamber

The base pressure in the UHV chamber is $3*10^{-10}$ mbar. The chamber was equipped with a QMS 200 quadruple mass spectrometer (Pfeiffer Vacuum), an X-ray source with non-monochromatized Mg/Al Kα radiation (XR50 SPECS), an UV discharge lamp (HIS13, OMICRON), a hemispherical analyzer (Phoibos 150, SPECS) and two

sputter guns (PHI 04-161, PERKIN-ELMER and IQE 12/38, SPECS). The sample was heated by electron-beam impact from the back side and the temperature was measured by a thermocouple type K.

The difference between these two sputter guns is: Ion source IQE 12/38 has two differential pumping apertures, which are mounted along the ion source axis. The first aperture is located between the ionization assembly and lens system and has a 1 mm opening. The second aperture with an inner diameter of 3 mm is placed between the lens and deflection system, which effectively prevents the gas in the main chamber going into the ionization chamber of the sputter gun.

To improve the signals of gas desorption in TPD measurement and to avoid the possible re-adsorption of the emitted gas particles on the sample, the mass spectrometer is also differentially pumped. An aperture is used to ensure that the measured signal is majorly contributed by the desorbed gas from the middle of the surface. The distance between the sample and the aperture is in the range of the aperture itself (1 mm). In this way, it can be assumed that the desorbed particle is only analyzed by MS once and after that, it is pumped away directly.

5.2 Sputtering

Sputtering is a process whereby atoms are removed from a solid target by bombarding the solid target with energetic particles. It is commonly used for cleaning metal surfaces, thin-film deposition (PVD), etching and analytical techniques (e.g. LEIS) and it can also be used to modify structural, electrical and chemical properties of a given material. The ion range in solids depends on the nature of the irradiating ions and target material[1]. In our investigation, sputtering methods were used to modify the graphite surfaces. Sputtering can generate defects on the HOPG surface and in the body, so that oxygen can absorb on the surface defects and form functional groups.

5.3 Temperature programmed desorption (TPD)

There are numerous methods for studying the surface processes. One important method is temperature programmed desorption spectroscopy. It is generally known that gas molecules can adsorb on the surface of a metal solid. It is important to know the energy necessary for the desorption and if the gas molecule will recombine or not during the desorption process. From TD-spectra all this information can be obtained.

On non-metal surfaces such as graphite and CNTs, gases can adsorb on the defect sites and react to form different functional groups. In this case, the product of desorption is corresponding to the product of dissociation of the functional groups and the energy of desorption is the same as the energy of dissociation. In this chapter the TPD method is described briefly.

Polanyi – Wigner Equation

In TPD spectra, the gas desorption rate is measured. With the Polanyi-Wigner equation[2] the desorption rate can be described.

Polanyi-Wigner equation:

$$r_{des} = -\frac{d\theta}{dt} = v_x^0(\theta) \cdot e^{\frac{-\Delta E_{des}(\theta)}{RT}} \cdot \theta^x \cdot N_{\max}^{x-1} \approx v_x^0(\theta) \cdot e^{\frac{-\Delta E_{des}(\theta)}{RT}} \cdot \theta^x$$

- θ: Coverage (is a function of pressure and temperature)
- v_x^0: Frequent factor (depending on the configuration of adsorbed particles)
- *x*: Order of desorption.
- ΔE_{des}: Activation energy of desorption (in kJ/Mol, it is a function of θ, if the particles interact with each other).

v_x^0, x, ΔE_{des} are often considered as constants, in reality they are often a function of coverage θ and temperature T.

Quantification of TPD spectra

(a) Quantification with Kinetic gas theory

The measured signal of TPD measurement is the ion current (in ampere) of the mass spectrometer. Nevertheless, we are interested in the desorbed gas amount. The following steps are necessary to obtain this quantity.

Through a calibration curve of each desorbed gas, each measured signal (MS signal) can be correlated to the gas pressure p*. For instance, the CO gas pressure can be calculated with the following equation, which is obtained from the CO calibration curve in figure 5.2.

$$P_{CO} = \frac{MS\ signal - 2.89 * 10^{-12}}{3.31 * 10^{-4}}$$

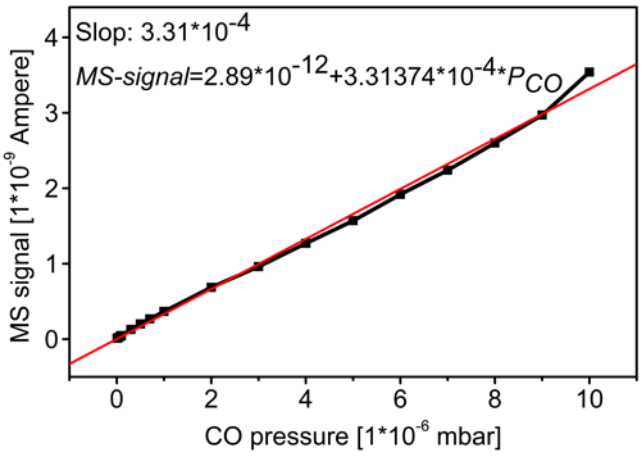

Figure 5.2 Calibration curve of CO gas

In combing the TD data with kinetic gas theory the amount of the desorbed gas particles can be calculated. It is known from kinetic gas theory[3] that the following formula holds:

$$^{1}Z_w = \frac{p^* N_A}{\sqrt{2\pi MRT}}$$

- M(kg/mol) = M(g/mol)/1000 (Molar mass)
- T(K) = T(°C) + 273 (Temperature)
- N_A = 6.0221 x 10^{23} /mol (Avogadro constant)
- R = 8.3145 J/mol·K (Gas constant)
- p^*: Pa. Value can be obtained from the MS signal via the calibration curve
- $^{1}Z_w$: $m^{-2}\cdot s^{-1}$ (Gas amount per time unit and per area unit)

This allows us to calculate $^{1}Z_w$, because all the parameters on the right hand side are known. When $^{1}Z_w$ is multiplied by the surface area of the HOPG sample (A=1*10^{-4} m^2), the amount of gas desorbing from the HOPG surface per time unit can be obtained.

Integration of $^{1}Z_w \cdot A$ over the time (t) corresponds to the total amount of desorbed gas from the HOPG surface. In our TPD measurement the heating rate $\mathrm{dT/dt}$ is 5.67 K/sec. The total desorbed gas amount can be calculated with the following integration.

$$\text{Total desorbed gas amount} = \int_{t1}^{t2} \Delta\ ^{1}Z_w \cdot A \cdot dt = \frac{1}{5.67} \cdot \int_{T1}^{T2} \Delta\ ^{1}Z_w \cdot A dT$$

(b) Quantification by comparison with CO on Pt (111)

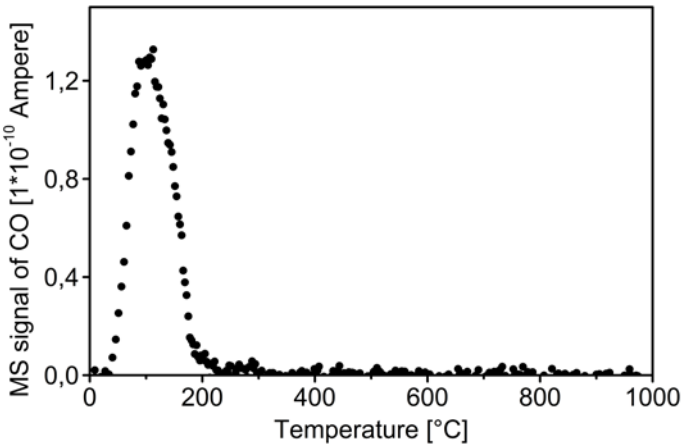

Figure 5.3 TPD of 20 L CO adsorption on Pt (111) at room temperature

20 L CO are adsorbed on Pt (111) at room temperature. This CO dose ensures the saturation coverage of CO on Pt (111) at room temperature. From the desorption curve the value of the CO integral can be obtained and this value corresponds to a certain amount of CO molecules, as reported in literature[4-6]. Comparing the CO integral from HOPG with the CO integral from Pt (111), the desorbed CO gas amount can be estimated. The desorbed oxygen amount calculated by this method is in agreement with the desorbed oxygen amount calculated by the kinetic gas theory. In chapter 6 kinetic gas theory was used to calculate the desorbed oxygen amount.

Calculation of desorption energy

The Polanyi-Wigner equation was modified by Redhead[7]. According to Redheads calculation the first order desorption (x = 1) can be described like this:

$$\frac{\Delta E_{des}}{RT_p} = \ln\frac{\nu_1^0 T_p}{\beta} + \ln\frac{RT_p}{\Delta E_{des}} \quad \text{.....(1)}$$

- T_p: Temperature of the maximal Desorption rate (K)
- ν_1^0: Frequent factor (s^{-1})
- ΔE_{des} : Activation energy of desorption (in kJ/Mol).
- β : Heating rate (in K s^{-1})

For ν_1^0 = 10^{13} s^{-1} and for different values of β ($10^{13} > \nu_1^0 / \beta > 10^8$), a family of curves ΔE_{des} to T_p was obtained[7]. From these curves it can be seen that each curve is almost

linear and that the slopes differ only slightly. Thus, the following approximated equation is obtained.

$$\frac{\Delta E_{des}}{RT_p} = \ln \frac{\nu_1^0 T_p}{\beta} - 3.64\,,\ \nu_1^0 = 10^{13}\,s^{-1}\,[7] \quad \text{.....(2)}$$

With this equation, the activation energy of the desorption state can be estimated.

5.4 Photoelectron spectroscopy

Photoelectron spectroscopy is a very powerful and versatile technique to study the composition and electronic structure of the surface region of a material[8;9]. It utilizes photoionization and analysis of the kinetic energy distribution of the emitted photoelectrons. Two different sources of the exciting radiation are in use and therefore two varieties of the photoelectron spectroscopy exist, namely the X-Ray Photoelectron Spectroscopy (XPS) and the Ultraviolet Photoelectron Spectroscopy (UPS). XPS uses x-ray radiation with photon energies of 200-2000 eV as the excitation source to examine core levels of a sample surface and UPS use UV radiation with a photon energy of 10-45 eV to examine the valence band state of a sample surface.

5.4.1 X-Ray Photoelectron Spectroscopy (XPS)

XPS, also known as Electron Spectroscopy for Chemical Analysis (ESCA), was developed as a useful analytical tool by Kai Siegbahn from Sweden, who received the Nobel Prize in 1981 because of this. In the last 30 years, both theory and experimental technology have been developed further. In the beginning, XPS was mainly used for qualitative analysis of chemical elements, whereas nowadays XPS has become one of the most important and widely used techniques for surface analysis. Examples for its use are the qualitative and quantitative analysis of surface elements, oxidative states of chemical elements and depth and boundary analysis of thin films. With XPS, measurements can be taken from the whole surface or just from a specific area. Furthermore, XPS is considered as a nondestructive technique for most materials. Therefore, XPS is widely applied in industry, e.g. in the related fields of polymer surface analysis, catalyst analysis, corrosion and adhesion analysis, thin film coating and semiconductors.

Equipment and Work principle

XPS must be operated in UHV system. The work pressure should be below $1*10^{-5}$ mbar and a pressure below $1*10^{-8}$ mbar is considered as an optimal pressure. XPS basically consist of an x-ray source and an energy analyzer. For the x-ray source Al and Mg anodes are usually used in order to generate the x-ray radiation.

The principle of XPS is based on the photoelectron effect. Core level electrons of a material can be ejected by the x-ray radiation and the emitted photoelectron can escape from the force of the atom core with a certain kinetic energy to be a free photoelectron, while the atom itself is in an excited state. The kinetic energy of the emitted electrons is dependent on incident energy (*hv*), instrument work function (Φ_{sp}) and element binding energy (E_B^F) (described in Eq.(3)). The sample work function (Φ_s) is canceled out in the derivation process of equation (3).

$$E_B^F = hv - E_{kin} - \emptyset_{sp} \quad \text{..... (3)}$$

To get a correct value for the binding energy of an element, a proper energy reference has to be used. All binding energies here are referenced to the Fermi level. Additionally, it has to be noted that the vacuum level is not a good reference level in this case. For example, consider two metals. Metal A has smaller work function than metal B (referenced to vacuum level). When these two metals come into electrical contact, they are going to have the same Fermi level. This process leads to a contact potential difference $\Delta\Phi$ (CPD). In this case, the energy of the core level referenced to the Fermi level does not change for the two metals. If the vacuum level is used as reference, the core level energy of metal changes for the value of CPD. Additionally, the work function of a surface referenced to vacuum level can change with different chemical environment. Therefore, the vacuum level is not a suitable reference level for binding energy calibration.

The resolution of XPS spectra depends on three factors: Analyzer resolution, width of the exciting radiation and lifetime of the excited state of sample. They obey Eq. (4)

$$(\Delta E_{tot})^2 = (\Delta E_{anal})^2 + (\Delta E_{line})^2 + (\Delta E_i)^2 \text{..... (4)}$$

The line width of non-monochromatized Mg *Kα* radiation is about 0.7 eV[7;10].

The limitation for this method is that the samples have to be conductive. If the conductivity of the sample is poor, the sample will be charged positive and form a

surface potential (surface charging), and this potential makes it more difficult for the photoelectron to leave the sample and reach the analyzer, e.g. the kinetic energy of the escaped electrons is reduced. This results in a shift of the binding energy to higher energy. Additionally, surface charging can also result in peak broadening. This might result in a wrong analysis of the material. Therefore, it is very important to calibrate the binding energy of the measured spectra.

Analysis of XPS spectra

(a) Qualitative analysis

In a XPS spectrum, there are various types of peaks. It is important to distinguish them correctly. In general, there is always increased background-intensity in XPS spectra with increased binding energy. The background consists of the amount of the secondary electrons and most of the secondary electrons are in the very low kinetic energy region.

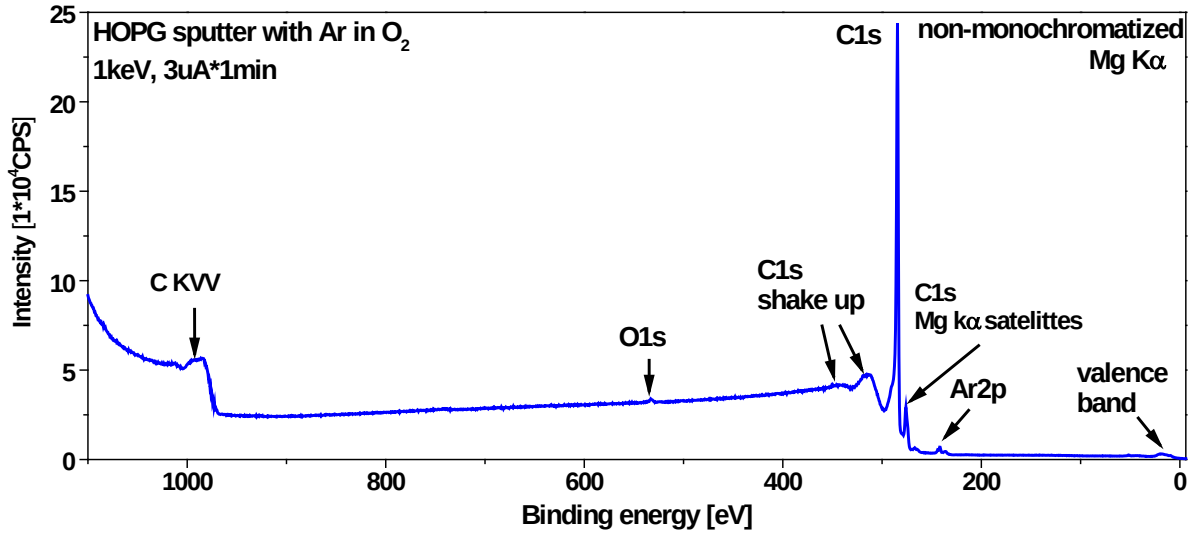

Figure 5.4 XPS survey of modified HOPG

- Main peaks

The main peaks are used to identify the element. The core-level binding energies of a certain element may be subject to variations depending on the chemical state of the atom, for instance its oxidation state. Chemical shifts of core-levels are an initial state effect. The nature and especially the ionicity of the bonds of an atom to its neighbours influence the charge density in the valence orbitals. Its change influences also the effective core charge and thus their $E_{B.}$ A change of bonding (change of oxidation state, change of ligands) will therefore result in a shift of core levels. Such

shifts are typically in the range of some eV or less[8;11]. Because of the spin-orbit-coupling the p, d and f lines split and show up as doublet in XPS spectra (final effects[8]). Ar 2p-XPS in figure 5.5b features the doublet with proper area ratio (1:2) of the $2p_{1/2}$ peak and $2p_{3/2}$ peak.

For most conductive samples the main peaks exhibit asymmetry. This asymmetry results from the neutralization of electrons in the conduction band with positively charged holes created during photoionization process. The main peak is asymmetrically broadened towards higher binding energy[11]. These final state effects are especially strong in metal samples. For non-conductive samples, the main peaks can also show asymmetry because of the positive charging effect. HOPG and graphitic-like compounds have an asymmetric C1s peak-shape centered at 284.5 eV (figure 5.4 and figure 5.5a).

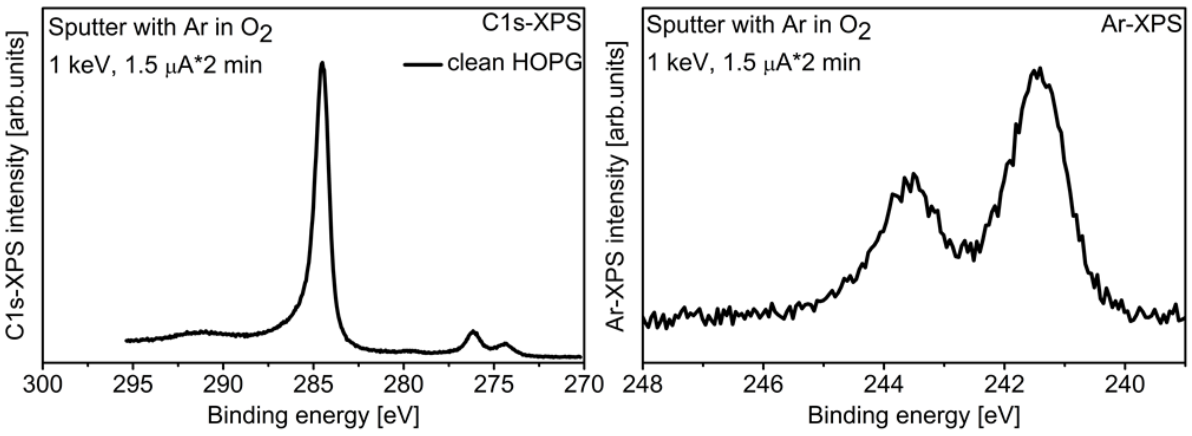

(a) (b)

Figure 5.5 (a) XPS-C1s spectrum of fresh cleaved HOPG; (b) XPS-Ar 2p spectrum of sputtered HOPG

- Shake-up peaks

When the sample is irradiated with X-ray radiation, the core electron (electron 'a') from the sample in ground state is emitted. “As the result of a sudden change in the central potential of an atom, an electron (electron 'b') in a given orbital may go in to an excited state (electron shake-up). This change in potential may occur as the results of a change in the nuclear charge”[12;13] and thereby the kinetic energy of the emitted core electron is reduced because of the atom potential. Consequently, it results in peaks at higher binding energy than the main peak. These peaks are called shake-up peaks. In HOPG the photoelectrons have coupling effects with these electrons in the π -π^* transition state. This shake-up peak in XPS lies at about 291 eV[14;15] (figure 5.5a). This peak is characteristic for graphitic structure.

- Auger peaks

The auger peaks are usually broader peaks in a XPS spectrum. Auger peaks carry also element information. With this peaks, the kind of element can be also identified. In figure 5.4 carbon KVV auger peaks lie between 1020 eV and 970 eV. Oxygen KLL peaks (790-720 eV) cannot be seen in figure 5.4 because of the extreme small amount of oxygen on HOPG surface.

- Valence lines and bands

Peaks between Fermi level and about 20 eV are developed by the emitted electron from the valence and conduction band (for metals and semiconductors). When the form and position of the main peaks of different materials e.g. polymers are very similar, the valence lines and band spectra can be used to differentiate the materials. Crosssection from the valence band region is usually weak and structureless due to the limited instrumental resolution[8]. Therefore, analysis of the valence band is usually based on UPS spectra described in chapter 5.4.2.

- Satellite peaks

In the XPS spectra measured with a non-monochromatic X-Ray source, there are several satellite peaks at higher binding energy beside the main peak. This is because the non-monochromatic X-Ray radiation contains more kinds of radiation, for instance Mg Kα radiation contains Mg K α1, 2, Mg K α3 and Mg K α4, which carry different value of energy. (See table 5.3). The shift and intensity ratio of the satellite peaks compared to the main peak is given below. In figure 5.4 the two strong overlapping small peaks at 276 eV and 274.4 eV beside the C1s peak are the C1s satellite peaks. The relative intensity of these two satellite peaks together is about 12% of the main C1s peak. In HOPG XPS measured at BESSY these satellite peaks are not present.

Table 5.3 Line sources and their characteristic data[16]

Main lines and satellites	energy [eV]	rel.intensity	Satellite shift [eV]
Mg K α1,2	1253.7	100	0
Mg K α3	1262.1	8.0	8.4
Mg K α4	1263.8	4.1	10.1
Further satellites		<1	
Al K α1,2	1486.7	100	0
Al K α3	1496.5	6.4	9.8
Al K α4	1498.5	3.2	11.8
Furthers atellites		<1	

(b) Quantitative analysis

Depth profile: The inelastic mean free path curve for electrons is well-known[17]. With certain photo energy of x-ray radiation, the kinetic energy of the excited core level electrons for a certain element in the sample can be calculated. It is therefore easy to estimate from which depth electrons can reach the surface. This is the decisive factor for the surface sensitivity of the measurement. Changing the photo energy of x-ray radiation, information from different depths of the sample can be obtained. To calculate the atomic concentration, several sample models can be used, which are described in the book of Ertl and Küppers in detail[8]. To ensure a correct calculation, it is important to choose a meaningful and suitable model for the given sample system. In following two models are described.

- Homogenous distribution of element ***A*** + ***B*** model[8]

When element A and B distributed homogenous on the sample surface region, the composition of the surface sheets can be quantified with this model. Because the probability to emit electrons of different elements is different, atomic sensitivity factor (ASF) for each element must be introduced in the calculation. For instance in modified HOPG surface, there are C, O and Ar. The atomic ratio of Ar to C ($\frac{X_{Ar}}{X_C}$) can be calculated.

$$\frac{X_{Ar}}{X_C} = \frac{I_{Ar}/ASF_{Ar}}{I_C/ASF_C}$$

- I_{Ar}, I_C: Intensity of Ar2p- peak and C1s- peak in XPS spectrum.
- ASF_{Ar}: Atomic sensitivity factor of argon. $ASF_{Ar} = 2.991$ [10].
- ASF_C: Atomic sensitivity factor of carbon. $ASF_C = 1$ [10]

- Substrate ***B*** + adsorbate ***A*** model[8]

Gases adsorb on some sample surfaces and form an over layer on the top of the substrate, e.g. CO on Pt (111) surface. The coverage of the gas is $\boldsymbol{\theta_A}$.

$$\frac{I_A I_B^0}{I_B I_A^0} = \frac{\Theta_A}{1 - \theta_A * (1 - e^{-a_A * \cos\theta / \lambda_A})}$$

- a_A: Size of compound ***A***.
- θ: Angular between analyser and surface normal.

- λ_A : Mean free path of electrons in adsorbate
- $I_{A,}I_B$: Intensity of measured compound ***A*** and ***B***.
- I_A^0, I_B^0 : Intensity recorded for pure compound ***A*** and ***B***

When the system of oxygen on HOPG is analyzed with this model, the oxygen coverage is:

$$\Theta_O = \frac{1}{\frac{I_C I_O^0}{I_O I_C^0} + 1 - \exp(^{-a_O * \cos\theta}/_{\lambda_O})}$$

5.4.2 Ultra violet Photoelectron Spectroscopy (UPS)

Work principle

Normally, the irradiated radiation for UPS measurement is UV light of the He I and He II line. The energy and intensity of the radiation is given in table 5.4.

Table 5.4 UV light energy, satellites and intensity[25]

Main lines	Energy [eV]	Rel. intensity	Satellite shift [eV]
He I	21.22	100	0
	23.09	about 1.5	1.87
	23.74	0.5	2.52
He II	40.81	100	0
	48.37	<10	7.56
	51.02		10.2

The working process is described in two parts. We give here only the most important formulas, omitting their derivation.

(a) $\Phi_s > \Phi_{sp}$

In this case the following equation can be derived.

$$hv = E_F - E_{cutoff} + e\Phi_s \ldots\ldots\ldots\ldots\ldots\ldots\ldots\ldots\ldots\ldots \quad (5)$$

(b) $\Phi_{sp} > \Phi_s$

In this case the work function of the spectrometer instead of the work function of the sample is considered:

$$hv = E_F - E_{cutoff} + e\Phi_{sp} \ldots\ldots\ldots\ldots\ldots\ldots\ldots\ldots\ldots\ldots \quad (6)$$

- $\Delta\Phi$: Contact potential difference. $\Delta\Phi = \Phi_{sp} - \Phi_s$

- E_F: Zero energy point.
- E_{cutoff}: Energy at cutoff edge.

From Eq. (5) and Eq. (6) it can be easily seen that the sample work function can be measured when the value of the sample work function is larger than that of the spectrometer. In case (b) the value of the spectrometer work function is measured.
In UPS and XPS measurements, lots of secondary electrons come from the spectrometer itself. These secondary electrons mix with the real photoelectrons and are measured by the spectrometer. This problem can be circumvented by putting a negative potential on the sample, whereby the secondary electrons from the spectrometer can be separated from the electrons emitted from the sample.

Energy calibration

(a) Using Fermi edge of metal

In UPS, the Fermi energy of a sample can be determined by measuring the Fermi edge of a clean metal surface. With this Fermi energy, an exact energy calibration of the spectrometer can be obtained.

(b) Using σ-peak of HOPG

In HOPG UPS spectrum, there is an intense peak of emitted secondary electrons located at E_{kin} = 7.57 ± 0.03 eV above the sample Fermi level. This secondary electron peak is due to scattering of π-band electrons into a distinct final state related to σ-bands. Therefore, this peak is called ‘σ-peak’. It is proved that the energy position of the σ-peak is independent on the temperature and excitation energy of the light source. Consequently, with the σ-peak of HOPG the energy of spectrometer can also be exactly calibrated[18].

Analysis of UPS spectra

With UPS spectra, the information about the electronic density of state (DOS) close to the Fermi level can be obtained, e.g. the valence band structure. The interpretation of UPS spectra is often quite difficult. Knowing the band structure of the measured material can help to understand the UPS spectra.

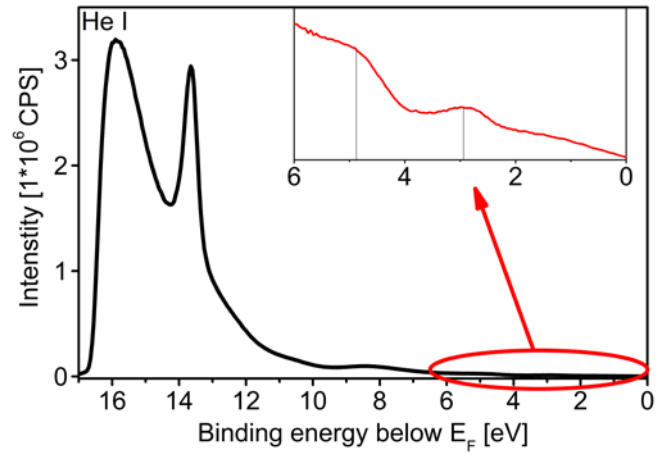

(a)

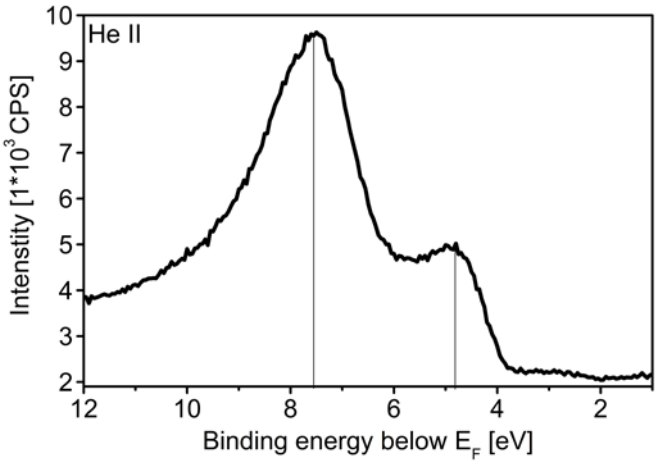

(b)

Figure 5.6 UPS-spectra of fresh cleaved HOPG. (a) He I-UPS; (b) He II-UPS

In UPS spectra, there is always the He I line in the He II line and some He II line in the He I line as well. Therefore, in He I-UPS spectra, the analyzer always measures a small amount of electrons excited by He II light. Consequently, there is some intensity in the region of $E_B > 21.2$ eV. In figure 5.6 He I and He II-UPS spectra are displayed for freshly cleaved HOPG. The two excitation energies are used for taking advantage of the different cross sections for σ-bands and π-bands. The He I beam has a large cross section for π-bands and the He II beam has a large cross section for σ-bands. In combination with the band structure of HOPG[19], an assignment of the peaks in UPS and the bands can be made. Furthermore, with the energy at cut off edge the work function of the HOPG sample can be calculated.

5.5 Scanning Tunneling Microscopy (STM)

The scanning tunneling microscope was invented in 1981 at the IBM lab by Gerd Binning and Heinrich Rohrer[20], who won the noble price in physics in 1986. STM is a powerful instrument for observing surfaces at the atomic level[21]. With this method it is possible to research the diffusion of particles, defects on the surface area and even measure the local electronic structure of a surface. Additionally, at low temperature (4 K) the metal tip of STM can be used to manipulate the surface atoms exactly[22]. STM is an extremely surface sensitive and local method, the information depth of the images is about the first atom layer.

Work principle

The theory of STM is based on the concept of quantum theory tunneling. When a conducting tip is brought very near to the surface to be examined, a bias (voltage difference) applied between the two can allow electrons to tunnel. For a negative bias, electrons tunnel out of occupied states in the sample into the tip and for a positive bias, electrons tunnel out of occupied states in the tip into the sample.
Knowing the wave function allows one to calculate the probability density for that electron to be found at some location. The probability, *P* that an electron tunnels through the space (d) between tip and surface and arrive the sample is:

$$P(E, eU_T) = \exp\left(-2d\sqrt{\frac{2m}{\hbar^2}\left(\overline{e\varphi} - E - \frac{eU_T}{2} \right)} \right)$$

From this equation, it can be seen that P depends exponentially on the distance between surface and tip, d, and the voltage U_T that we put on. This voltage increases the energy level of the tip, so that the electrons of the sample are able to tunnel across the barrier. On the other side of the barrier, where the electron tunnel into, an empty level of the same energy as the electron is required for accepting the tunnel electrons. If there are unoccupied states to accept a tunnel electron, this leads to change in the tunnel current.
The Tunneling current is a function of tip sample distance (d), applied voltage (U_T) and the local density of states (ρ) of the sample and tip (not changeable). The changeable parameters are I_T, d and U_T. Different measure modes can be used by fixing two of these three parameters.

Measure forms and information

(a) Image: From the image we can get information about lattice constant, surface structure e.g. (111), (110) and surface roughness such as defects, steps, edges, terrace.[23;24]

(b) Line scan: Helps to calculate the lattice constant and calibrate the STM image.

(c) I-U_T curve: A point measurement. 'd' is kept constant at a point, and then U_T is changed. With this curve we can get the local electronic structure of semiconductors in the band gap and the value of conductance (dI / dV) at this location[23].

Reference List

[1.] J.F.Ziegler, J.P.Biersack, U.Littmark, in *The stopping and range of ions in solids* ,*Vol*. *1*, **1985**.

[2.] K. Christmann, *Introduction to surface physical chemistry* **1991,** *Springer Verlag, New York* .

[3.] Gerd Wedler, in *Lehrbuch der Physikalischen Chemie* **1987**, p. 676-689.

[4.] G. Ertl, M. Neumann, K. M. Streit, *Surface Science* **1977,** *64* 393-410.

[5.] C. T. Campbell, G. Ertl, H. Kuipers, J. Segner, *Surface Science* **1981,** *107* 207-219.

[6.] P. R. Norton, J. W. Goodale, E. B. Selkirk, *Surface Science* **1979,** *83* 189-227.

[7.] P. A. Redhead, *Vacuum* **1962,** *12* 203-211.

[8.] G.Ertl, J.Küppers, *Low Energy Electrons and Surface Chemistry*, VCH Verlagsgeselllschaft, **1985**.

[9.] M.Henzler, W.Göpel, in *Oberflächenphysik des Festkörpers* **1994**.

[10.] Specs, Quatification in XPS using SpecsLab and CasaXPS, p.11-12, 2005

[11.] D.A.Shirley, *Photoemission in Solids* , Springer, **1978**.

[12.] Thomas A Carlson, *Photoelectron and Auger spectroscopy*, Plenum Press, **1975**.

[13.] R.J.Behm, K. Christmann, G. Ertl und M.A. van Hove, *J.Chem.Phys.* **1980, 73** 2984-2993.

[14.] S. Svensson, B. Eriksson, N. Mârtensson, G. Wendler, U. Gelius, *Journal of Electron Spectroscopy and Related Phenomena* **1988,** *47* 327-384.

[15.] A.M. Bradshaw, S.L. Cederbaum, W. Domcke, U. Krause, *Journal of Physics C: Solid State Physics* **1974,** *7* 4503.

[16.] J.F.Moulder, W.F.Stickle, P.E.Sobol, and K.D.Bomben, *Handbook of X-ray photoelectron spectroscopy*, Perkin-Elmer Corporation, Eden Prairie, Minnesota, **1992**.

[17.] M. P. Seah, W. A. Dench, *Surf.Interface Anal.* **1979,** *1* 2-11.

[18.] P. Oelhafen, J. L. Freeouf, *Journal of Vacuum Science & Technology A-Vacuum Surfaces and Films* **1983,** *1* 96-97.

[19.] I. T. McGovern, W. Eberhardt, E. W. Plummer, J. E. Fischer, *Physica B+C* **1980,** *99* 415-419.

[20.] G.Binnig, H Rohrer, *IBM J.Res.Dev.* **1986,** *30* 355-369.

[21.] M. Kuwabara, D. R. Clarke, D. A. Smith, *Applied Physics Letters* **1990,** *56* 2396-2398.

[22.] D. M. Eigler, E. K. Schweizer, *Nature* **1990,** *344* 524-526.

[23.] H.Fuchs, E.Tosatti, *EPL (Europhysics Letters)* **1987,** *3* 745.

[24.] J.Cervenka, C.F.J.Flipse, *Journal of Physics: Conference Series* **2007,** *61* 190.

[25.] Focus and Omicron. Instruction manual, VUV discharge lamp HIS13. Version 1.7, 1998, Focus-Omicron, instruments for surface science.

6. Results and discussion

6.1 Sample preparation

The size of HOPG samples is 9*9*2 mm^3. After HOPGs were cleaved freshly in air, they were transferred in UHV immediately. After that, XPS measurements were taken at room temperature with the freshly cleaved sample, see figure 6.1. The O1s-XPS indicates that the sample was covered by some oxygen functional groups. This is because of the existence of various edges on the surface after cleaving, which can be attacked by oxygen in air (described in chapter 2.2).

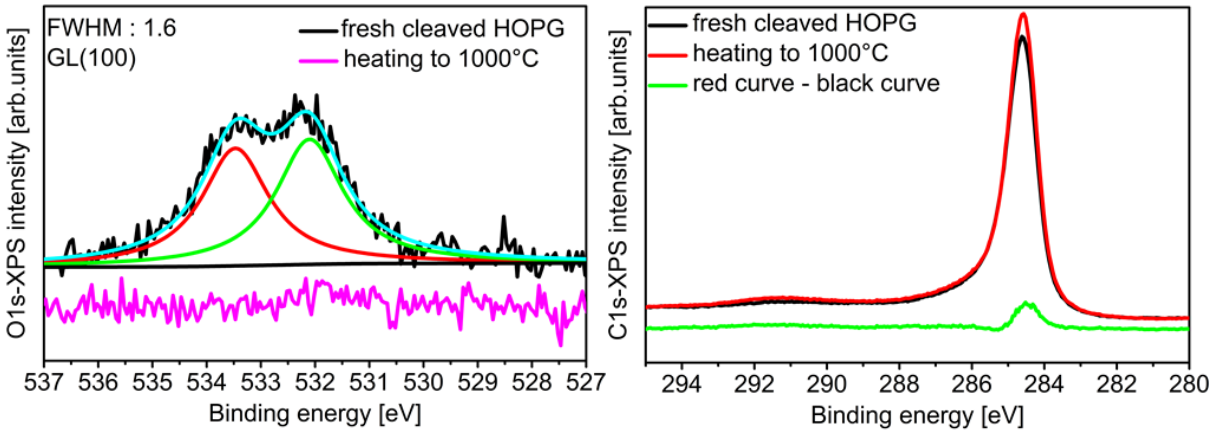

(a) (b)

Figure 6.1 XPS spectra of fresh cleaved HOPG (a) O1s-XPS (b) C1s-XPS

To degas the sample and sample holder, the HOPG was heated in UHV up to 1000 °C for several times. The CO-TPD is shown in figure 6.2. After three heating cycles, the amount of desorbed gas did not change much anymore. Furthermore, there was no oxygen-intensity in O1s-XPS. Therefore, the samples were considered as clean after undergoing three heating cycles. Every HOPG that was used in this study underwent the described procedure for degasing.

There is always CO desorption above 900 °C. The reason is still unknown. One of the possible explanations for that is, that there are CO molecules stored in the HOPG bulk and that they require a very high temperature to diffuse to HOPG surface.

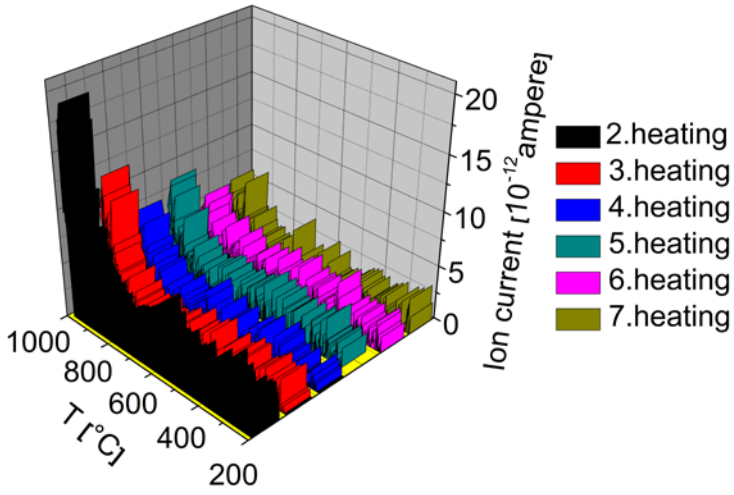

Figure 6.2 CO-TPD spectra of fresh cleaved HOPG-sample

6.2 A new concept for assessing the structure quality of Highly Oriented Pyrolytic Graphite

Abstract

It is very difficult to ascertain the quality of different HOPG because of minimal structural differences. In this paper we demonstrate a new application of the method “Temperature programmed desorption spectra of Ar”. We show how this method can be used to discern the quality of HOPG. We observed in Ar-TPD that the spectra of different HOPG samples differ drastically in the location of the spectrums peak and the shape of the peak. In each Ar TPD spectrum, three different desorption states (Ar-α, Ar-β and Ar-γ) can be noted. We conclude from these results, together with surface sensitive measurements (X-ray Photoelectron Spectroscopy (XPS), UV Photoelectron Spectroscopy (UPS) and Scanning Tunneling Microscopy (STM)), that the desorption temperature of the Ar-γ state mirrors the graphitic part of HOPG. It is the desorption temperature of the Ar-γ state that allows for a classification of the HOPG quality.

6.2.1 Introduction

HOPG is a highly ordered form of pyrolytic graphite with an angular spread of the c axes of less than 1 degree[1]. The weak bonding between graphene layers allows HOPG to serve as host for intercalation of various compounds. The effects of intercalation are generally discussed in view of the measured spectrum of pristine HOPG for instance XPS, UPS and secondary electron spectroscopy[2-6]. Due to the ordinary graphite structure and low impurities quota of HOPG, it is also a very promising reference material for ion bombardment related defect investigation[7-9]. For all of these investigations a comparable quality of HOPGs is required. However, HOPG is not a perfect material. There are many construction defects such as lattice vacancies, stacking faults, displacement of small graphite crystals and parallelism deviation of graphene layers[10]. In reality, HOPG is built from many small crystals[11] oriented the same way. Typical lengths of the crystals are several microns to several hundred microns[11]. According to the norm of HOPG production firm MiroMasch, HOPGs with good quality should have few construction defects, large grains and crystallites and a uniform surface with minimal steps[10]. Moreover, they should also allow easy cleaving of very thin layers. Various techniques such as X-Ray Diffraction

(XRD) and X-Ray Photoelectron Spectroscopy (XPS) have been applied to structural studies of HOPG[12;12;13] or graphite based material[14;15]. However, all of these techniques are not very sensitive to pristine HOPG structure. To differentiate the quality of HOPG is unfortunately very difficult.

In this paper a very sensitive new concept was developed for assessment of the original HOPG quality using Ar ion etching on HOPG. Energies of 0.5 and 1.0 keV were used to bombard HOPG. Temperature programmed desorption (TPD) was measured to detect the desorbed Ar from HOPG. X-Ray Photoelectron Spectroscopy (XPS), UV Photoelectron Spectroscopy (UPS) and Scanning Tunneling Microscopy (STM) were used to characterize the core level of Ar implants and the HOPG surface morphology. The results show: There is a strong correlation between the desorption behavior of Ar implants and the original HOPG structure. Additionally, different defect environments of Ar implants have an influence on the Ar core level position in XPS spectra.

6.2.2 Experimental

Experiments were carried out in an ultra-high vacuum (UHV) chamber with a base pressure of $3*10^{-10}$ mbar. The chamber was equipped with a QMS 200 quadruple mass spectrometer (Pfeiffer Vacuum), an X-ray source with non-monochromatized Mg/Al Kα radiation (XR50, SPECS), a hemispherical analyzer (Phoibos 150, SPECS) and a sputter gun with two differential pumping apertures (IQE 12/38 SPECS). The mass spectrometer for TPD was differentially pumped as well and the distance between the sample and the aperture was in the range of the aperture itself (1 mm). The aperture was located in the middle of the top site of the sample. The sample was heated by an electron-beam impact heater from the back side and the temperature was measured by a thermocouple type K. The thermocouples were proofed with Thermoguss 2000 and were mounted in the center of the HOPG body through a predrilled 0.6 mm diameter hole from the narrow side of HOPG. In XPS measurement Mg Kα radiation (1253.6 eV) was used for excitation. The STM measurements were done in air.

The size of the used HOPG samples (ZYB-graded) is 1 cm^2 × 0.2 cm. At first, HOPG was cleaved freshly in air, after that it was transferred in UHV immediately. To degas the sample and sample holder, the HOPG was heated inside UHV to 1000 °C for several times until no gas desorption can be measured below 900 °C. Table 6.1

gives an overview of the different HOPG samples. Two different HOPG samples were used, they are termed A and B. On sample B different surfaces were cleaved (sample B1 – B5). The sputter procedure was carried out with the IQE 12/38 ion source. The HOPG samples A and B1 – B5 were irradiated with Ar in different gas background. For the sputtering process ion energies of 1 keV and 0.5 keV at 90° to the sample surface were used (table1). The Ar implantation range is about 1 and 2 nm for 0.5 and 1.0 keV Ar ion kinetic energy[16]. After sputtering, XPS and UPS were measured at room temperature. Subsequently, surveys of Ar-TPD were carried out in the temperature range from room temperature up to 930 °C. After the TPD measurement, samples were cooled down to room temperature and were again characterized by XPS and UPS.

Table 6.1 Samples of HOPG overview

Sample	Sputtering condition		Sputtered ion amount
A	Sputtering with Ar in O_2	1 keV, 1.5 uA*2min	$5.6*10^{14}$ ions/cm^2
B1	Sputtering with Ar in H_2O		
B2			
B3	Sputtering with Ar in H_2O	500 eV, 0.1 uA*3min	$1.1*10^{14}$ ions/cm^2
B4		500 eV, 0.1 uA*6min	$2.2*10^{14}$ ions/cm^2
B5		500 eV, 0.1 uA*24min	$8.8*10^{14}$ ions/cm^2

6.2.3 Results and discussion

6.2.3.1 HOPG surface structure after sputtering

As mentioned above, HOPG is built from many small crystals[11]. Because of possible stacking fault and displacement of small graphite crystals, there are mainly 3 kinds of construction defects in HOPG: lattice vacancy, cross-linking between graphene layers and 3d-construction defects. Especially cross linking defects and 3d-construction defects are very sensitive to the sputtering process: During the sputtering process, Ar is irradiated to HOPG surface. Ar ions cross through the graphene layer, lose energy and in the end stay somewhere between the graphene layers. When Ar ions bombard graphene layers with cross-linking and 3d-construction defects, these defects make the graphene layer stiffer and hence prevent the relaxation effect like in flexible graphene. Therefore, the sputter damage on these stiff layers due to construction defects is more pronounced.

The damage on the surface area after sputtering can be related to the UPS-spectra in figure 6.3. The complete breakdown of the σ-peak at 13.6 eV indicates destruction of the graphite electronic structure[4], as can be seen in the curve of sample B1 in fig. 6.3a (UPS of sample A and B2 is very similar to the curve of B1). Sample B3, B4 and B5 were sputtered with increased Ar dose at the same sputter energy (500 eV, table 6.1). The remaining σ-peak of sample B3, B4 and B5 indicates that the graphene layers in the surface area were not completely amorphous. The peaks at 5 eV and 7.5 eV in He II-UPS spectra are contributed by the top σ-band and π-band[17-19], the intensity of these two peaks decreases with increased sputter dose and shifts slightly to Fermi energy side. The shift of the peak at 7.5 eV (see figure 6.3b) indicates that the π-band moves in the direction of the Fermi energy, one possible explanation for the shift is the conversion of π-states to σ-states after sputtering. The surface morphology of clean HOPG, sputtered for 3 min and 24 min respectively is shown in STM images in figure 6.4. The mean roughness of HOPG sputtered for 3 min is about 0.2 nm. This means that only sputter damages in the first graphene layer are visible. The species in the first layer are mobile on interaction with the fast scan direction of the STM tip. Whereby, the mean roughness of HOPG sputtered for 24 min is about 1.2 nm, which means about 4 monolayers of graphene are damaged. Obviously, the surface of the sample sputtered for 24 min has much larger corrugation and is more destroyed than the sample sputtered for 3 min. The loss of atomic resolution is due to the mobile species in the 3 min case and due to partly amorphous carbon[8] in the first layers in the 24 min case. The σ-peak in the UPS measurement of sample B3 (3 min) and B5 (24 min) still shows graphitic character. Comparing the results of UPS and STM it can be concluded that parts of the HOPG surface are amorphous and some parts remain graphitic in character after sputtering. The higher the sputter dosage, the smaller is the amount with graphitic character. For sample B5, the deeper graphene layers are more destroyed than for sample B3. Simultaneously, this destruction in deeper layers affected strongly the surface morphology. The identity of the mobile surface groups is still unknown, they could be mobile small graphite island generated during the sputter process.

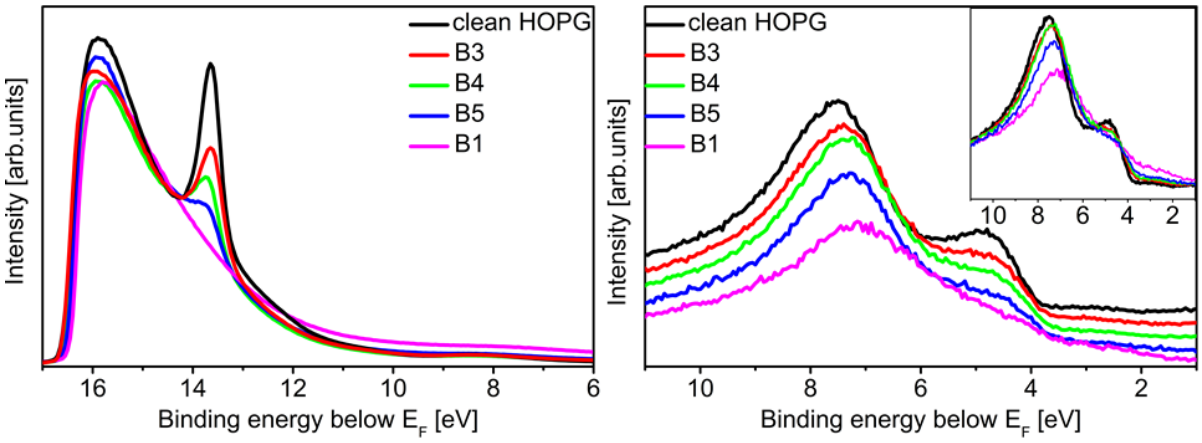

(a) (b)

Figure 6.3 UPS of sample B3, B4 and B5 and B1 after sputtering. The black curve is UPS of clean HOPG sample before sputtering (a) He I-UPS; (b): He II-UPS;

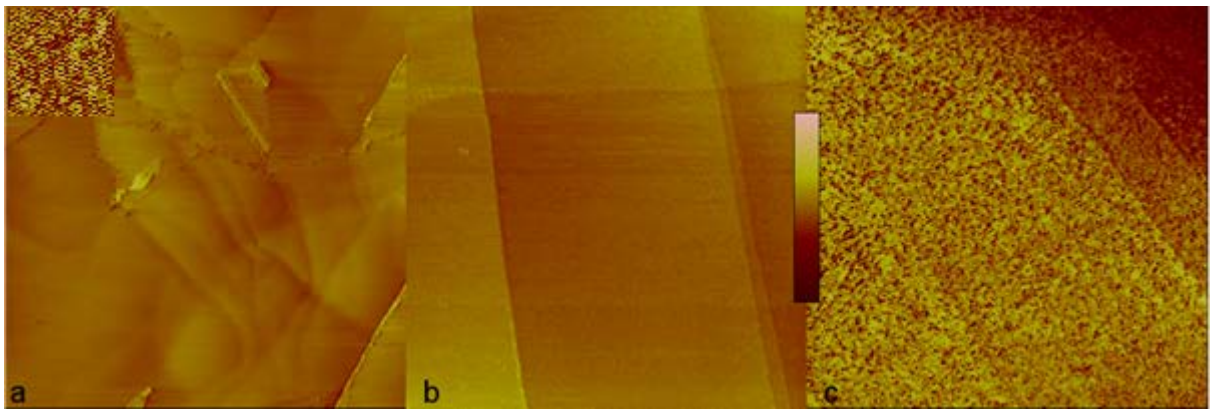

Figure 6.4 STM images of HOPGs (1mm×1mm, I=2nA), the height of the scale is 10nm for all three images (a) freshly cleaved HOPG (U=20mV). Inlet: atomic resolved image (5nm×5nm, U=20mV, I=2nA); (b) 500V, 0.1uA*3min (U=150mV); (c) 500V, 0.1uA*24min (U=150mV)

6.2.3.2 Influence of original HOPG structure on Ar-TPD spectra

Sample A, B1 and B2 were irradiated with the same Ar doses of $5.6*10^{14}$ ions/cm^2 at the same sputter energy of 1 keV. It is expected that the Ar desorption spectra of these three samples should be similar, but it is remarkable that the Ar-TPD spectra differ dramatically (figure 6.5). In Ar-TPD three desorption states α, β and γ can be observed. Ar-α desorbed in the low temperature range around 300 °C and the intensity of this state is quite low. Ar-β desorbed around 500 °C. The Ar-γ desorbed at high temperatures above 800 °C and the desorption temperature of Ar-γ for the three samples follow $T_A < T_{B1} < T_{B2}$. It has to be noted at this point, that the desorption temperature of Ar is dependent on the heating rate. The desorption amount of Ar-β and Ar-γ is relatively high compared to the Ar-α state. Additionally, the ratio of the integration of Ar-β and Ar-γ states for different samples is quite different: The ratio of sample A is much larger than the ratio of sample B1 and B2 (R_A

> $R_{B1,}$ R_{B2}). It has to be noted that T_{B2} is above our planned measurement range. Therefore, R_{B2} cannot be calculated exactly.

Since the sputter condition for the three samples is the same, the difference of TPD-spectra can only be caused by the structural difference of the pristine HOPGs. This assumption can be established by the C1s-XPS and UPS spectra of the three samples. In C1s-XPS small differences can be seen (figure 6.6a). The width of the C1s line (FWHM) of the three samples differs slightly: FWHM of sample A > B1 > B2. According to literature, the smaller the line width, the better the graphitization of the sample[20]. In He I-UPS (figure 6.6b) the secondary electron peak (σ-peak) at 13.6 eV of the three samples is shown. The σ-peak is due to scattering of HOPG π-band electrons into a distinct final state related to σ-bands[18]. This peak is extremely sensitive to the graphitic structure. The intensity of the σ-peak mirrors the graphitization degree of HOPG. According to both, XPS and UPS spectra, the graphitization degree of the three samples after sputtering is: B2 > B1 > A.

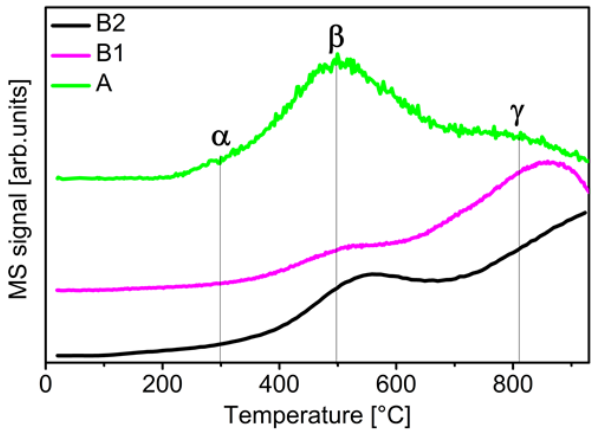

Figure 6.5 Normalized Ar-TPD spectra of sample A, B1 and B2

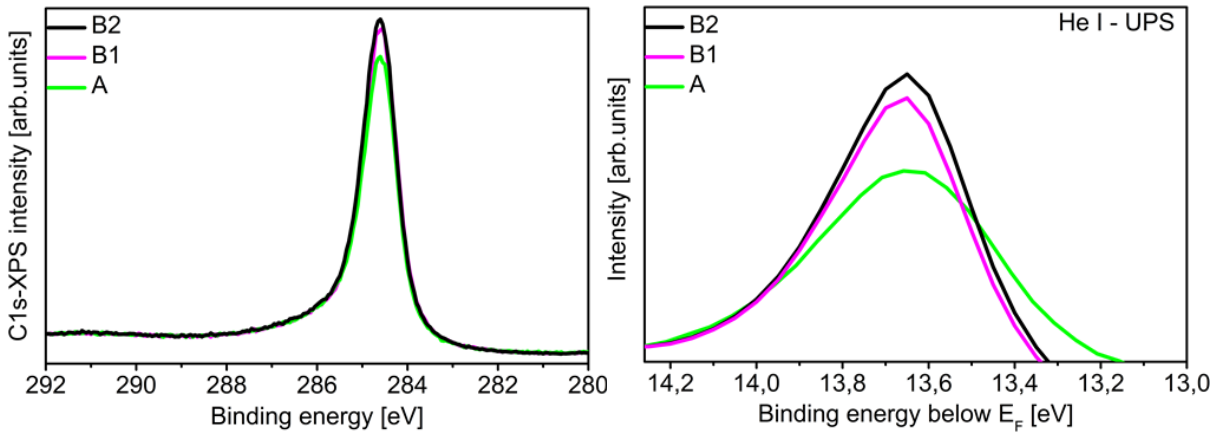

(a) (b)

Figure 6.6 (a) normalized C1s-XPS of sample A, B1 and B2 before they are sputtered; (b) normalized He I-UPS of sample A, B1 and B2 before they are sputtered

The question is why there are three different Ar desorption states. It is well known that under normal conditions it is very difficult to form bonds between Ar and other gases. Therefore, a correlation between the binding energy of Ar to carbon and the Ar desorption temperature is not meaningful. To resolve the question, the HOPG structure is looked into. The original graphitic structure with construction defects lead to three major escape ways for Ar implants: vertical sites in direction of the (a, b)-plane, lattice vacancies and hexagonal graphite rings in direction of the c-axes (figure 6.7). Desorption of Ar implants from HOPG can be considered as a self-diffusion process in heterogeneous system. Therefore, the desorption energy of Ar in TPD is rather a consequence of different diffusion barriers than binding energy. After sputtering, vacancy defects (VDs) and interstitial defects (IDs) in HOPG are generated[21;22]. These sputter-VDs lead to additional escape channels for Ar. The surface sputter-VDs, which appear as small hillocks in STM images[23;24], can be considered as a kind of vertical site. Other kind of sputter-VDs can be considered as a kind of lattice vacancy. The IDs, which are often observed in STM images as large scale protrusions[7;25], can lead to the partial increase of the inter layer distance between the graphene layers[21], but they don‘t offer any escape channels for Ar. To sum up, after sputtering there are still three major diffusion ways for Ar: Vertical sites (vertical sites in the (a, b)-plane and surface sputter-VDs included), vacancies (lattice vacancies and non-surface sputter-VDs included) and hexagonal graphite rings.

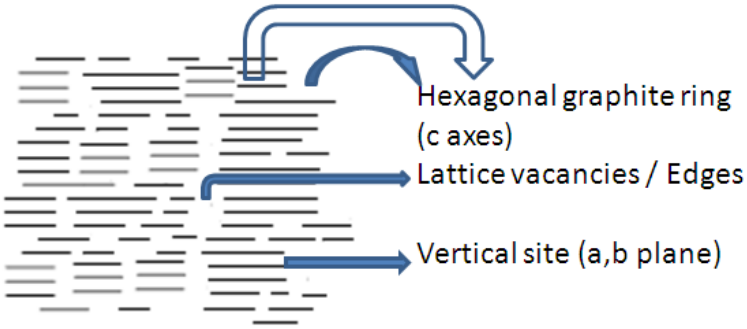

Figure 6.7 Structure of HOPG

In chapter 6.2.3.1 it is mentioned that small mobile graphite islands on the top graphite layer could be generated during sputtering. Ar located beneath these small islands could desorb from the edges of the islands. The diffusion channel at these edges can be regarded as a vertical site. However, because these islands are located on the top surface of HOPG, the Ar beneath these islands can escape more easily than the Ar in the normal vertical sites in HOPG. For Ar to escape through the vacancies, it first has to overcome the diffusion barrier in vertical sites to reach the vacancies. This barrier, together with the escape probability through VDs, was investigated by Choi, Kim and Kang[26]. They found desorption temperatures between 200 and 400 °C and a very broad desorption signal for surface implanted Ar (sputter energy 100 eV). Therefore, the desorption temperature is a function of the number and the kind of the generated VDs and hence also a function of the implantation depth. In principle, Ar can also escape through hexagonal rings. Nevertheless, at room temperature this is difficult if not impossible, because the diameter of Ar (0.414 nm) is much larger than that of the hexagonal rings. To conclude, the barriers of these 3 diffusion ways are in sequential order: $E_{C6} > E_{a,b}$ (surface) > $E_{a,b}$ (deep layers). This conclusion can be supported by the intercalation process of molecules in graphite reported in literature[27-29]. For the intercalation process of different compounds into HOPG, the self-diffusion process is dominant. There is no exchange between surface adsorbent and compounds. The diffusion of the compounds into HOPG initiates at graphite edges and vertical sites (see figure 6.7). The activation energy of the diffusion process is about 8-50 kJ/mol[27-29]. From the intercalation process it can be deduced that the diffusion barrier of the edges and vertical sites is lower than that of the Ar through the graphite surface. Correlating this result with Ar diffusion in HOPG, it can be concluded that the diffusion process of Ar implants in HOPG initiates at edges and vertical sites. Hence Ar desorbs at first from vertical

sites at surface layers, followed by vertical sites from deep layers through edges and VDs. Diffusion of Ar through hexagonal graphite surface is very difficult at room temperature.

Correlating the diffusion barrier with the Ar desorption temperature in TPD, the three Ar desorption states can be assigned with these three diffusion ways:

Firstly, Ar-α around 300 °C corresponds to the Ar escaped from vertical sites of the surface near HOPG layers. Because the aperture of TPD is located on the top site of HOPG, the desorbed Ar from vertical sites in the (a, b)-planes through edges cannot be measured. Therefore, the intensity of the mass spectrometer signal corresponding to the Ar-α state should be mainly contributed to by the Ar desorbed from the mobile graphite islands on the top surface of HOPG and the first layers. Considering the mean implantation depth of 2 nm, the amount of Ar implanted in the first three surface layers is low.

Secondly, Ar-β around 500 °C corresponds to the Ar escaped from deeper layers through VDs.

Thirdly, Ar-γ above 800 °C corresponds to the Ar escaped from HOPG hexagonal rings. In other words, the desorption-temperature of Ar-γ can be correlated with the remaining, nearly VD-free graphitic structure after sputtering. Combining with the TPD results, after which $T_A < T_{B1} < T_{B2}$, a logical rule can be extracted. The desorption-temperature of Ar-γ mirrors the intact graphitic structure after sputtering. The higher this temperature is, the better the graphitic structure remains after sputtering. This corresponds to less lattice vacancies in HOPG before sputtering and better quality of the original HOPG. We name this result the 'T_γ rule of HOPG quality'. According to this rule, it is obvious that the quality of sample B2 is the best, sample B1 is the second best and sample A has the worst quality. This is in agreement with C1s-XPS and UPS result (figure 6.6a and 6.6b).

6.2.3.3 Influence of Ar implantation dose on Ar binding energy

The surface damage on samples B3, B4 and B5 increases with the sputter dose (see chapter 6.2.3.1). The sequence of the graphite fraction (G) of the three samples in the surface area after sputtering is: $G_{B3} > G_{B4} > G_{B5}$. From Ar-TPD spectra in figure 6.8 it is obvious that the desorption temperature of Ar-γ of sample B3, B4 and B5 follows: $T_{B3}, T_{B4} > T_{B5}$. For sample B5, fewer graphene layers in the surface remain than for sample B3 after sputtering. That means Ar implants in sample B5 have to

move through fewer graphene layers than Ar in sample B3. This is the reason for the lower desorption temperature of Ar-γ. This result demonstrates the correctness of our "T_γ rule of HOPG quality" directly.

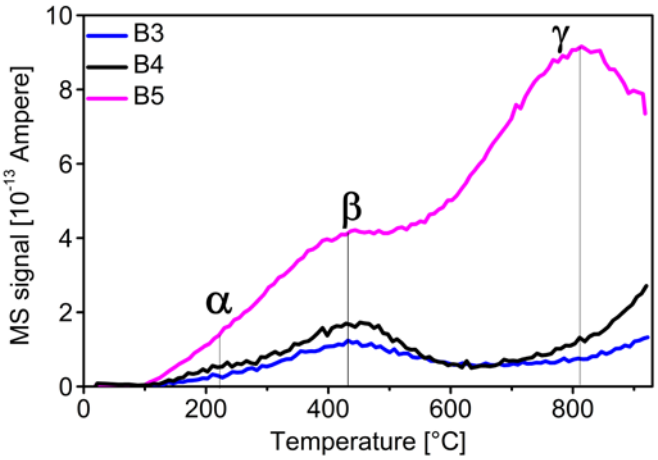

Figure 6.8 Ar-TPD spectra of sample B3, B4 and B5.

From Ar-XPS spectra (inlet in figure 6.9) it is seen that there is nearly no Ar detectable for sample B3 and only a minimal change of Ar core level position for sample B4 and B5 after sputtering. In table 6.2 the atomic ratio of Ar to C after sputtering (R_1) and the ratio of C1s intensity after sputtering to C1s intensity before sputtering (R_2) in XPS were calculated. The R_1 value shows the Ar implant concentration in the HOPG surface and this value increases dramatically with increased Ar sputter dose. The R_2 value shows the decrease of the graphitic carbon fraction with increased sputter dose. It is proven with the depth profile measurement of Ar-XPS that Ar implants are mainly distributed in deep graphite layers rather than on the HOPG surface. The measured Ar intensity of sample B3 is extremely low (blue curve in figure 6.9), because the trapped Ar in deep layers is not accessible by XPS due to the mostly intact graphitic surface layers (R_2 value in table 6.2 and STM image in figure 6.4b). In contrast, the measured Ar intensity of sample B4 (6 min, black curve in figure 6.9) is much higher than that of sample B3 (3 min) and this is not only because of the increased sputter dose. One important reason is that partly removed/destroyed first layers make the Ar trapped in deep layers accessible to XPS. In table 6.2 the R1 value shows that the amount of Ar in sample B5 is twice as large as in sample B4. In comparison to this, the TPD spectra (figure 6.8) indicate that the amount of Ar in sample B5 is more than twice as large as in sample B4. This further corroborates that Ar implants are mainly distributed in deep graphite layers, which are not accessible by XPS. Combining the Ar-XPS with the R_1 and R_2 value, it

can be concluded that neither a change of Ar concentration, nor a change of the graphitic carbon amount would have a strong influence on the Ar-XPS position. This result will be used in the next section 6.2.3.4.

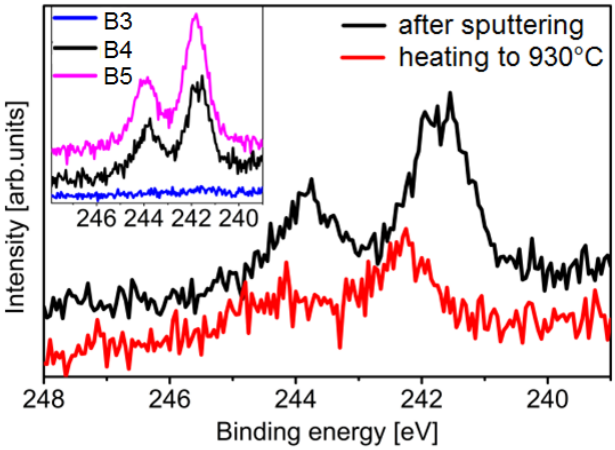

Figure 6.9 Ar-XPS of sample B4. Black curve was measured directly after sputtering, red curve was measured after heating the sample to 930°C. Inlet: Ar-XPS of sample B3, B4 and B5 after sputtering.

Table 6.2		
Sample	Atomic ratio of Ar to C: $R_1 = \frac{I_{Ar}/ASF_{Ar}}{I_C/ASF_C}$ (calculated by XPS with homogenous distribution model[30;31])	$R_2 = \frac{I_{C-sputtering}}{I_{C-clean\ HOPG}}$
B3, 3 min	0.00003 ≈ 0	0.98
B4, 6 min	0.002	0.92
B5, 24 min	0.004	0.91

6.2.3.4 Influence of defects on Ar binding energy

Figure 6.9 shows Ar-XPS of sample B4 before and after heating. It is obvious that after heating the Ar core level position shifted to the high binding energy side by 0.56 eV. Simultaneously, the R_1 value dropped from 0.002 (before heating) to 0.001 (after heating) and the R_2 value increased slightly. These phenomena are similar for other sputtered samples. In stepwise heating experiments, when the sample was heated stepwise to higher temperatures (e.g. 100 °C, 200 °C, 300 °C, 500 °C), the Ar binding energy shifted to the higher binding energy in small steps as well. During the heat treatment, four factors of the HOPG system changed. Firstly, interstitial carbon could change to sp^2 graphitic carbon, this can be observed in C1s-XPS spectra. Secondly, the amount of Ar implants decreased because of Ar-desorption. Thirdly, large

amounts of interstitial defects (ID) were removed by heating while vacancy defects (VD) survived. Fourthly, the depth profile of Ar position changed. It was already demonstrated in section 6.2.3.3, that changes in the Ar concentration and graphitic carbon amount don't result in a big shift of the Ar core level position. The reasons for the shift are the changes of the implantation depth of Ar in HOPG and the change of the amount of interstitially trapped Ar and C while heating. The defective carbon layers reestablishment of the graphitic sp^2 layers together with the removal of interstitial carbon, as well as the desorption of argon leads to an increase of graphene layers in the upper layers of the surface. This thick stack of graphene increases the probability of electron energy losses for the Ar core level electrons in a way analog to the losses responsible for the C1s asymmetry[32]. Another possibility is the change of the matrix[33] for trapped Ar into more relaxed and intact carbon layers, or Ar trapped in VDs rather than in IDs. The distance of intact graphene layers without interstitial carbon and a low amount of interstitial argon leads to a stronger polarization and hence a decrease of the screening of core electrons perpendicular to the graphene layers.

6.2.4 Conclusion

The results in this investigation show that structures of different HOPG samples are different, because of the inherent construction defects. Ar desorption behavior is very sensitive to this structural difference. There are three desorption states Ar-α, Ar-β and Ar-γ in Ar temperature programmed desorption spectra, which correspond to different diffusion barriers for Ar. The desorption temperature of Ar-γ correlates with the remaining graphitic structure of the HOPG surface after sputtering. The higher T_γ is, the more graphitic structure of HOPG remains after sputtering. The desorption temperature of Ar-γ mirrors the quality of HOPG: The higher the temperature, the fewer construction defects there are, the better the quality of HOPG. It was also found that the kind of defect environment (interstitial defects and vacancy defects) for Ar implants after sputtering has a strong influence on the Ar core level position. When interstitial defects were removed by heating to 930 °C, the Ar core level shifted to the high binding energy site and the shift is about 0.56 eV. The Ar binding energy is a function of the interstitial defect amount and the thickness of the reestablished sp^2 layers without interstitial carbon.

Reference List

[1.] Robert Schlögl, in *Handbook of Heterogeneous Catalysis*Eds.: G.Ertl, H.Knözinger, F.Schüth, J.Weitkamp, **2008**.

[2.] R.Schlögl, *Graphite -A Unique Host Lattice*, **1994**.

[3.] G. K. Wertheim, P. M. T. Van Attekum, H. J. Guggenheim, K. E. Clements, *Solid State Communications* **1980,** *33* 809-811.

[4.] R. Schlögl, *Surface Science* **1987,** *189* 861-872.

[5.] P. Oelhafen, P. Pfluger, E. Hauser, H. J. Güntherodt, *Physical Review Letters* **1980,** *44* 197-200.

[6.] U. M. Gubler, P. Oelhafen, H. J. Güntherodt, *Solid State Communications* **1982,** *44* 1621-1623.

[7.] T. Li, B. V. King, R. J. MacDonald, G. F. Cotterill, D. J. O'Connor, Q. Yang, *Surface Science* **1994,** *312* 399-410.

[8.] R. Coratger, A. Claverie, F. Ajustron, J. Beauvillain, *Surface Science* **1990,** *227* 7-14.

[9.] A. Hoffman, I. Gouzman, R. Brener, *Applied Physics Letters* **1994,** *64* 845-847.

[10.] S. Wu, R. Yang, D. Shi, G. Zhang, *Nanoscale* **2012,** *4* 2005-2009.

[11.] Akira Yoshida, Yoshihiro Hishiyama Yutaka Kaburagi. Characterization of crystal grain shape and crystal axis orientation mapping on surface of HOPG using electron backscatter diffraction. 2004. The American Carbon Society.

[12.] R. Schlögl, H. P. Boehm, *Carbon* **1983,** *21* 345-358.

[13.] J. Fournier, D. Miousse, L. Brossard, H. Ménard, *Materials Chemistry and Physics* **1995,** *42* 181-187.

[14.] C. Underhill, T. Krapchev, M. S. Dresselhaus, *Synthetic Metals* **1980,** *2* 47-55.

[15.] W. Metz, D. Hohlwein, *Carbon* **1975,** *13* 84-86.

[16.] J.F.Ziegler, J.P.Biersack, U.Littmark, in *The stopping and range of ions in solids* ,*Vol*. *1*, (**1985**.

[17.] F. R. McFeely, S. P. Kowalczy, L. Ley, R. G. Cavell, R. A. Pollak, D. A. Shirley, *Phys.Rev.B* **1974,** *9* 5268-5278.

[18.] J. Krieg, P. Oelhafen, H. J. Guntherodt, *Solid State Communications* **1982,** *42* 831-833.

[19.] R. F. Willis, B. Fitton, G. S. Painter, *Phys.Rev.B* **1974,** *9* 1926-1937.

[20.] J. P. Tessonnier, D. Rosenthal, T. W. Hansen, C. Hess, M. E. Schuster, R. Blume, F. Girgsdies, N. Pfänder, O. Timpe, D. S. Su, R. Schlögl, *Carbon* **2009,** *47* 1779-1798.

[21.] J. R. Hahn, H. Kang, *Phys.Rev.B* **1999,** *60* 6007.

[22.] J. R. Hahn, H. Kang, *Surface Science* **1996,** *357-358* 165-169.

[23.] J. R. Hahn, H. Kang, S. Song, I. C. Jeon, *Phys.Rev.B* **1996,** *53* R1725.

[24.] H. X. You, N. M. D. Brown, K. F. Al-Assadi, *Surface Science* **1993,** *284* 263-272.

[25.] R. Coratger, A. Claverie, A. Chahboun, V. Landry, F. Ajustron, J. Beauvillain, *Surface Science* **1992,** *262* 208-218.

[26.] W. Choi, C. Kim, H. Kang, *Surface Science* **1993,** *281* 323-335.

[27.] S. Aronson, *Journal of Inorganic and Nuclear Chemistry* **1963,** *25* 907-918.

[28.] M. B. Dowell, D. S. Badorrek, *Carbon* **1978,** *16* 241-249.

[29.] W. Metz, L. Siemsglüss, *Carbon* **1978,** *16* 225-229.

[30.] G.Ertl, J.Küppers, *Low Energy Electrons and Surface Chemistry*, VCH Verlagsgeselllschaft, **1985**.

[31.] Specs, *Quantification in XPS using SpecsLab and CasaXPS*, **2005,** pp. 11-12.

[32.] D.A.Shirley, *Photoemission in Solids* , Springer, **1978**.

[33.] K. S. Kim, N. Winograd, *Chemical Physics Letters* **1975,** *30* 91-95.

6.3 Combined XPS and TPD study of oxygen groups on Highly Oriented Pyrolytic Graphite functionalized by two sputter procedures

Abstract

Temperature Programmed Desorption (TPD) combined with X-Ray Photoelectron Spectra (XPS) was used to study two functionalized HOPG systems. One HOPG system was sputtered with Ar and O_2, this sputter procedure introduces mainly bulk oxygen functionalities and the TPD and XPS results do not correlate. The other HOPG system was sputtered with Ar in O_2 atmosphere. This procedure introduces mostly surface oxygen functionalities and allows a successful correlation of TPD and XPS analysis.

6.3.1 Introduction

In recent years carbon materials present more and more important applications in various fields. For instance graphite, soot, CNTs and carbon Nano filaments etc. can be used as catalysts for oxidative dehydrogenation reactions of aromatic hydrocarbons, alkanes and alkenes[1-6]. The active sites of the catalyst are still unknown but they should be one or more of the oxygen functional groups. Furthermore, graphite, CNTs and CNFs are catalytic supports for metal particles[7-9].The prerequisite for their function as a catalyst support is the existence of functional groups which are anchoring sites to immobilize the metal particles. Due to the importance of oxygen functionalities on carbon, the nature of oxygen groups on different carbon material has been investigated for many years using various techniques. For instance Titration[10;11], X-Ray Photoelectron Spectroscopy (XPS)[11-18], Temperature Programmed Desorption spectroscopy (TPD)[11;13-16], Infrared Spectroscopy (IR)[14;16], Contact Angle Measurements (CAM)[14;14], and High-Resolution Electron Energy Loss Spectroscopy (HREELS)[19]. Nevertheless, the nature of the oxygen groups is still not clarified due to the complexity of the system. Firstly, various oxygen functionalities appear simultaneously in carbon and it is not possible to differentiate them. Secondly, the sensitivities of the techniques are different, e.g. some are sensitive to the surface, and some are sensitive to bulk, so that it is difficult to combine the measured results by different techniques. Therefore, a suitable model system, which can simplify the complexities of the oxygen-carbon system, will be very helpful.

In this paper we introduce two different sputtering procedures to functionalize HOPG: Sputtering with Ar and O_2 (procedure 'a') and sputtering with Ar in O_2 atmosphere (procedure 'b'). It is known that accelerated ions can go into the bulk of the sample. This means that both surface defects and bulk defects can be generated by sputtering. With procedure 'a' both Ar and O_2 gas are ionized and accelerated to sputter the sample. Therefore, the defects are generated not only by Ar^+ but also by O_2^+/O^+. With procedure 'b' the defects are only generated by Ar^+. The O_2 gas atmosphere ensures that the defects are saturated by O_2 molecules and not by other molecules. Compared to strong oxidants, the advantages of the sputter methods to oxidize the HOPG surface are: Firstly, amount of the defects can be well controlled by changing the sputter dosage[20]. Secondly, the sputter method and characterization methods mentioned below can be carried out in the same vacuum chamber without any contact of the sample with the outside of the chamber. This avoids any disruptions from outside factors. It was decided to use HOPG, because HOPG has a well-defined structure like a kind of mono crystal without any metal impurities and pores. Furthermore, HOPG is the basic component for many other carbon materials such as carbon nanotubes, active carbon and carbon nanofibers. The sputtered HOPGs were characterized with two powerful methods TPD and XPS. TPD is a bulk sensitive method and can detect the desorbed gas species which are the product of decomposition of surface functionalities. XPS is a surface sensitive method and can determine oxygen species on the surface.

The results of the two sputter systems show that the sputter method using Ar and O_2 introduces O_2 mainly into HOPG bulk. When the HOPG is heated, the O_2 diffuses to the surface, providing the continuous existence of oxygen functionalities on the surface. The other sputter method (HOPG sputtered with Ar in O_2 atmosphere) introduces only oxygen on the surface and this procedure can thus be used to build a suitable model system for the oxygen functionality investigation.

6.3.2 Experimental

Experiments were carried out in an ultra-high vacuum (UHV) chamber with a base pressure of $3*10^{-10}$ mbar. The chamber was equipped with a QMS 200 quadruple mass spectrometer (Pfeiffer Vacuum), an X-ray source with non-monochromatized Mg/Al Kα radiation (XR50 SPECS), a hemispherical analyzer (Phoibos 150, SPECS) and two sputter guns (PHI 04-161, PERKIN-ELMER and IQE 12/38, SPECS). The

difference between these two sputter guns is that Ion source IQE 12/38 has two differential pumping apertures. The mass spectrometer for TPD was also differentially pumped. The distance between the sample and the aperture is in the range of the aperture itself (1 mm). The sample was heated by an electron-beam impact heater from the back side and the temperature was measured by a thermocouple type K, which was mounted in the center of the HOPG body through a predrilled hole from the narrow side of the HOPG. The thermocouples were covered with Thermoguss 2000. In the XPS measurement Mg Kα radiation (1253.6 eV) was used for excitation.

Experiments were done with two HOPG pieces (A and B). Their size was 1 cm^2× 0.2 cm. After HOPGs were cleaved freshly in air, they were transferred in UHV immediately. Before doing the experiment each HOPG was heated in UHV up to 1000 °C for several times to gas out the adsorbed gas species on the HOPG surface plane. Sample A1 and A2 were two individually cleaved surfaces of the HOPG piece A. Sample A1 was irradiated with Ar and O_2 (Sputter procedure 'a':1 kV, 3 μA*min, $P_{Ar} = P_{O2} = 5*10^{-6}$ mbar, Table 6.3). This sputter procedure was carried out with ion source PHI 04-161. Sputtered sample A1 was heated to 1000 °C and thereby TPD was measured. With this TPD survey certain desorption temperatures of oxygen-contained gases were obtained. Sample A2 was treated with the same sputter procedure as sample A1 and afterwards was characterized with XPS at room temperature before and after sputtering. Subsequently, sample A2 was heated successively to several certain temperatures selected from the TPD-survey of sample A1. After each heating step sample A2 was cooled down to room temperature and characterized with XPS. In this way, a series step wise TPD and XPS spectra were obtained.

Sample B1 and B2 were two individually cleaved surfaces of the HOPG piece B and they were bombarded with Ar in O_2 atmosphere (procedure 'b':1 keV, 3 μA*min, $P_{O2} = 5*10^{-6}$ mbar, table 6.3), which is carried out with ion source IQE 12/38. After sputter treatment the same experiment was done with sample B1 and B2 as with sample A1 and A2.

Table 6.3 Analyzed HOPG samples

Sample	Sputtering treatment		Analysis
A1	procedure 'a'	with Ar and O_2	TPD
A2			Combined stepwise TPD and XPS
B1	procedure 'b'	with Ar in O_2	TPD
B2			Combined stepwise TPD and XPS

6.3.3 Results and discussion

In TPD measurements, CO, CO_2, H_2O, O_2 and Ar are desorbed. On sample A1 sputtered with Ar and O_2, CO is dominantly desorbed and a small amount of CO_2, H_2O and O_2 desorb above 500 °C. The desorption curves of CO_2, CO, H_2O, O_2 and Ar have very similar shapes and differ only in intensity (figure 6.10a). From the stepwise TPD-spectra of sample A2 (figure 6.11a), this phenomenon can be seen even more clearly. The intensity of desorbed CO shows the same trends as the intensity of desorbed Ar. This phenomenon indicates that the desorption behavior of O-contained gases is strongly correlated with Ar desorption. Our former investigation shows that Ar desorption spectra from HOPG is determined by the different Ar diffusion pathways[21] and they apply to other desorbed gases as well. The similarity of Ar TPD and O-contained gas TPD indicates: The oxygen-contained gas desorption from sample A1 and A2 is strongly influenced by the diffusion pathways in HOPG rather than the interaction between oxygen-containing gases and carbon.

In comparing the TPD of sample A1 and B1 (sample B1 was sputtered with Ar in O_2), it is seen that the intensity of desorbed CO, CO_2 and H_2O is about 10 times smaller for sample B1 than for sample A1. There is mainly CO desorbed and the amount of CO_2 and H_2O can be neglected. Furthermore, no O_2 desorption can be observed. This phenomenon is analyzed in detail later. The desorption spectra of CO and Ar-TPD are similar in shape. From our former investigation[21], it can be deduced that there should also be three diffusion pathways for CO the same as for Ar. Therefore, the three desorption states of CO are correlated with the three diffusion pathways in the TPD spectra which should be observed in CO TPD spectra, but it is relatively difficult to clearly differentiate the three CO states. The desorption peak of CO is very broad and not as intense as the Ar-desorption peak. An explanation for this could be that CO interacts much better with carbon atoms, defects and graphene layers than Ar. While Ar receives energy to overcome the diffusion barrier and escape from the diffusion channels without interaction with HOPG, CO receives energy initially to break the bond with HOPG. During diffusion, the diffusion rate of CO could be interrupted many times by the interaction with other carbon atoms and defects. Therefore, the oxygen-containing gases have very broad desorption peaks. Compared to the oxygen introduced by the first sputter procedure, desorption of CO here is not only strongly influenced by the diffusion pathways in HOPG, but also by the interaction between CO and carbon (for instance re-adsorption on defects and

desorption). Additionally, the integral of the CO curves in figure 6.11b is consistent with the CO curve in figure 6.10b.

Furthermore, there are three remarkable differences between the TPD spectra of sample A1 and B1. Firstly, the desorption of CO, CO_2, H_2O and Ar from B1 starts at about 200 °C, which is much lower than the starting temperature of desorption from A1 and the CO desorption curve of B1 is much broader than that of A1. Secondly, there is a desorption peak of CO, H_2O, CO_2 and Ar from B1 at about 500 °C, while that from A1 is at about 800 °C. The high desorption-temperature of the gases from A1 could be an indication that there are very stable oxygen functional groups formed by the sputter procedure 'a'. Desorption temperature is a very important, but unfortunately, not the only criteria for the thermal stability of oxygen groups. As mentioned above, the gas desorption from sample A1 and A2 is determined by the diffusion pathways in HOPG. Therefore, the high desorption temperatures here do not correspond to stable oxygen functionality. Thirdly, there are three desorption states α, β and γ in Ar-TPD. The desorption temperature of Ar-γ of sample B1 is about 800 °C and that of sample A1 is above 1000 °C, which is above our measurement range. This phenomenon was already observed and analyzed in our former investigation[21]: "The desorption temperature of Ar-γ correlates with the remaining quasi defect-free graphitic structure of the HOPG surface after sputtering. The higher T_γ is, the more graphitic structure of HOPG there is after sputtering." This means, the high desorption temperature of Ar-γ of sample A1 indicates that there is more graphitic carbon remaining on sample A1 than sample B1 after sputtering. From the literature[22], it is known that the ether groups can diffuse on the graphitic carbon layer. If they come in contact with each other, an O_2 molecule can be formed. Combining this with the graphitic structure of sample A1 and B1 after sputtering, it can be deduced that the probability that two ether groups meet to form O_2 on the surface of sample A1 is much larger than for sample B1. This could be one reason why there is O_2 desorption from sample A1 and none from sample B1.

Additionally, the evolution of CO desorption above 950 °C from samples A1 and B1 present the trend of further increase. The reason is still unknown. There could be several explanations for that. Firstly, there are too many oxygen functional groups, which cannot desorb completely even at high temperature. Secondly, there are many CO molecules stored in the HOPG bulk and they require very high temperature to diffuse to HOPG surface. Thirdly, it is supposed that there are plenty of small mobile

HOPG islands on the amorphous HOPG surface (described in chapter 6.2). It is known that the heat transfer of amorphous carbon is not as good as graphitic carbon[23]. Therefore, the temperature of the surface mobile graphite island could be much lower than the measured temperature (thermocouple was mounted in the middle of HOPG bulk). In this case, the high temperature CO in the TPD spectra in fact desorbed from the amorphous surface or from the surface graphite islands at low temperature.

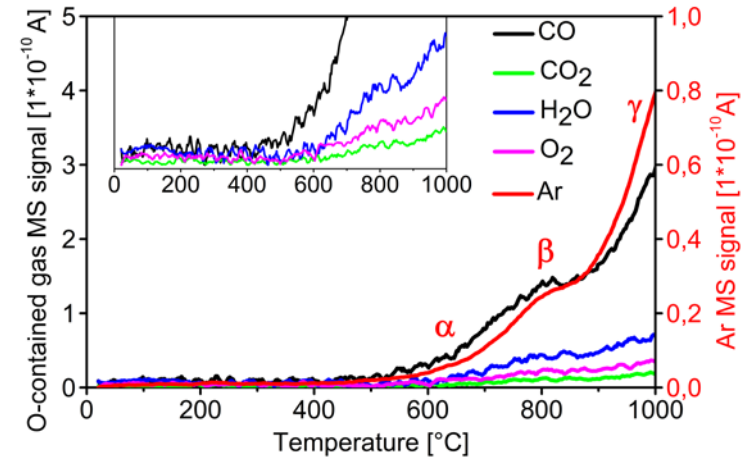

(a)

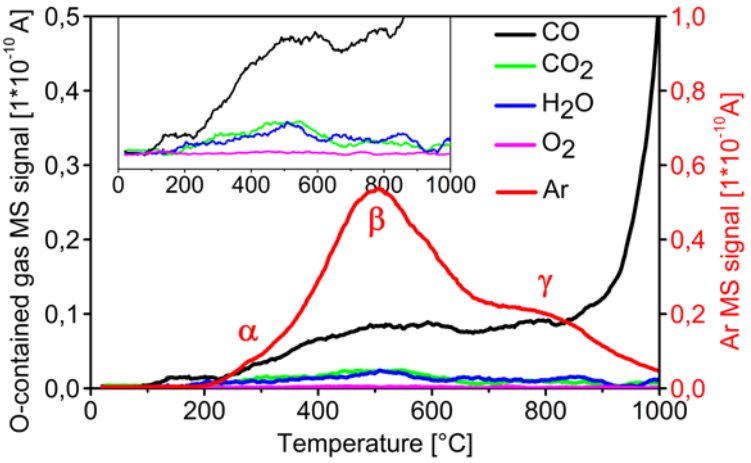

(b)

Figure 6.10 CO CO_2 H_2O O_2 and Ar-TPD spectra with heating rate of 5.7 K/sec. inlet: magnified CO CO_2 H_2O and O_2 TPD spectra (a) TPD spectra of sample A1; (b) TPD spectra of sample B1.

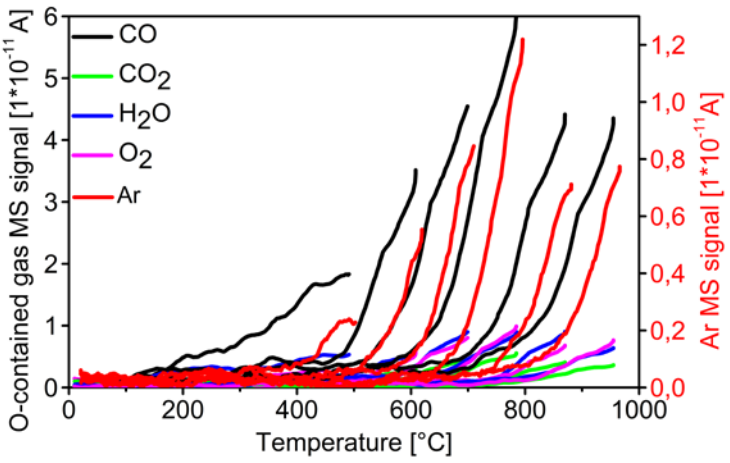

(a)

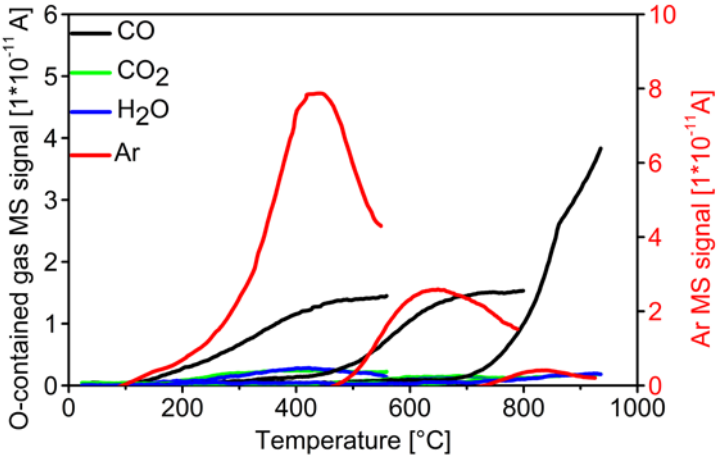

(b)

Figure 6.11 Step wise CO CO_2 H_2O O_2 and Ar-TPD spectra with heating rate of 5.7 K/sec. (a) TPD-spectra of sample A2 heated to 610, 710, 795, 880 and 965 °C successively. The intensities between room temperature and 100°C do not correspond to any gas desorption. It is only a signal of noises. (b) TPD-spectra of sample B2 heated to 560, 800 and 935 °C successively.

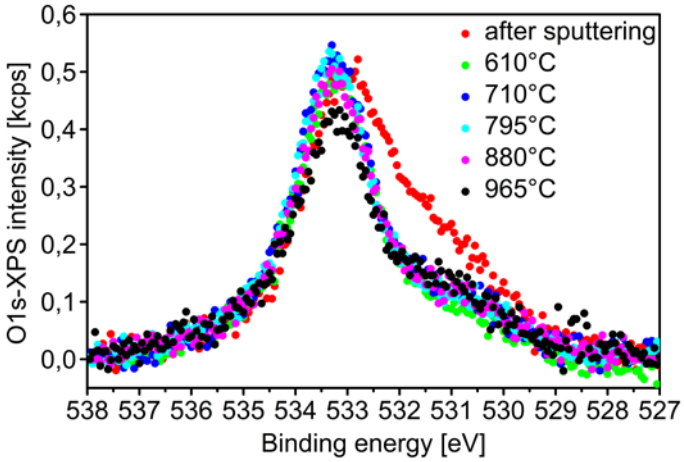

(a)

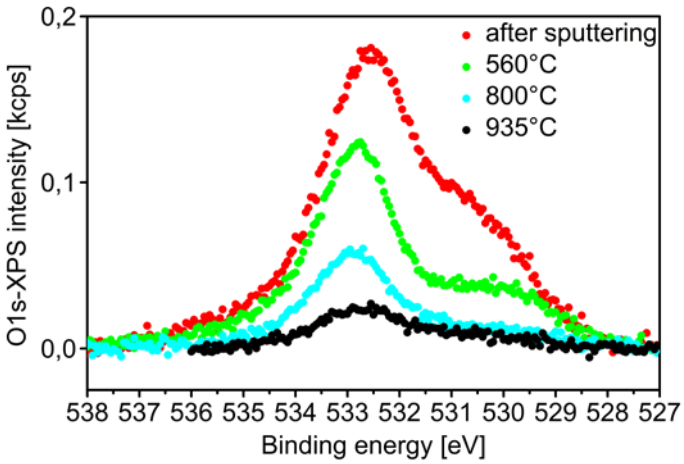

(b)

Figure 6.12 XP O1s-spectra of samples with different pretreatment temperatures, Shirley background is subtracted; (a) O1s-XPS spectra of sample; (b) O1s-XPS spectra of sample B2.

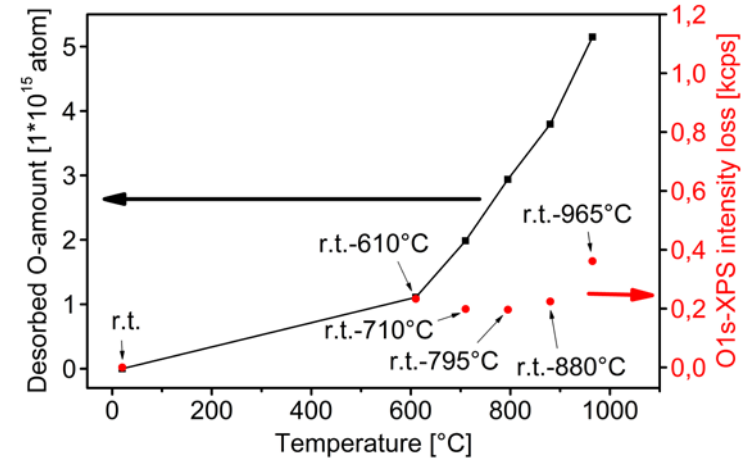

(a)

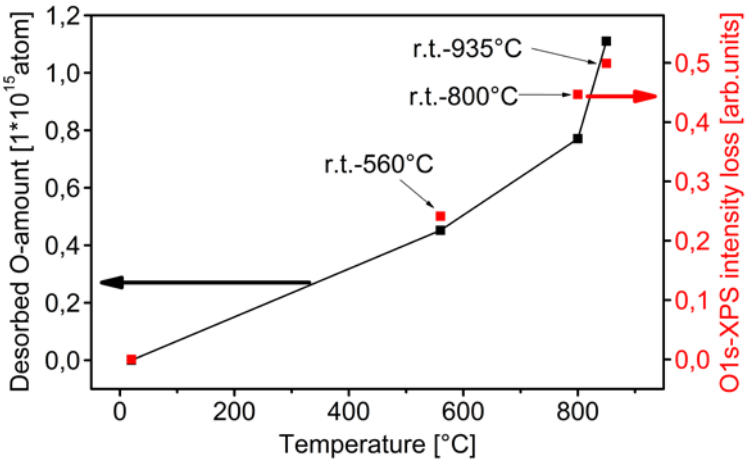

(b)

Figure 6.13 Correlated XPS-TPD curves: black points correspond to the accumulated desorbed oxygen amount after heating the sample B2 different temperature successively. Red points correspond to the difference of relative oxygen amount compare to the XP O1s spectrum after sputtering. The XPS and TPD intensities are adjusted with the first and second data point in the low temperature range (room temperature – 610°C) of the integrated TPD profile. Direct quantification and exact adjustment are hampered, due to the different probing depths of the two methods (a) correlated curve of Sample A2; (b) correlated curve of sample B2.

In figure 6.12a the step wise XPS spectra of A2 are presented. The broad O1s peak after sputtering indicates the successful introduction of various oxygen functionalities by the sputtering procedure. After the sample A2 was heated to 610 °C, the intensity of the O1s contribution around 532 eV decreases dramatically. In contrast, the intensity and shape of the O1s spectra measured after further heating steps show almost no change. The amount of desorbed oxygen in HOPG was calculated by integrating the TPD spectra with help of the calibration experiment[24]. The change of the oxygen amount on the surface while heating corresponds to the oxygen difference spectra. The correlation curve of the desorbed oxygen in HOPG (TPD) and on the surface (XPS) is illustrated in figure 6.13a. Obviously, between room

temperature and 610 °C the desorbed oxygen amount (TPD) is consistent with the intensity loss of the surface oxygen (XPS). Between 610 °C and 965 °C the intensity loss of surface oxygen (XPS) is much lower than the total desorbed oxygen (TPD). These phenomena demonstrate: The highly activated oxygen plasma generated through sputter procedure ‘a’ goes deeply into the HOPG bulk, the same as Ar plasma, and simultaneously saturates the bulk defects. Hence, oxygen distributes mainly in the HOPG bulk rather than on the surface area. When these bulk oxygen groups are going to decompose and desorb, they need not only energy for the decomposition but also for overcoming the diffusion barrier[21]. Different to Ar diffusion from HOPG, implanted O_2 and released oxygen groups can saturate bulk defects while heating. This means the repeated re-oxidation processes consume the released oxygen groups, so that the desorption of gases is hindered and delayed. On the other hand, oxidation of bulk defects while heating can block the diffusion pathways of the mobile Ar, O_2 and released oxygen groups. That could be the reason for the high starting temperature of gas desorption (figure 6.10a and figure 6.11a). When the sample was heated to 610 °C, a certain amount of oxygen groups on the surface area decomposed and desorbed. The bulk oxygen at this temperature is not able to saturate all the released defects. Therefore, there is loss of O1s intensity (figure 6.12a). When the temperature is higher than 610 °C, all the released surface defects can be saturated by the diffused bulk oxygen. Therefore, the oxygen peaks in the oxygen XP spectra show almost no change above 610 °C (figure 6.12a).

In figure 6.12b the step wise XP spectra of B2 are presented. In contrast to the O1s XPS of sample A2, the oxygen intensity decreases continuously while heating. Quantifying the TPD and XPS spectra in figure 6.11b and figure 6.12b, the correlation-curve (figure 6.13b) of the desorbed oxygen from HOPG (TPD) and from surface area of HOPG (XPS) was obtained. In contrast to the TPD-XPS correlation-curve of A2 (figure 6.13a), the trend of desorbed oxygen amount from HOPG is almost identical to the trend of desorbed oxygen on the surface area. This is a clear indication that introduced oxygen on sample B2 exists mainly on the surface and not in the bulk and means oxygen saturates only surface defects and oxygen functional groups were introduced only on the surface area.

In summary, there is much more oxygen stored in sample A1 and A2 (about 2 monolayers oxygen calculated with TPD) than in sample B1 and B2 (about 0.3 monolayers oxygen calculated with TPD). Sputter procedure ‘a’ generates Ar plasma

and highly activated oxygen plasma, which can be stored in the bulk in the form of oxygen functionalities, oxygen molecules and even oxygen atoms. Sputter procedure 'b' generates only Ar plasma. The O_2 atmosphere can only saturate the defects on the surface area. O_2 molecules were not able to stay on the surface individually. This is the reason why there is no O_2 desorption from sample B1 and B2. The bulk defects generated with sputter procedure 'b' are properly saturated though the relaxation and restructuring of the carbon atoms, for instance graphitic configuration (sp^2) of carbon atoms to diamond configuration (sp^3).

6.3.4 Conclusion

For HOPG systems sputtered with Ar and O_2, the increase of total desorbed oxygen from HOPG during heat treatment (calculated with TPD spectra) is much larger than the increase of the oxygen intensity loss from the surface during heating (calculated with XPS spectra), and the O1s XPS intensity doesn't change from 610 °C to 965 °C. For the HOPG system sputtered with Ar in O_2 atmosphere, the increase of total desorbed oxygen and the increase of the oxygen intensity loss from the surface while heating is almost identical, and the O1s XPS intensity decreases continuously after the sample is heated to 935 °C. These results demonstrate: Sputtering with Ar and O_2 introduces mainly bulk oxygen into HOPG. This oxygen can be delivered continuously to the surface area while heating, so that the amount of surface oxygen can be held at a constant level. In contrast, sputtering with Ar in O_2 atmosphere generates only an extremely small amount of surface oxygen. This surface oxygen can be removed successively by heating. With this sputter method a suitable model of oxygen on the HOPG surface can be built for combining the bulk sensitive methods and surface sensitive methods together to analyze the oxygen functionalities.

Reference List

[1.] M. Muhler, R. Schlögl, G. Ertl, *J.Cat.* **1992,** *138* 413-444.

[2.] Nicolas Keller, *Angewandte Chemie International Edition* **2002,** *41* 1885-1888.

[3.] D. S. Su, N. I. Maksimova, G. Mestl, V. L. Kuznetsov, V. Keller, R. Schlögl, N. Keller, *Carbon* **2007,** *45* 2145-2151.

[4.] Z. J. Sui, J. H. Zhou, Y. C. Dai, W. K. Yuan, *Catalysis Today* **2005,** *106* 90-94.

[5.] X. Liu, D. S. Su, R. Schlögl, *Carbon* **2008,** *46* 547-549.

[6.] G. Mestl, N. I. Maksimova, N. Keller, V. V. Roddatis, R. Schlögl, *Angewandte Chemie-International Edition* **2001,** *40* 2066-2068.

[7.] K. P. De Jong, J. W. Geus, *Catalysis Reviews: Science and Engineering* **2000,** *42* 481-510.

[8.] E. Auer, A. Freund, J. Pietsch, T. Tacke, *Applied Catalysis A: General* **1998,** *173* 259-271.

[9.] P. Serp, M. Corrias, P. Kalck, *Applied Catalysis A: General* **2003,** *253* 337-358.

[10.] H. P. Boehm, *Carbon* **1994,** *32* 759-769.

[11.] M. L. Toebes, J. M. P. Van Heeswijk, J. H. Bitter, A. Jos van Dillen, K. P. De Jong, *Carbon* **2004,** *42* 307-315.

[12.] C. Kozlowski, P. M. A. Sherwood, *J.Chem.Soc., Faraday Trans.1* **1985,** *81* 2745-2756.

[13.] R. Schlögl, G. Loose, M. Wesemann, *Solid State Ionics* **1990,** *43* 183-192.

[14.] U. Zielke, K. J. Hüttinger, W. P. Hoffman, *Carbon* **1996,** *34* 983-998.

[15.] S. Kundu, Y. Wang, W. Xia, M. Muhler, *J.Phys.Chem.C* **2008,** *112* 16869-16878.

[16.] J. H. Zhou, Z. J. Sui, J. Zhu, P. Li, D. Chen, Y. C. Dai, W. K. Yuan, *Carbon* **2007,** *45* 785-796.

[17.] Y. Xie, P. M. A. Sherwood, *Chemistry of Materials* **1991,** *3* 164-168.

[18.] J. Harvey, C. Kozlowski, P. M. A. Sherwood, *Journal of Materials Science* **1987,** *22* 1585-1596.

[19.] M. J. Nowakowski, J. M. Vohs, D. A. Bonnell, *Surface Science* **1992,** *271* L351-L356.

[20.] J. Fournier, D. Miousse, L. Brossard, H. Ménard, *Materials Chemistry and Physics* **1995,** *42* 181-187.

[21.] Henan Li, Dirk Rosenthal, Robert Schlögl, *not published* **2011**.

[22.] R. Larciprete, S. Fabris, T. Sun, P. Lacovig, A. Baraldi, S. Lizzit, *Journal of the American Chemical Society* **2011,** *133* 17315-17321.

[23.] D. Dasgupta, F. Demichelis, A. Tagliaferro, *Philosophical Magazine Part B* **1991,** *63* 1255-1266.

[24.] J. M. Gottfried, K. J. Schmidt, S. L. M. Schroeder, K. Christmann, *Surface Science* **2002,** *511* 65-82.

6.4 A systematic characterization of oxygen functional groups on Highly Oriented Pyrolytic Graphite

Abstract

Temperature Programmed desorption (TPD) and X-Ray Photoelectron Spectroscopy (XPS) were used to study various functionalized HOPG systems. HOPG samples were sputtered in different gas atmospheres (O_2, H_2O and H_2) under different sputter conditions. Additionally, HOPG samples were oxidized in HNO_3 solvent for comparison. The surface damage of HOPG was characterized with UV Photoelectron Spectroscopy (UPS), Scanning Electron Microscopy (SEM) and Scanning Tunneling Microscopy (STM). Our investigation shows that at least five oxygen components are necessary for fitting the O1s spectra.

6.4.1 Introduction

Graphite, carbon nanotubes (CNTs) and carbon nanofibers (CNFs) are used as catalytic supports for metal particles[1-3] due to their excellent chemical stability and electrical conductivity. Due to their inert character, pristine graphite, CNTs and CNFs can only load metal particles with very low dispersion. Introducing oxygen functional groups to the surface of these carbon materials can change their surface character. The oxygen functionalities offer anchoring sites to immobilize metal particles, thereby achieving a high dispersion of metal particles on carbon surface[4;5]. Furthermore, graphite[6] and CNTs possess excellent electrochemical properties and are widely used as electrodes in batteries. In lithium batteries, Li^+ ions are stored by intercalation and also by surface oxygen via reaction with the functional groups. For instance, surface C-OH groups adsorb Li^+ through formation of C-O^- Li^+ salt. On the other hand the formation of Li-salts can also result in the attenuation of reversible storage capacity. Thereby the stability of the batteries can be disturbed. Therefore, the quantity and the chemical properties of the surface oxygen groups play an very important role for the high specific charge capacity and for the cycle stability of the battery[7;8]. In short, knowing the nature of the oxygen functionalities on carbon materials is crucial. Over the years, the nature of oxygen functional groups on carbon materials has been investigated using numerous techniques such as Titration, Infrared Spectroscopy (IR), High-Resolution Electron Energy Loss Spectroscopy (HREELS), X-Ray Diffraction (XRD), X-Ray Photoelectron Spectroscopy (XPS),

Temperature Programmed Desorption (TPD) and Scanning Tunneling Microscopy (STM). Despite the efforts in this field, there is still an incomplete picture of the nature of oxygen groups, due to their complexity.

XPS is perhaps the most powerful method for identifying a material's surface oxidation states. With XPS the surface oxygen species can be differentiated because of their different chemical shifts of the core levels. Unfortunately, the O1s binding energies of various oxygen components occur only in a narrow range of 2.5 eV[9;10], such that they overlap with one another. Therefore, it is very difficult to unambiguously identify oxygen components and assign them to one or more specific functional groups. In the literature, O1s peaks are often fit using between two and seven oxygen components. Table 6.4 shows an overview of all existing fitting models in the literature. The most widely used fitting model is O1s-fitting with two oxygen components[11-17]. The first oxygen component is in the 531 eV range, corresponding to oxygen doubly bounded to carbon (C=O)[11;18;19]. The other oxygen component is at 533 eV range, corresponding to oxygen singly bound to carbon (C-O)[11;18;19].

Table 6.4 XPS-O1s fitting components in the literature

BE (eV) / Literature	> 535.6	535.0 - 535.6	534.2 - 534.9	533.1 - 533.8	532.1 - 532.8	531.0 - 532.0	530.0 - 530.7
[11-17]				532.7-533.6		531.0-532.0	
[20]				533.8	532.5		530.7
[21]				533.1	532.5-532.8	531.3	
[22;23]			534.7	533.2-533.4		531.6-532.0	
[24]	537.5			533.5		531.0-532.0	
[25;26]			534.3-534.9		532.1-532.8	531.0-531.3	
[12;27-29]	535.7-536.9			532.3-533.7		531.1-531.8	
[30]		534.6-535.4		532.2-533.4		531.2-531.6	
[31]		534.8-535.6		532.4-533.1			530.4
[32]				533 range	532 range	531.6	530.3
[19;33]		534.3-535.4		533.1-533.8	532.3-532.8	531.0-531.9	
[34]	536.1		534.2	533.3	532.3	531.1	
[35]	537.8	535		533.4	532.8	532	531	530

The assignment for the oxygen components in the literature is not consistent. Several studies exist on polymers where solely one single oxygen functional group can be analyzed[9;10;18;36]. Several authors follow the early works of Clark and co-workers[37;38] leading to an interpretation like:

530 range: O in metal oxide [19;35]

531 range: C=O in carbonyls [11;18], aldehydes [11;18],
C=O in O=C-O- containing groups [11;18;19]

532.2: -O- in ether [18;19;39], alcohols [19], ester/lactones [18]
C=O in isolated carbonyls [19],

533.0 - 533.3 : -O- in H_2O [19;40], ether [11], hydroxyls [11;18;40]
-O- in O=C-O- containing groups [11;18;19]
O_2^- [41],

534 range: -O- in carbonates[19]

535, 536 range: H_2O[34],

The discrepancies shall be illustrated with two examples: Firstly, Zielke et al. argued with the fast intramolecular exchange of H in carboxyl groups that both O in carboxyl groups shall occur at 534.2 eV binding energy[34]. This is in contrast to the mentioned polymer literature and also to the pioneering work of Siegbahn et al. where it was shown, that CH_3COOH show two O1s signals in the gas phase and only one in the solid state[42]. This nicely shows that intramolecular H exchange is not fast enough, but intermolecular exchange (i.e. via hydrogen bridge bonding) is indeed fast enough. Secondly, Papirer et al.[43] followed the Scienta ESCA database by Beamson and Briggs[44] and arrived at a similar model with slight shifts of the range. The problem is that there is still no consistent fitting method until now. So far, neither a consistent reasoning has been proposed why a certain number of oxygen groups should be used for O1s-XPS fitting, nor any evidence has been presented for the oxygen components used for O1s-fitting. Although a bulk of literature exists on the topic, the oxygen functionalities have not been characterized systematically. The aim of our investigation is to choose a simplified carbon-oxygen model system to separate the oxygen components in O1s-XPS, in order to build a new fitting-model as reference for other oxygen related investigations. The aim is realized through introducing the oxygen functionalities on HOPG by different functionalization

conditions and characterizing the oxygen functionalities systematically with distinct powerful characterization methods.

HOPG is a suitable material for this investigation, because there are no metal impurities and pores in HOPG compared to CNTs or CNFs. The next step is to find a suitable functionalization method to introduce oxygen groups on HOPG. Pristine HOPG does not adsorb gases at room temperature in UHV[45] due to the inert chemical property, the basal plane of HOPG is relatively inactive toward molecular oxygen. Even after exposure of HOPG in O_2 ($8*10^{-8}$ mbar) at 820 ˚C for 2 hours no measurable oxygen can be determined[46]. According to our prior investigation[47], we chose to sputter HOPG in different gas atmospheres (O_2, H_2O and H_2) to introduce oxygen on the HOPG surface. The change of the gas atmosphere results in a change of the population of the various oxygen components in O1s-XPS, so that different shapes of O1s-XPS can be obtained. This is very useful for the analysis of oxygen components. With this sputter method, extremely small amounts of oxygen functional groups can be generated, mainly on the HOPG surface. With this method it is possible to combine the bulk sensitive method of TPD and surface sensitive method of XPS to analyze the oxygen functionalities. Additionally, for a comparison with the oxygen groups introduced by the most common method, HOPG was functionalized in HNO_3 solution.

To characterize the surface defects, UPS, SEM and STM were used. UPS delivers important information about the electronic structure of the valence band of HOPG. SEM and STM were used to observe the morphological damage directly after sputtering. TPD and XPS were used to investigate the bonding nature of the induced oxygen groups. TPD can detect the gas species that desorb from HOPG, due to the decomposition of surface functionalities that occurs during heating. XPS can provide information about the oxygen species that remain after heating. According to the statistical appearance of oxygen components in O1s-XPS and O1s-XPS difference spectra, we find that at least five oxygen components are necessary to fit the O1s spectra. Our investigation provides a new O1s fitting model for oxygen-functionalized graphitic materials.

6.4.2 Experimental

Experiments were carried out in an ultra-high vacuum (UHV) chamber, with a base pressure of $3*10^{-10}$ mbar. The UHV chamber was equipped with a QMS 200 quadruple mass spectrometer (Pfeiffer Vacuum), an X-ray source with non-monochromatized Mg/Al Kα radiation source (XR50 SPECS), a UV discharge lamp (HIS13, OMICRON), a hemispherical analyzer (Phoibos 150, SPECS) and a differentially pumped sputter gun (IQE 12/38, SPECS). The mass spectrometer for TPD is differentially pumped. The distance between the sample and the mass spectrometer aperture is in the range of the aperture itself (1 mm). The sample was heated by an electron-beam impact heater from the back side of the sample, and the temperature was measured using a type K thermocouple, mounted in the center of the HOPG body through a predrilled hole from the narrow side of the HOPG sample. The thermocouples are proofed with Thermoguss 2000. In the XPS measurement, Mg Kα radiation (1253.6 eV) was used for excitation. Additionally, HOPG was characterized with SEM (Hitachi S-4800FEG) and STM (Bruker Multimode 3) in air. The material of the STM tip was Pt/Ir.

The size of the HOPG samples (ZYB) was 1 cm^2 × 0.2 cm. HOPG was freshly cleaved in air and transferred immediately to UHV. To degas the sample and sample holder, HOPG was heated inside UHV to 1000 °C several times. The sputter procedure was done using an ion source IQE 12/38. HOPG samples were irradiated with argon in an oxygen/water/hydrogen atmosphere under various different sputter conditions (table 6.5). In general, UPS and XPS were measured at room temperature after the sputter procedure. Samples were subsequently heated to different temperatures, while TPD was measured. After each heating step, samples were cooled down to room temperature and characterized by UPS and XPS. For a comparison, some of the sputtered samples were characterized by XPS in the high pressure XPS chamber in “Berliner Elektronen-Speicherring Gesellschaft für Synchrotronstrahlung” (BESSY). The X-ray source for the XPS is monochromatized radiation. The preparation (sputter procedure) of the samples was done in the UHV chamber at FHI and afterwards the samples were transported in air to Bessy.

Table 6.5 Overview of HOPG samples analyzed in this study			
Sample preparation		Heat treatment	Analysis
500eV,0.1uA*3min ≈1.1*10^{14}Ar$^+$	Sputtering with Ar *in O_2* P_{O2} = 5*10^{-6} mbar	Heating to 930°C	UPS,TPD,XPS,STM,SEM
500eV,0.1uA*6min ≈2.2*10^{14}Ar$^+$			UPS,TPD,XPS
500eV,0.1uA*24min ≈8.8*10^{14}Ar$^+$			UPS,TPD,XPS,STM,SEM
1keV,1.5uA*2min ≈1.1*10^{15}Ar$^+$		Stepwise heating	UPS,TPD,XPS
500eV,0.1uA*3min ≈1.1*10^{14}Ar$^+$	Sputtering with Ar *in H_2O* P_{H2O} = 5*10^{-6} mbar	Heating to 930°C	UPS,TPD,XPS
500eV,0.1uA*6min ≈2.2*10^{14}Ar$^+$			UPS,TPD,XPS
500eV,0.1uA*24min ≈8.8*10^{14}Ar$^+$			UPS,TPD,XPS
1keV,1.5uA*2min ≈1.1*10^{15}Ar$^+$			UPS,TPD,XPS
500eV,0.1uA*3min ≈1.1*10^{14}Ar$^+$	Sputtering with Ar *in O_2* P_{O2} = 5*10^{-6} mbar	Stepwise heating -- Bessy	XPS(Bessy)
1keV,1.5uA*2min ≈1.1*10^{15}Ar$^+$			XPS(Bessy)
500eV,0.1uA*3min ≈1.1*10^{14}Ar$^+$	Sputtering with Ar *in H_2* P_{H2} = 5*10^{-6} mbar	No	XPS(Bessy)
1keV,1.5uA*2min ≈1.1*10^{15}Ar$^+$			XPS(Bessy)
500eV,0.1uA*3min ≈1.1*10^{14}Ar$^+$	Sputtering with Ar *in O_2* P_{O2} = 5*10^{-6} mbar	Stepwise heating in *0.5 mbar O_2* -- Bessy	UPS,XPS(Bessy),SEM
500eV,0.1uA*6min ≈2.2*10^{14}Ar$^+$			UPS,XPS(Bessy),SEM
1keV,0.1uA*3min ≈1.1*10^{14}Ar$^+$			UPS,XPS(Bessy),SEM
HOPG in 65% HNO_3solution at 100°C for 2 hours		Stepwise heating	UPS, TPD, XPS

6.4.3 Results and discussion

6.4.3.1 Amount of oxygen in HOPG - TPD results

On clean HOPG, no desorption peak can be seen above room temperature, this is in agreement with other literature reports[45]. After sputtering, in all TPD spectra, CO, H_2O, CO_2, Ar and H_2 desorbed from HOPG. Ar and H_2 TPD are not processed here because they don't contribute to oxygen functionalities. CO, H_2O, CO_2 are the decomposition products of the surface oxygen species. Unfortunately, the desorption temperatures of the gases do not correspond to the decomposing temperature of oxygen functionalities, as shown in our former investigation[47;48], because the desorption temperatures are not only dependent on the type of oxygen species, but also strongly influenced by gas diffusion through defects in HOPG[47;48]. Therefore, a correlation between desorption temperature and thermal stability of oxygen species is not possible.

For HOPG sputtered with Ar^+ in O_2, there is dominantly CO desorption and fewer amounts of CO_2 and H_2O desorption (figure 6.14). With increased sputtering intensity, the amount of desorbed CO increases dramatically. The ratio of desorbed CO_2 and

H_2O does not change (figure 6.14). In contrast, for HOPGs sputtered with Ar^+ in H_2O, the amount of desorbed CO, CO_2 and H_2O are comparable. The increased sputter intensity does not result in considerably more gas desorption. In table 6.6 the amount of desorbed oxygen in HOPG was calculated by integrating the TPD-spectra with the help of gas calibration experiments. For the HOPG samples sputtered with Ar^+ in O_2, there are less than 0.13 monolayers of oxygen introduced. For HOPG sputtered with Ar^+ in H_2O, less than 0.002 monolayers of oxygen are introduced on the HOPG surface. This is an indication that the surface defects generated during the sputtering procedure can split O_2 molecules much better and more effectively than they can split H_2O molecules. For a comparison, HOPG was treated with 65% HNO_3 solution at 100 °C for 2 hours. This method is widely used to functionalize carbon materials. The analysis of TPD spectra shows, that there are 43 monolayers of oxygen introduced in HOPG by this functionalization method. This is more than 1000 times greater than the amount of oxygen introduced by the sputtering procedure (table 6.6). It shall be noted that, in contrast to the literature, the TPD and XPS results presented here were obtained with very small amounts of oxygen. The expected advantage of this extremely small amount of oxygen species is that the overlap of various O1s-XPS components can be reduced, in order to better resolve the shape of the O1s peaks e.g. figure 6.15a.

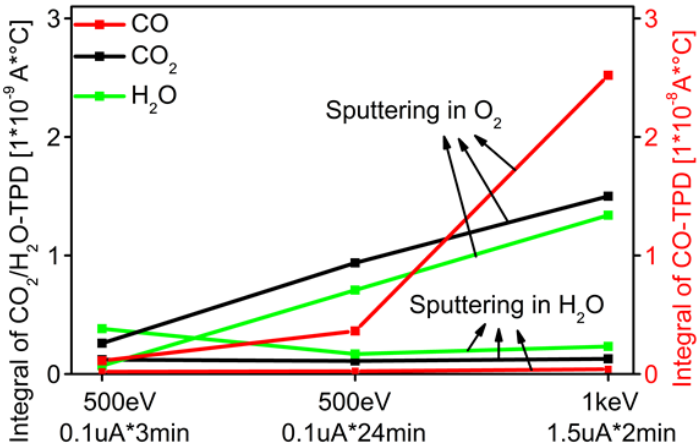

Figure 6.14 Integral of CO, CO_2 and H_2O TPD spectra for samples sputtered with Ar in O_2 / H_2O atmosphere under different sputter intensity.

Table 6.6 Introduced oxygen and argon amount by different oxidation processes			
Oxidation methods		Amount of introduced oxygen (calculated by TPD)	
		in *atom*	in *monolayer*
Sputtering with Ar *in* O_2	500eV, 0.1uA*3min	$1.5*10^{13}$	0.004
	500eV, 0.1uA*24min	$7.5*10^{13}$	0.02
	1keV, 1.5uA*2min	$4.8*10^{14}$	0.13
Sputtering with Ar *in* H_2O	500eV, 0.1uA*3min	$3*10^{12}$	0.0008
	500eV, 0.1uA*24min	$4.5*10^{12}$	0.0012
	1keV, 1.5uA*2min	$7.5*10^{12}$	0.002
In *HNO_3* solution	HOPG in 65% HNO_3 solution at 100°C for 2 hours	$1.6*10^{17}$	43

6.4.3.2 Characterization of oxygen functionalities on HOPG - XPS results

6.4.3.2.1 O1s-XPS fitting model

The aim of this work is the establishment of an O1s-XPS fitting model by determining three essential quantities: the FWHM of a single O1s signal, the minimum number and the positions of all these O1s signals. This approach consists of measuring series of O1s-XPS spectra with an oxygen modified HOPG as starting point followed by thermal decomposition of the oxygen functional groups. The series in figure 6.15 to figure 6.19 are chosen as examples, in which the FWHM values and the peak positions can be recognized from the difference spectra within one series. Measurement of each O1s-XPS spectrum at FHI (XPS with non-monochromatized radiation) took about 8 hours. The O1s spectrum taken in the first two hours is the same as the spectrum taken in the last two hours. There were no changes observed during the long time of measurement. In the following, the recognized oxygen components are analyzed in detail from a mathematical point of view:

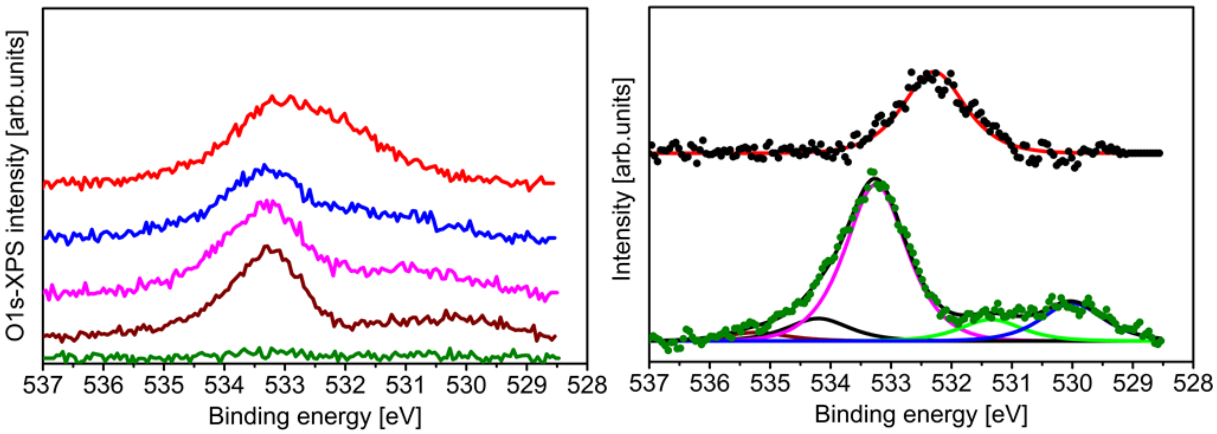

(a) (b)

Figure 6.15 (a) O1s-XPS spectra of HOPG sputtered with Ar in O_2 atmosphere (500eV, 0.1uA*3min), sample was heated to different temperatures in 0.5mbar O_2 atmosphere at BESSY, red curve: heating to 150°C in O_2, blue: 250°C in O_2, magenta: 400°C in O_2, wine: 550°C in O_2, olive: 700°C in O_2. Energy of radiation: 680eV; (b) O1s-XPS difference spectra of O1s XPS in figure 6.15a, black: red curve minus blue curve in figure 6.15a, olive: wine curve minus olive curve in figure 6.15a. Shirley background is subtracted, fitting parameter: FWHM=1.2

Recognition in figure 6.15b: FWHM = 1.2, O1s-component at 532.2 eV (upper curve in fig.6.15b), at 533.3 eV (magenta curve in fig.6.15b), in 531 eV range and 530 eV range (green and blue curves in the bottom curve in fig.6.15b). In the bottom curve in fig.6.15b O1s-component at 534.2 eV is needed, in order to deconvolute the curve correctly because of the asymmetry.

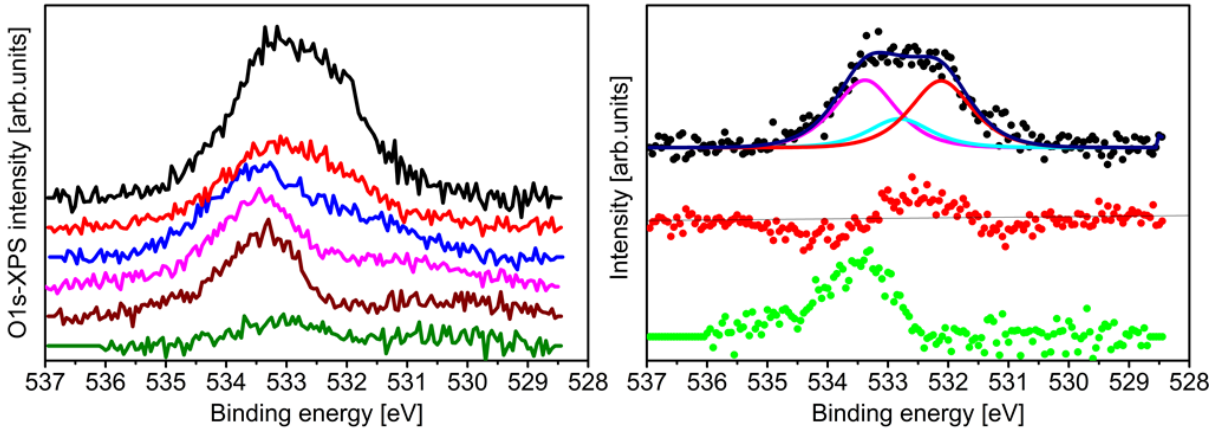

(a) (b)

Figure 6.16 (a) O1s-XPS spectra of HOPG sputtered with Ar in O_2 atmosphere (1keV, 0.1uA*3min), sample was heated to different temperatures in 0.5mbar O_2 at BESSY, black curve: heating to 150°C in vacuum, red: 150°C in O_2, blue: 250°C in O_2, magenta: 400°C in O_2, wine: 550°C in O_2, olive: 700°C in O_2. Energy of radiation: 680eV; (b) O1s-XPS difference spectra of O1s XPS in figure 6.16a, black: black curve minus red curve in figure 6.16a, red: red curve minus blue curve in figure 6.16a, green: wine curve minus olive curve in figure 6.16a. Shirley background is subtracted, fitting parameter: FWHM=1.2

Recognition in figure 6.16b: O1s-component in 534 eV range (middle curve in fig.6.16b), at 533.3eV (magenta cuve in the upper curve in fig.6.16b and bottom curve in fig.6.16b), 532.2 eV and 532.7 eV (upper curve in fig.6.16b)

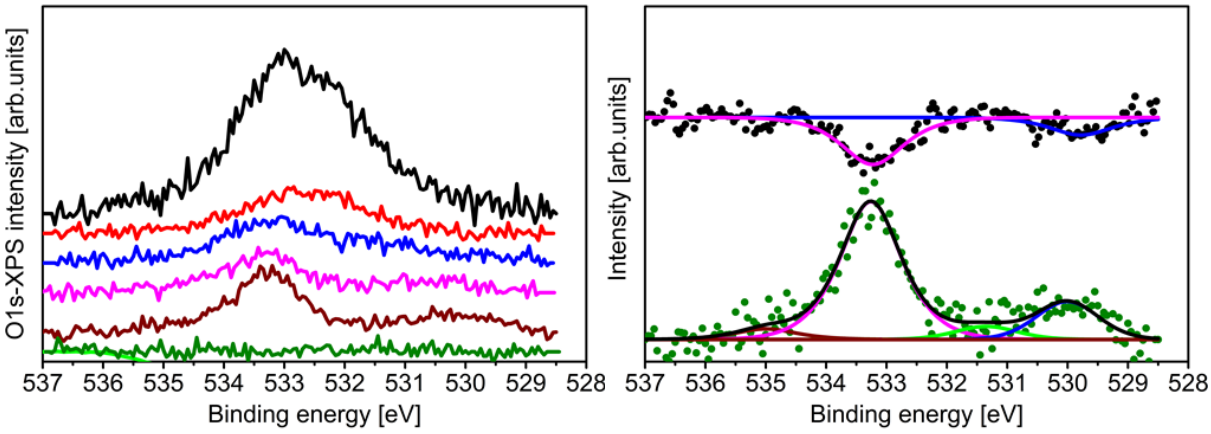

(a) (b)

Figure 6.17 (a) O1s-XPS spectra of HOPG sputtered with Ar in O_2 atmosphere (500eV, 0.1uA*6min), sample was heated to different temperatures in 0.5mbar in O_2 at BESSY, black curve: heating to 64°C in vacuum, red: 150°C in O_2, blue: 250°C in O_2, magenta: 400°C in O_2, wine: 550°C in O_2, olive: 700°C in O_2. Energy of radiation: 680eV; (b) O1s-XPS difference spectra of O1s XPS in figure 6.17a, black: magenta curve minus wine curve in figure 6.17a, olive: wine curve minus olive curve in figure 6.17a. Shirley background is subtracted, fitting parameter: FWHM=1.2

Recognition in figure 6.17a and 6.17b: FWHM = 1.2, O1s-component in 535 eV range (black curve in fig.6.17a), at 533.3 eV and in 530 eV range (upper and bottom curve in fig.6.17b).

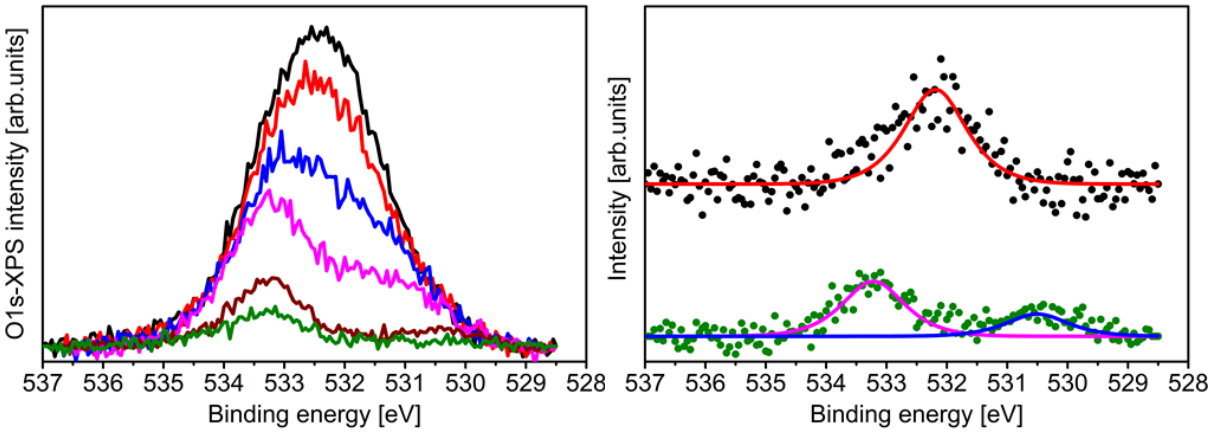

(a) (b)

Figure 6.18 (a) O1s-XPS spectra of HOPG sputtered with Ar in O_2 atmosphere (1keV, 1.5uA*2min), sample was heated to different temperatures at BESSY, black curve: 20°C, red: 100°C, blue: 200°C, magenta: 300°C, wine: 500°C, olive: 700°C. Energy of radiation: 680eV; (b) O1s-XPS difference spectra of O1s-XPS in figure 6.18a, black: black curve minus red curve in figure 6.18a, olive: wine curve minus olive curve in figure 6.18a. Shirley background is subtracted, fitting parameter: FWHM=1.2

Recognition in figure 6.18a and 6.18b: FWHM = 1.2, O1s-component at 533.3 eV (magenta curve in fig.6.18b), 532.2 eV (upper curve in fig.6.18b) and in 530 eV range (blue curve in the bottom curve in fig.6.18b).

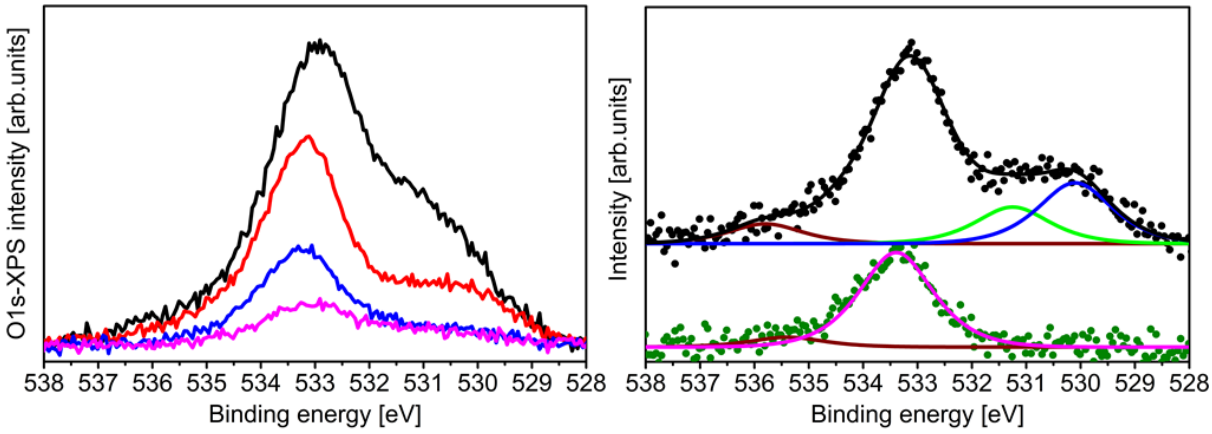

(a) (b)

Figure 6.19 (a) O1s-XPS spectra of HOPG sputtered with Ar in O_2 atmosphere (1keV, 1.5uA*2min), sample was heated to different temperatures, black curve: 20°C, red: 560°C, blue: 800°C, magenta: 935°C; (b) O1s-XPS difference spectra of O1s XPS in figure 6.19a, black: red curve minus blue curve in figure 6.19a, olive: blue curve minus magenta curve in figure 6.18a. Shirley background is subtracted, fitting parameter: FWHM=1.6

Recognition in figure 6.19a and 6.19b: FWHM = 1.6, O1s-component in 535 eV range (black curve in fig.6.19a and fig.6.19b), at 533.3 eV (upper and bottom curve in fig.6.19b), in 531 eV range (green curve in the upper curve in fig.6.19b) and 530 eV range (blue curve in the upper curve in fig.6.19b).

(a) O1s in 535 eV range

This oxygen component has extremely low intensity (figure 6.19, figure 6.20), and it cannot be seen in all spectra, e.g. in figure 6.15 and figure 6.16 this component is missing. Oxygen in the 535 eV range appears only occasionally. The desorption behavior of this component does not have any correlation with temperature while heating. Additionally, the position of this component is not fixed and it always lies in the energy range above 535 eV. Therefore, this O1s component is defined as an optional but not necessary component for the O1s fitting.

(b) O1s at 534.2 eV

From the O1s difference spectra (olive curve in figure 6.15b and figure 6.17b, the red and green curves in figure 6.16b) a very unclear O1s contribution at 534.2 eV with extreme low intensity can be observed. This O1s contribution has never been observed as a clear and individual peak, but without the contribution of this oxygen component most of the O1s peak cannot be fitted perfectly (olive curve in figure

6.15b). Therefore, this oxygen component is taken as a fixed O1s component for O1s fitting

(c) O1s at 533.3 eV

O1s contribution at 533.3 eV is reported frequently in the literature, compared to other O1s components it is the most uncritical component. In our experiment, this peak can be observed as an individual peak in the O1s difference spectra, after stepwise heating experiments (figure 6.17b, olive curve in figure 6.15b, 6.18b and 6.19b). This is a clear indication that this oxygen component corresponds to one or more oxygen species, which decompose while heating. Therefore, O1s at 533.3 eV is chosen as a fixed component for O1s fitting.

(d) O1s at 532.2 eV and 532.75 eV

The O1s peak at 532.2 eV can be observed as an individual peak after stepwise heating experiments in the O1s difference spectra (black curve in figure 6.15b and figure 6.18b). Therefore, O1s at 532.2 eV is chosen as a fixed component for O1s fitting. In literature all the reported fitting models have used only one oxygen component in the 532 eV range. In our XPS experiment measured with non-monochromatized X-ray radiation, there is obviously intensity loss in 532 eV range in O1s difference spectra, but the position of the component in 532 eV range cannot be resolved clearly (red points in 532 eV range in table 6.7). However, in the O1s spectra measured with monochromatized X-ray radiation, there is an obvious indication of an additional O1s component between the two fixed oxygen components at 532.2 eV and O1s 533.3 eV (see black curve in figure 6.16b). The black curve in figure 6.16b has a flat plateau with two clear shoulders at 533.3 eV and 532.2 eV. It is not possible to fit this curve with only these two components, a third component in between is necessary for a successful deconvolution. In this case, the component at 532.75 eV was selected as the most suitable match according to the fitting program ‘CASA XPS’. Therefore, O1s 532.75 eV was chosen as another fixed O1s component.

(e) O1s in 531 eV range

In all O1s spectra of HOPGs after sputtering, there is O1s intensity in the 531 eV range, but in most of the O1s spectra (black curves in figure 6.15a-6.19a), the

oxygen component in the 531 eV range cannot be easily recognized because of its overlap with other oxygen components. Nevertheless, there are two O1s spectra in figure 6.20a and figure 6.20b, which show a clear shoulder at 531.3 eV. Even more, from the black curve in figure 6.19b, there is a plateau between 532 eV and 530 eV and a shoulder in the 530 eV range that can be seen clearly. This means that, to deconvolute this plateau, an oxygen peak in the 531 eV range is necessary. In contrast to the O1s spectra, no intensity of this oxygen component can be identified in most of the O1s difference spectra. The absence of this oxygen component in most O1s difference spectra indicates that the corresponding oxygen groups - having contributions in the 531 eV range - cannot be decomposed easily through heating. Therefore, the related oxygen species should be essentially stable groups with high thermal stability. To conclude, the oxygen component in the 531 eV range is a necessary component for O1s fitting and the related oxygen groups has high thermal stability.

(f) O1s at 530 eV range

For all strongly sputtered HOPG samples, with sputter doses greater than $5.6*10^{14}$ ions/cm^2, measured with non-monochromatized and monochromatized X-ray radiation, the O1s spectra before heating need oxygen components in the 530 eV range to deconvolute the O1s peak. In the O1s difference spectra (olive curves in figure 6.15b and 6.17b and black curve in figure 6.19b) there is a clear shoulder in the 530 eV range. Even more, for the strongly sputtered HOPG samples (olive curve in figure 6.18b) and the sputtered HOPG heated in 0.5 mbar oxygen atmosphere (black curve in figure 6.17b), the oxygen contribution in the 530eV range can be recognized clearly as an individual peak. For the O1s spectra measured with *non-monochromatized* x-ray radiation, to deconvolute the O1s spectra of weakly sputtered HOPG (with sputter dose below $2.2*10^{14}$ ions/cm^2 in different gas atmosphere of O_2 and H_2O) before heat treatment (not showed here), no intensity in this range can be identified both in O1s spectra and in O1s difference spectra. In contrast, for the O1s spectra of weakly sputtered HOPG before heat treatment measured with *monochromatized* x-ray radiation, a component in the 530 eV range is necessary for O1s fitting. Both samples were weakly sputtered under the same sputtering conditions, but it is unclear why the oxygen component in the 530 eV range only exists on the sample measured at Bessy. It should be mentioned, the

samples measured with monochromatized x-ray radiation at Bessy were transported to Bessy in air. In other words, sputtered samples lay in a high concentration of mixture of oxygen and water atmosphere during transport. This could be the reason for the existence of O1s 530 eV in these weak sputtered samples measured at Bessy. From these Phenomena a brave conclusion can be made: The oxygen component in the 530 eV range can be formed on HOPG in two cases: Firstly, when the HOPG surface is strongly destroyed in oxygen contained gas atmosphere (O_2 and H_2O in our experiment; in H_2 there is no O1s 530 eV formed). Secondly, sputtered HOPG (slightly damaged as well as strongly damaged) was heated in present of high concentration of O_2. In other words, O1s in the 530 eV range is correlated with strong disorder of the HOPG surface (more surface defects) and high concentration of oxygen. To sum up, O1s in 530 eV range is not necessarily an essential O1s component, the existence of this component is highly dependent on the surface morphology and the surrounding gas atmosphere.

Comparing the O1s peaks measured with non-monochromatized x-ray radiation (figure 6.19) with O1s peaks measured at Bessy (figure 6.15-6.19), the width of the total O1s peak is comparable. This indicates that many kinds of oxygen components should be in the O1s peak at the same time. In table 6.7, an overview of the clearly recognized O1s peaks in the O1s difference spectra is given. In all the O1s spectra, components at the 533.3 eV, 531.4 eV and 532 eV ranges can be recognized. In total there are seven oxygen components recognized in all O1s difference spectra.

Table 6.7 Clear recognized O1s components from O1s difference spectra										
	Treatment / XPS BE (eV)		535 range	534.2 (±0.1)	533.3 (±0.1)	532.75 (±0.1)	532 range	532.2 (±0.1)	531.3 (±0.2)	530 Range
AC FHI	Sputter with Ar *in O_2*	500eV, 0.1uA*3min								
		500eV, 0.1uA*6min			●			●	●	
		500eV, 0.1uA*24min								
	Sputter with Ar *in O_2* – stepwise heating	1keV, 1.5uA*2min	●		●		●		●	●
	Sputter with Ar *in H_2O*	500eV, 0.1uA*3min								
		500eV, 0.1uA*6min			●	●		●	●	
		500eV, 0.1uA*24min								
		1keV, 1.5uA*2min	●		●		●		●	
Bessy	Sputter with Ar *in O_2* – stepwise heating	500eV, 0.1uA*3min			●	●		●	●	
		1keV, 1.5uA*2min			●	●		●	●	●
	Sputter with Ar *in O_2* – stepwise heating *in O_2*	500eV, 0.1uA*3min								
		500eV, 0.1uA*6min		●	●	●		●	●	●
		1keV, 0.1uA*3min								
		1keV, 1.5uA*2min		●	●	●		●	●	●
	Sputter with Ar *in H_2*	500eV, 0.1uA*3min				●		●		
		1keV, 1.5uA*2min					●			

To conclude, from the statistic possibility of the appearance of all oxygen components in all measured O1s-XPS spectra and O1s difference spectra, a new fitting model for O1s-XPS is developed. According to the analysis above, O1s-peaks should be fit with five fixed components at 534.2 (± 0.1 eV), 533.3 (± 0.1 eV), 532.75 (± 0.1 eV), 532.2 (± 0.1 eV), 531.2 (± 0.2 eV) and with two non-fixed components at 530 eV and 535 eV ranges. From the O1s difference spectra, the parameters for fitting the O1s-spectra can be fixed. The full width at half maximum (FWHM) of the O1s difference spectra is about 1.2 eV for oxygen measured with monochromatized X-ray radiation (figure 6.15b and 6.17b) and 1.6 eV for oxygen measured with non-monochromatized X-ray radiation (figure 6.19b). The shape of the peak can be described very well with mixed Gauss-function and Lorenz-function. The fitting parameters are shown in table 6.8. All the measured XPS O1s spectra can be fitted with this model perfectly. In figure 6.20a-6.20d four examples are presented that show the fit for different shapes of the O1s-XPS.

Additionally, our seven-component fitting model is applied on O1s-XPS of two real samples of functionalized carbon nanofiber[19]. The first sample is CNF oxidized by H_2O_2 and the other sample is CNF oxidized by O_3. Obviously, with our model the two samples can be well fitted (see figure 6.21a and 6.21c). For comparison, the two samples are fitted with the most widely used two-component fitting model reported in literature[11-17] (see figure 6.21b and 6.21d). As mentioned above, the FWHM of one oxygen component in the oxygen difference spectra is 1.6 eV. Therefore, FWHM of 1.6 eV is used for the O1s-XPS fitting with the two-component model (see figure 6.21b and 6.21d, fitting parameter is given in table 6.8). This model has two shortcomings. It is unable to fit O1s in the 530 and 535 eV range and, more importantly, the oxygen components in the 532 eV range are missing. When a fitting model takes only two components into account, these two components have to cover all oxygen functionalities. For this to work, it is necessary to either increase the value of FWHM of the two fitting components, or to reduce the types of surface oxygen groups. However, to increase the FWHM only makes the analysis of oxygen functionalities more imprecise, because the number of different oxygen types does not change with the value of FWHM. To reduce the number of oxygen functionalities is not realistic as well, because we are interested in analyzing all oxygen groups existing on the surface of carbon samples. In contrast, in our seven-component fitting model oxygen groups are differentiated precisely according to the oxygen difference

spectra. Therefore, we are able to gain further insight into the nature of oxygen functionalities and give an assessment of these in the following chapter.

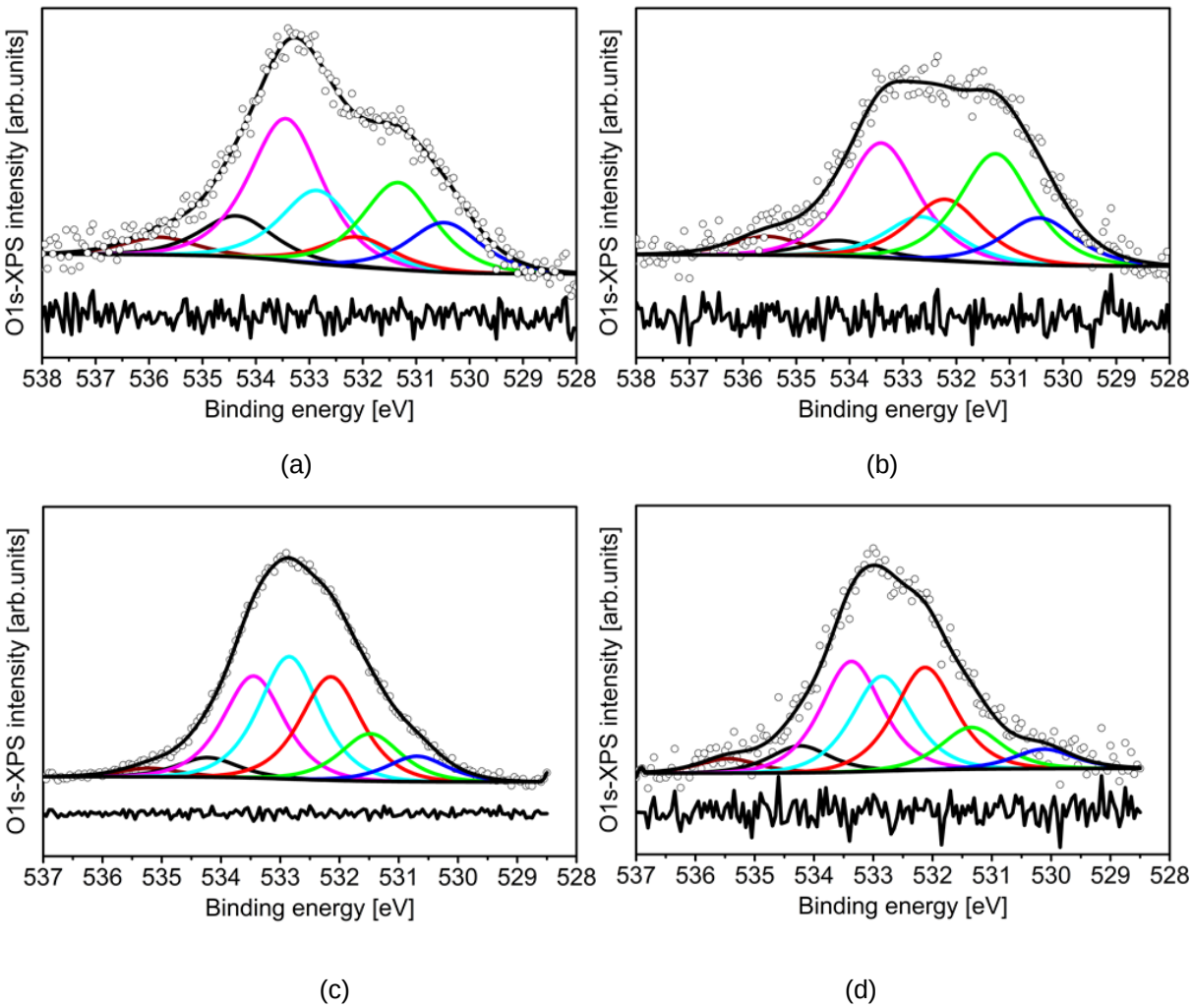

Figure 6.20 Fitting examples with our 7-component fitting model. (a) O1s-XPS spectra of HOPG direct after sputtering with Ar in O_2 atmosphere. 500eV, 0.1uA*24min. Fitting parameter: FWHM=1.6; (b) O1s-XPS spectra of HOPG direct after sputtering with Ar in H_2O atmosphere, 1keV, 1.5uA*2min. Fitting parameter: FWHM=1.6; (c) O1s-XPS spectra of HOPG sputtered with Ar in O_2 atmosphere (500eV, 0.1uA*3min), sample was measured at room temperature at BESSY. Energy of radiation: 680eV. Fitting parameter: FWHM=1.2; (d) O1s-XPS spectra of HOPG sputtered with Ar in O_2 atmosphere (500eV, 0.1uA*6min), sample was heated in vacuum to 64 °C at BESSY. Energy of radiation: 680eV. Fitting parameter: FWHM=1.2

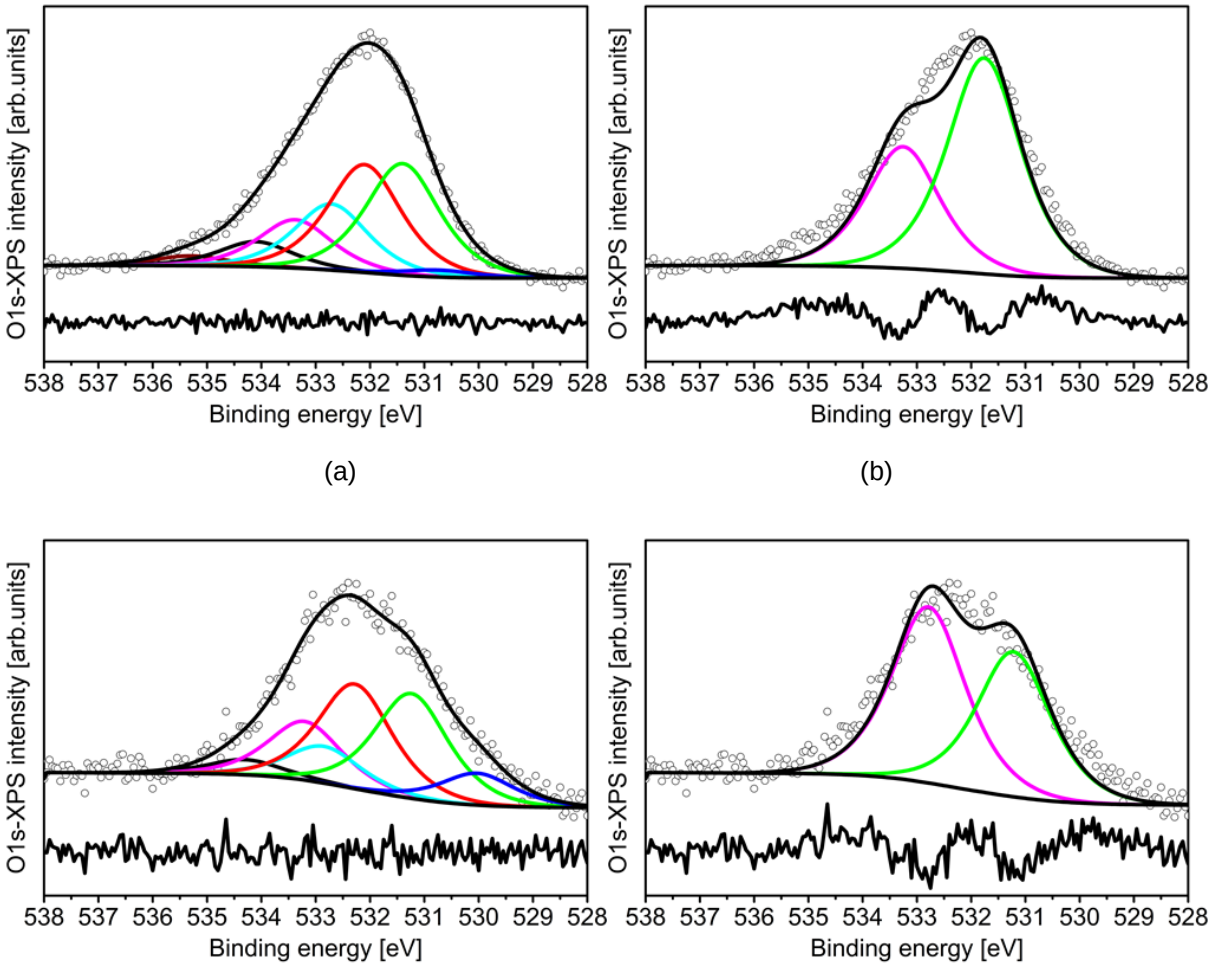

Figure 6.21 Application of our fitting model on the real sample reported in the literature[19] and comparison of two-component fitting model with our 7-component fitting model. (a) and (b)O1s -XPS spectra of CNF/$SMF_{Inconel}$ reported in literature (sample C2, oxidized in H_2O_2)[19]. O1s-XPS is fitted with (a) our fitting model and (b) two-component fitting model in literature. Fitting parameter: FWHM=1.6; (c) and (d) O1s -XPS spectra of CNF/$SMF_{Inconel}$ reported in literature (sample D4, oxidized in O_3)[19]. O1s-XPS is fitted with (c) our fitting model and (d) two-component fitting model in literature. Fitting parameter: FWHM=1.6

Table 6.8 Fitting parameters for O1s-XPS in figure 6.20 and figure 6.21 (Shirley background)				
Fitting model	X-ray source	O1s component [eV]		FWHM of O1s components [eV]
Our fitting model (seven-component)	Non-monochromatized	Fixed	534.20 ± 0.1	1.6
			533.30 ± 0.1	
			532.75 ± 0.1	
			532.20 ± 0.1	
			531.20 ± 0.2	
		Not fixed	530 range	
			535 range	
	Monochromatized (Bessy)	Fixed	534.20 ± 0.1	1.2
			533.30 ± 0.1	
			532.75 ± 0.1	
			532.20 ± 0.1	
			531.20 ± 0.2	
		Not fixed	530 range	
			535 range	
Two-component fitting model	Non-monochromatized	Fixed	533.2 ± 0.5	1.6
			531.5 ± 0.5	

6.4.3.2.2 Assignment of oxygen components in O1s-XPS

6.4.3.2.2.1 Oxidation state of oxygen components

The chemical shift of oxygen components in the functional groups is strongly influenced by the surrounding atoms and groups. This influence can be described as an electron-withdrawing inductive effect of atoms or functional groups, also known as the − *I* effect. Graphite is considered to have a similar induction effect as C_6H_5. The – *I* effect of the functional groups is assumed to be the following:

$$COOH > C{=}O > OH > OR > C_6H_5 > H > CH_3 > MeCH_2–$$

In XPS spectra, when the surrounding groups of an oxygen component have strong – *I effect*, the binding energy of the closest oxygen component to it will shift to higher binding energy. The extreme case is that this oxygen component loses its electron completely and becomes an oxygen cation. Therefore, combining the – *I* effect of the oxygen groups with our O1s-XPS fitting model, the order of the binding energy of the oxygen can be briefly deduced theoretically. Additionally the binding energy of several functional groups (ether, alcohols, carbonyls, carboxyls) differs strongly by up to 1eV for carbonyl groups depending on the aromatic/aliphatic nature of the carbon substrate[36]. This is due to the mesomeric effect (m-effect) of the aromates and/or

the group itself. The +m-effect of oxygen directly bonded to aromates leads to an increase of the binding energy, while the –m-effect of C=O in carbonyls and carboxyls leads to a decrease of the binding energy compared with the bonding to aliphatic carbon. In the following it is generally assumed that the functional groups are attached to aromatic (extended π) systems.

The possible binding energy of the oxygen components is supposed to be:

O^{n+} >O=C-O-C=O >O=C-O-R >C-O-C >C-OH >H_2O >-O---H >O=C-O-C=O>O=C-O-R >R-C=O >O^{n-}

535 534 533 range 532 range 531 range 530

It is important to note that carboxyl groups are divided into two kinds of carboxyls. One kind is like gaseous COOH, which has contributions at two positions about 531 eV and 533 eV in the O1s spectra[42]. The other kind of carboxyl group is carboxyls in a solid, in which hydrogen bridge bonds can be formed. These carboxyls have only one contribution in 532 eV range in the O1s spectra[42].

6.4.3.2.2.2 Assignment of oxygen components

In figure 6.22 the developments of the O1s components at 534 eV, 533 eV, 532 eV, 531 eV and 530 eV in XPS while heating in UHV and in 0.5 mbar O_2 atmosphere are illustrated. The development curves of O1s components heated in UHV show the thermal stability of the corresponding oxygen components and the development curves of O1s components heated in O_2 atmosphere show the oxidizabilitiy of the corresponding oxygen components. It is assumed at first, that the assignment of the oxygen components according to the – *I* effect order above is correct. Afterwards we analyze if the behavior of the thermal stability and oxidizability (in figure 6.22) of the assigned O1s components corresponds to their nature.

On the HOPG surface, seven oxygen containing groups (–OH, C=O, C-O-C, H_2O, -COOH, COOC, COOOC) could be generated after sputtering. When these functional groups on the HOPG surface were heated in UHV conditions, large oxygen functional groups (COOH, COOC, COOOC) could decompose completely to CO or CO_2 and resulted in the intensity loss of the oxygen components in O1s-XPS spectra. –OH, C-O-C and C=O groups are three thermally stable groups. According to theoretic calculations[49] they can only decompose at very high temperatures. When HOPG samples were heated in UHV conditions, much H_2 was desorbed beside desorption of other gases. This phenomenon can be observed in each TPD spectrum.

Desorption of H_2 could take place because of the existence of some oxygen groups such as hydroxyls and hydroxyl carbons, which can produce H_2 (for instance reaction (3) to (6)). On the other hand, the presents of H_2 means reduction reactions of oxygen functional groups by H_2 could happen as a competing reaction to the thermal decomposition reaction of oxygen functional groups. The development curves of O1s components to temperature in figure 6.22 under UHV conditions correspond to the summation of the decomposition reactions and reduction reactions of the oxygen groups. When the functional groups are heated in 0.5 mbar O_2 atmosphere, some of the functionalities can be oxidized to large functional groups, and the large functional groups decompose at the same time as well. Therefore, the development curves of oxygen components to temperature in oxygen atmosphere correspond to an equilibrium state of oxidation and decomposition of the functional groups.

Reactions (1) to (8) are the possible decomposition, reduction and oxidation reactions:

Decomposition:

(1) $2\ COOH \leftrightarrow CO_2 + CO + H_2O$

$COOC \leftrightarrow CO_2 + C$

$COOOC \leftrightarrow CO_2 + CO$

(2) $C\text{-}OH + \text{-}OH \leftrightarrow CO + H_2O$

$C{=}O \leftrightarrow CO$

Reduction:

(3) $2\ C{=}O + H_2 \leftrightarrow 2\ C\text{-}OH$

(4) $COOH + H_2 \leftrightarrow C\text{-}OH + H_2O$

$COOC + H_2 \leftrightarrow 2\ C\text{-}OH$

$COOOC + 2\ H_2 \leftrightarrow 2\ C\text{-}OH + H_2O$

(5) $C\text{-}O\text{-}C + H_2 \leftrightarrow C\text{-}OH + CH$

(6) $C\text{-}OH + H_2 \leftrightarrow CH + H_2O$

Oxidation:

(7) $C{=}O + C + O_2 \leftrightarrow COOOC \leftrightarrow CO + CO_2$

(8) $2\ C\text{-}OH + O_2 \leftrightarrow 2\ COOH \leftrightarrow CO_2 + CO + H_2O$

Hydrogen bridge bonds:

(9) $COOH + H_2O \leftrightarrow H\text{-}(O\text{-}C\text{-}O\text{-})\text{-}H\text{-}O\text{-}H$

(10) $2COOH \leftrightarrow H\text{-}(O\text{-}C\text{-}O\text{-})\text{-}H\text{-}O\text{-}C\text{-}O$

(11) $C{=}O + H_2O \leftrightarrow C\text{-}O\text{--}H\text{-}O\text{-}H$

Other reactions:

(12) $COOH + C\text{-}OH \leftrightarrow COOC + H_2O$

(13) $2C\text{-}OH \leftrightarrow C\text{-}O\text{-}C + H_2O$

(14) $2COOH \leftrightarrow COOOC + H_2O$

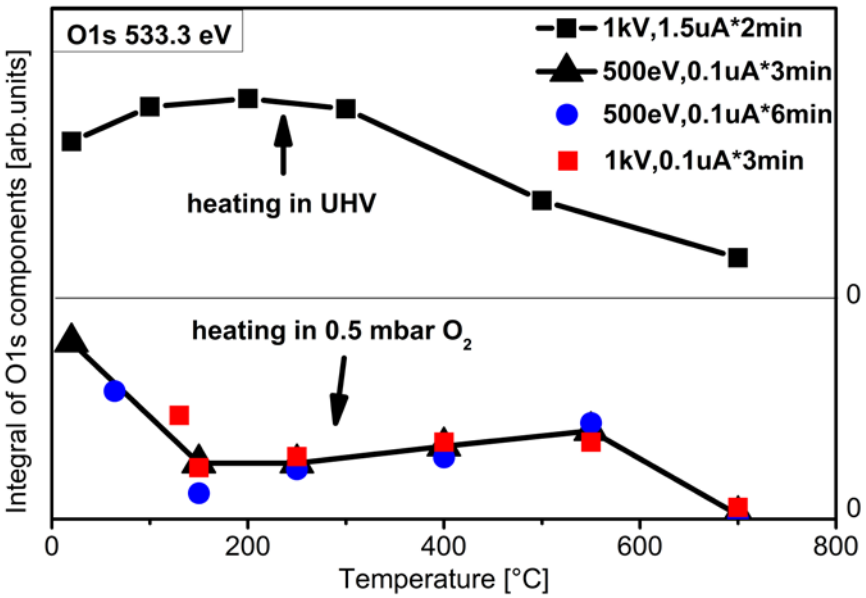
O1s 533.3 eV
1kV,1.5uA*2min
500eV,0.1uA*3min
500eV,0.1uA*6min
1kV,0.1uA*3min
heating in UHV
heating in 0.5 mbar O2
Integral of O1s components [arb.units]
0
0
0
200
400
600
800
Temperature [°C]

(a)

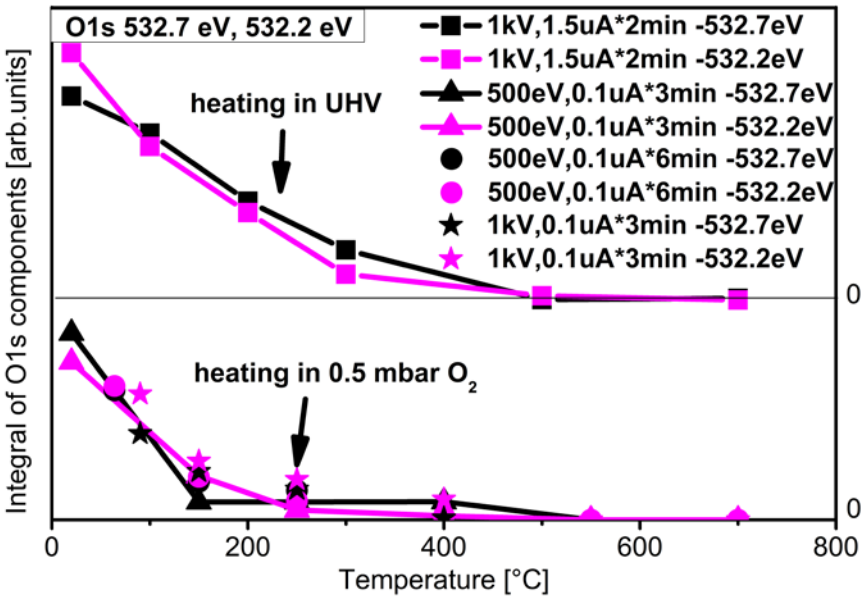
O1s 532.7 eV, 532.2 eV
1kV,1.5uA*2min -532.7eV
1kV,1.5uA*2min -532.2eV
500eV,0.1uA*3min -532.7eV
500eV,0.1uA*3min -532.2eV
500eV,0.1uA*6min -532.7eV
500eV,0.1uA*6min -532.2eV
1kV,0.1uA*3min -532.7eV
1kV,0.1uA*3min -532.2eV
heating in UHV
heating in 0.5 mbar O2
Integral of O1s components [arb.units]
0
0
0
200
400
600
800
Temperature [°C]

(b)

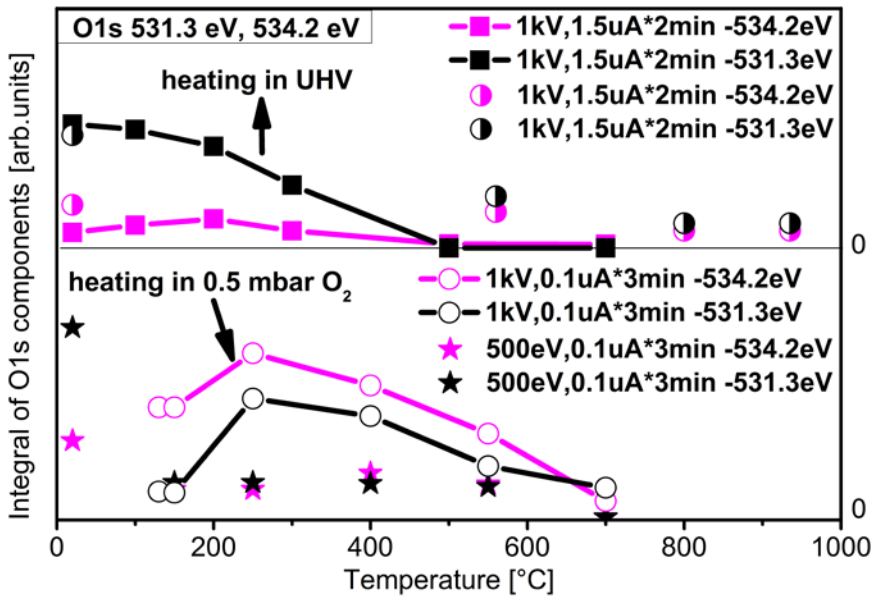

(c)

Figure 6.22 Integration of O1s-components at different temperatures, (a) O1s component at 533.3eV (b) O1s component at 532.7eV and 532.2eV (c) O1s component at 531.3eV and 534.2eV. The data points indicated by half circles in figure 6.22c were measured with non-monochromatized radiation at FHI, all other data points were measured with monochromatized radiation at Bessy. All the O1s-XPS spectra were fitted with O1s fitting model described in chapter 6.4.3.2.1.

In figure 6.22a, the development of O1s at 533.3 eV while heating in UHV shows at first an increase. This increase occurs because new –OH groups could be produced by the reduction reaction of carbonyls and large oxygen groups (carboxyls, lactone and anhydride). Above 300 °C the amount of this component begins to decrease. The reason for the decrease could be that hydroxyls begin to decompose. At 700 °C there is still an O1s signal at 533.3 eV, this is indication for ultra-stable ether groups. The development curve of O1s at 533.3 eV under 0.5 mbar O_2 condition shows at first a fast decrease. The main reason for this decrease could be the decomposition of carboxyls and lactones. Between 200 °C and 500 °C, new -O- in lactones or carboxyls can be produced by reaction (7), (8) and these carboxyls and lactones can decompose at the same time. This is the reason that the curve between 200 °C and 500 °C is almost constant.

Comparing the development curves of all oxygen components heated in UHV and in 0.5 mbar O_2, only oxygen at 532.7 eV and 532.2 eV (figure 6.22b) have the same behavior in terms of the thermal stability curve and oxidizability curve. Both components decrease continuously while heating. At about 500 °C, both components disappear completely. These phenomena indicate that these two components are strongly correlated with each other. Figure 6.22b shows that when HOPG was heated

in 0.5 mbar O_2, both components at 532.2 eV and 532.7 eV decreased continuously while heating. This behavior is the same as when HOPG was heated in UHV. The continuous decrease indicates that these two oxygen components are not oxidizable and they are at the end of oxidation states. In all the oxygen groups, only water and hydrogen bridge bond (reaction (9), (10)) between different oxygen groups can fulfill this condition. Combining the *–I* effect order of the oxygen groups, it is assumed that O1s at 532.2 eV is from the oxygen in –O---H group, which has a hydrogen bridge bond.

Regarding O1s at 531.3 eV and 534.2 eV, the development trend of O1s at 534.3 eV follows the same trend as O1s at 531.3 eV. This indicates that there should be one oxygen group that contains two kinds of oxygen components and the components contribute to O1s at 534.2 eV and at 531.3 eV. Combining the *– I* effect of the oxygen groups, it is supposed that this group is anhydride. Anhydride can be produced in oxidation reaction (for instance reaction (7)) and that explains the increase of O1s at 531.3 eV and 534.2 eV between 100 and 300 °C. If the single bonded oxygen in anhydride corresponds to O1s at 533.3 eV instead of 534.2 eV, the development curve of O1s at 533.3 eV under 0.5 mbar O_2 should have a similar trend as O1s at 531.3 eV. However, the development curve of O1s at 533.3 eV does not correlate with O1s at 531.3 eV. This supports indirectly that -O- in anhydride corresponds to O1s 534.2 eV. The continuous decrease of these oxygen components under UHV is due to the decomposition of large oxygen groups (reaction (1), (2)). It is remarkable, that at high temperature above 800 °C, in some of the experiments there is still O1s at 531.3 eV and 534.2 eV left. This is an indication for the existence of another ultra-stable group. After sputtering there could be some small aromatic system such as pyrone (figure 6.23) remaining on the surface. Pyrone consists of one carbonyl (531.3 eV) and one ether group. Normal ether group has binding energy at 533.3 eV, but because of the following equilibrium reaction, the ether group can be positively charged. Therefore, the binding energy of this ether group in pyrone could shift to higher binding energy, which is at 534.2 eV.

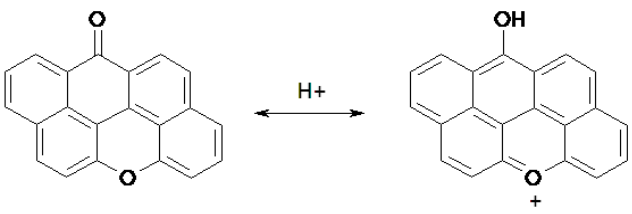

Figure 6.23 Structure of pyrone

For O1s in 535 eV range, there are no rules to follow (analyzed in chapter 6.4.3.2.1). They should correspond to some positively charged oxygen-containing particles. Typically graphite flakes occur on HOPG with bad contact to the Fermi-sea observable in SEM measurements as flakes with light contrast. For O1s in 530 eV range, this component strongly correlates with highly destroyed HOPG surface and high concentration of oxygen. This is an indication that they could be some negative charged particles with high oxygen concentration, for instance CO_3^{2-} or some oxygen atoms concentrated at electron-rich defects sites on HOPG. However, we cannot completely exclude the occasional occurrence of some metal particles which are exposed after sputtering.

To conclude, the assumption of assignment of oxygen components in O1s-XPS is:

535 range:	positively charged particles such as graphite flakes
534.2 range:	-O- in anhydride, pyrone
533.3 range:	-O- in hydroxyls, ether, lactone, carboxyls
532.7 range:	-O- in H_2O
532.2 range:	-O- in hydrogen bridge bond
531 range:	=O in carbonyls, lactone, anhydride, carboxyls
530 range:	negatively charged molecules such as CO_3^{2-}

The assignment of O1s at 533.3 eV and O1s in 531 eV range is consistent with literature[11;18;19].

6.4.3.3 Electronic structure of sputtered HOPG - UPS results

From UPS spectra (figure 6.24 and 6.25), it can be seen that damage to the HOPG surface increases with increasing sputter intensity. Complete breakdown of the σ-peak at 13.6 eV indicates destruction of the graphite electronic structure[50]. The remaining σ-peak indicates the graphene layers in surface area were not completely amorphous. The peak at 5 eV and 7.5 eV in He II-UPS spectra are contributed by the top σ-band andπ-band[51-53], the intensity of these two peaks decreases with increased sputter dose and shifts slightly to the Fermi energy side. The shift of the peaks at 7.5 eV indicates that the π-band moves to the Fermi energy, corresponding to the conversion of π-states to σ-states after sputtering. With the same sputter intensity, the damages of HOPGs sputtered in H_2O and in O_2 are comparable. However, HOPGs sputtered in O_2 show a little bit more graphitic character than

HOPGs sputtered in H_2O. The reason could be: After HOPGs were sputtered in O_2, aromatic oxygen groups could form, which are still graphitic. In contrast, after HOPG was sputtered in H_2O, hydroxyls were formed, so that the surface contained rather aliphatic structure than aromatic structure.

Obviously, defect formation very quickly destroys the graphene structure and a small surplus of functional groups does not allow concluding that the main carbon structure is graphitic. The analysis of UPS spectra supports these notions. Furthermore, one of the challenges in this work is to find suitable sputter conditions that produce as small amounts of small defects as possible, in order to reduce the amount of oxygen on the surface and to reduce the complexity of the oxygen functionalities. Sputter conditions such as sputter energy, sputter intensity and sputter time and the oxygen-containing gas atmosphere (acting as the oxygen source) were varied. UPS was used to obtain reference spectra that allowed the selection of suitable sputtering parameters and served for benchmarking and comparing the state of functionalized HOPG surface.

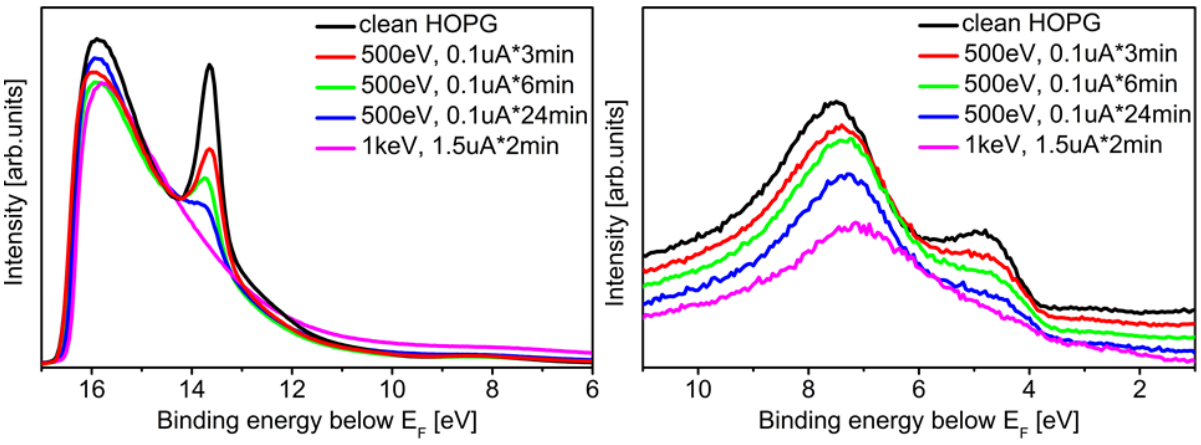

(a) (b)

Figure 6.24 UPS spectra of HOPGs after sputtering in H_2O atmosphere under different sputter conditions. The black curve is UPS of all HOPG sample before sputtering. (a) He I-UPS; (b) He II-UPS

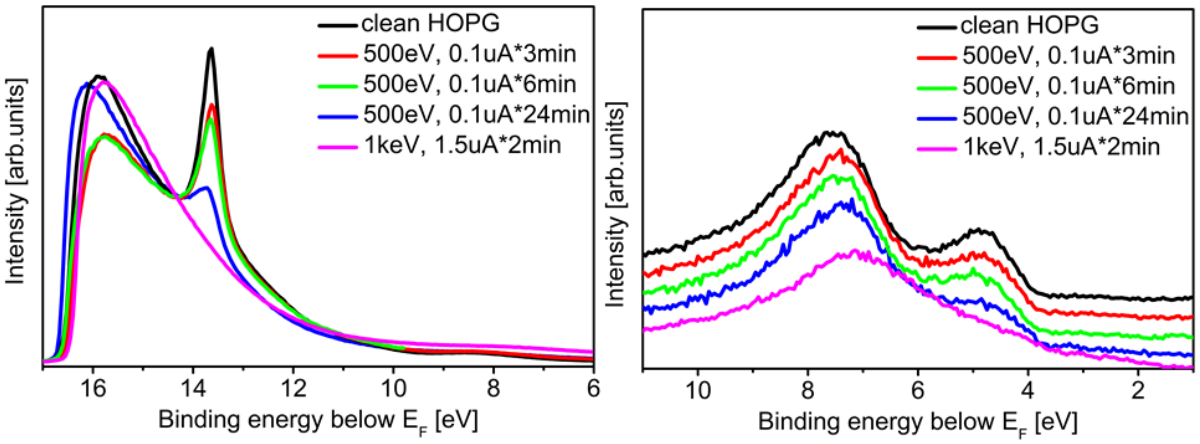

(a) (b)

Figure 6.25 UPS spectra of HOPGs after sputtering in O_2 atmosphere under different sputter conditions. The black curve is UPS of all HOPG sample before sputtering. (a) He I-UPS; (b) He II-UPS

6.4.3.4 Surface morphology of sputtered HOPG - SEM and STM results

Surfaces of fresh cleaved HOPG, weak sputtered HOPG (500 eV, 0.1 uA*3min) and strongly sputtered HOPG (500 eV, 0.1 uA*24min) were characterized by SEM (figure 6.26) and STM (figure 6.15 in chapter 6.2). SEM images in figure 6.26 were measured with an accelerating voltage of 1.5 kV, which is very surface sensitive. For the strongly sputtered sample (figure 6.26c) the contrast is blurred, indicating that the roughness of the sample is much higher than that of the freshly cleaved (figure 6.26a) as well as that of the weakly sputtered sample (figure 6.26b). Nevertheless, the roughness differences between images (a) and (b) are so small that they can be neglected. With STM the roughness differences of the three samples can be resolved very well (see figure 6.4 in chapter 6.2). The mean roughness of HOPG sputtered for 3 min is about 0.2 nm and the mean roughness of HOPG sputtered for 24 min is about 1.2 nm. This means there is about only one graphene layer damaged on the weakly sputtered sample. In contrast, about 4 graphene layers were damaged for the strongly sputtered sample. The blurred contrasts observed in the SEM images are resolved in the STM images as corrugations. The weakly sputtered sample shows mobile surface particles moving with the direction of the STM tip. This phenomenon is in agreement with the literature[54]. In both cases of weakly and strongly sputtered surfaces, no atomic resolution is feasible due to the mobile species and the amorphous surface character[54] respectively.

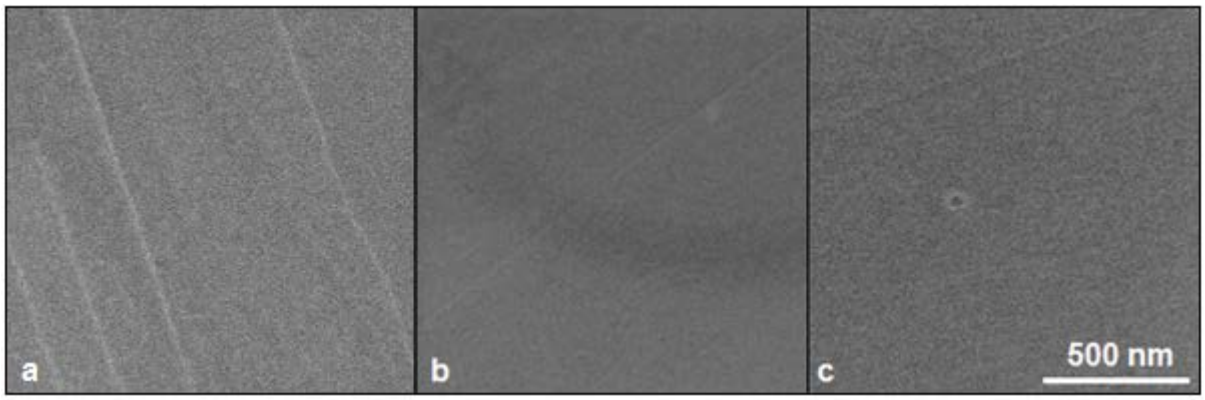

Figure 6.26 SEM images of (a) fresh cleaved HOPG (b) 500eV, 0.1uA*3min (c) 500eV, 0.1uA*24 min. Measure condition: 15.0 kV, SE

6.4.3.5 Correlation of surface morphology and O1s-XPS

Figure 6.27a to 6.27c shows the O1s-XPS directly after sputtering with Ar in H_2O atmosphere with increasing sputter time. The O1s-XPS spectra are fitted with our fitting model described above. Figure 6.27a shows when HOPG was sputtered for 3 min, oxygen components at 533.3 eV (-O- in hydroxyls, ether, lactone, carboxyls), 532.7 eV (H_2O) and 531.4 eV (=O in carbonyls, carboxyls and anhydride) were introduced dominantly on the HOPG surface. The extremely low intensity (can be considered as zero) of the O1s component at 534.2 eV (-O- in anhydride and pyrone) indicates the absence of the anhydride group. Combining these results with STM image and the assignment of oxygen components given before, it can be concluded that sputtering HOPG for 3 min yields a barely destroyed surface and primarily hydroxyls, ether, carbonyls, lactone, carboxyls and H_2O are generated on the HOPG surface. As the sputter time increased the amount of the different oxygen groups introduced on the HOPG surface changed. From figure 6.27a to 6.27c the integral of the fitted oxygen components (which corresponds to the amount of the oxygen component) to the sputter time are illuminated in figure 6.28. For the O1s component at 535 eV range and 530 eV range, it was already discussed before that these two components come out occasionally and there are no rules to follow. Therefore, in figure 6.28 the development of these two oxygen components with the sputter time was not shown. From figure 6.28 it can be seen that the amount of oxygen component at 533.3 eV (hydroxyls, ether, lactone, carboxyls), 532.2 eV (hydrogen bridge bonds) and 534.2 eV (anhydride and pyrone) increased when sputter time increased from 3 min to 24 min. Especially the amount of oxygen at 533.3 eV increased almost linearly. In contrast, the amount of oxygen at 531.4 eV (carbonyls, lactone, carboxyls and anhydride) and 532.7 eV (H_2O) increased at first and began

decreasing when sputter time was longer than 6 min. The total oxygen amount increased continually, but from 3 min to 6 min it increased much faster than from 6 min to 24 min. Combining this results with the surface morphology of sputtered HOPG, it can be concluded: With increased sputter time up to 24 min, which corresponds to the strongly destroyed HOPG surface (figure 6.26c), the amount of hydroxyls, ether, hydrogen bridge bonds and anhydride/pyrone increased continually with the increased sputter time. Hydroxyls and ether became the dominate oxygen groups on HOPG surface after HOPG was sputtered for 24 min. It is not necessary, that the amount of carbonyls, lactone, carboxyls and H_2O increased with the sputter time. Our results show that the amount of carbonyls, lactone, carboxyls and H_2O on HOPG surface sputtered for 24 min is lower than that for 6 min.

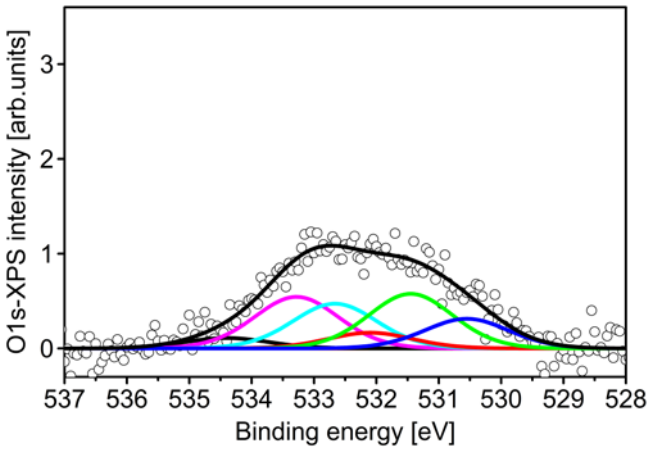

(a)

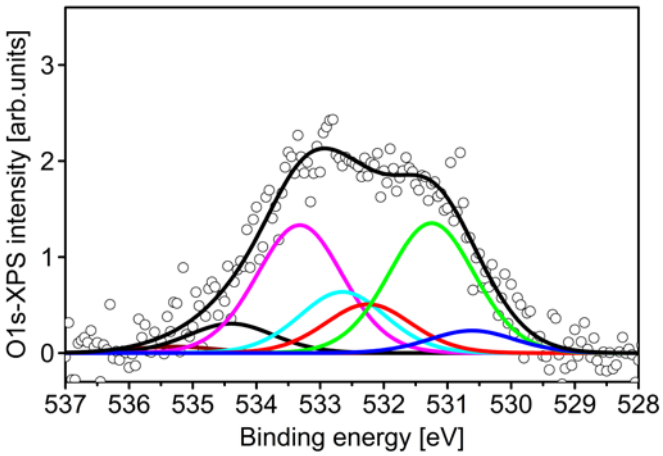

(b)

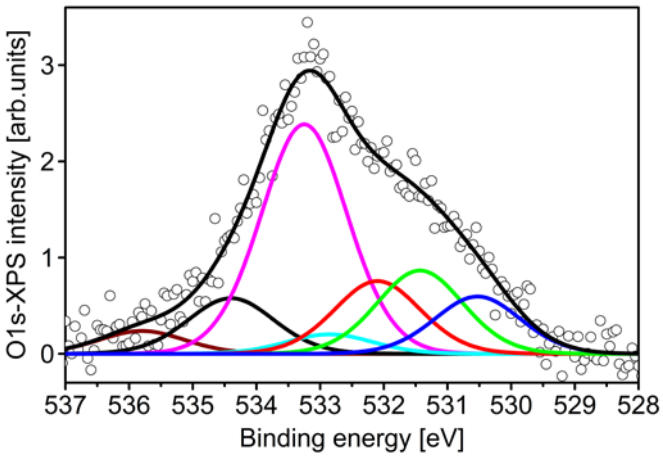

(c)

Figure 6.27 (a)-(c) normalized O1s-XPS spectra of sputtered HOPG with Ar in H_2O atmosphere (a) 500eV, 0.1µA*3min; (b) 500eV, 0.1µA*6min; (c) 500eV, 0.1µA*24min. Fitting parameter: FWHM=1.6

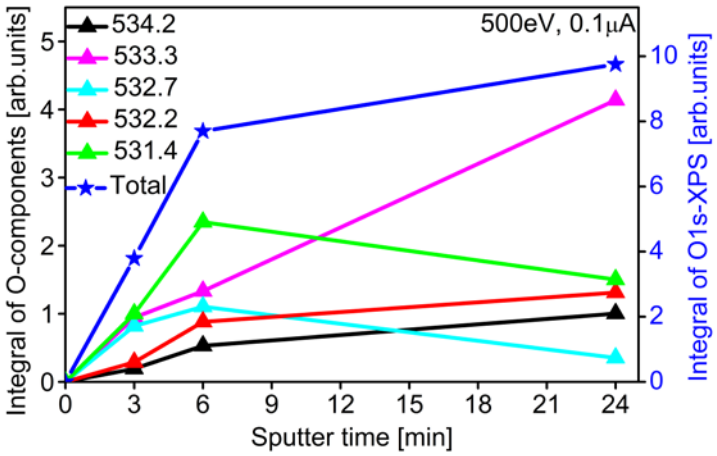

Figure 6.28 Development of oxygen components amount in figure 6.27a, 6.27b and 6.27c with sputter time. The dark blue curve corresponds to the development of total oxygen amount with the sputter time.

6.4.4 Conclusion

Oxygen functionalities were introduced on the surface of HOPG by sputtering in different gas atmospheres of O_2, H_2O and H_2. HOPGs were irradiated with four sputter doses $1.1*10^{14}$ Ar^+, $2.2*10^{14}$ Ar^+, $8.8*10^{14}$ Ar^+ and $1.1*10^{15}$ Ar^+ under 500 eV and 1 kV of beam voltage. The σ-peak at 13.6 eV in UPS spectra is very sensitive to the graphitization degree of the surface area. UPS results show that the surface damage level increases with sputter dose and when sputter dose is above $1.1*10^{15}$ Ar^+, HOPG surface gets completely amorphous. This is in agreement with STM images, where all the strongly sputtered sample surfaces were completely amorphous. With SEM surface roughness, differences between different samples cannot be clearly seen. The reason for the different results of UPS, SEM and STM are that the measured depth of surface with these three methods is different. With TPD the introduced oxygen amount can be calculated. With all these 4 sputter doses, less than 0.13 monolayer oxygen are introduced on the surface. The successive removing of the functionalities by heating results in the changes of the shape and intensity of the O1s-XPS spectra. According to the statistic appearance of O1s components in O1s difference spectra of various experimental series, a new O1s fitting model with five fixed O1s components and two flexible components is build. Five fixed O1s components are at 534.2 (± 0.1 eV), 533.3 (± 0.1 eV), 532.75 (± 0.1 eV), 532.2 (± 0.1 eV), 531.2 (± 0.2 eV). Two flexible components are in 530 eV and 535 eV ranges. With this fitting model all the measured XPS O1s-spectra can be fit very well. Furthermore, differently functionalized HOPGs were heated in UHV

condition and in 0.5mbar O_2 atmosphere, to investigate the thermal stability and oxidizability of the different functional groups with the help of XPS. Combining the thermal stability and oxidizability of the oxygen groups with the theory of electron induction effects from various groups, an assignment of the oxygen component in O1s-XPS to the functional groups is interpreted as follows:

535 range:	positively charged particles such as graphite flakes
534.2 range:	-O- in anhydride, pyrone
533.3 range:	-O- in hydroxyls, ether, lactone, carboxyls
532.7 range:	-O- in H_2O
532.2 range:	-O- in hydrogen bridge bond
531 range:	=O in carbonyls, lactone, anhydride, carboxyls
530 range:	negatively charged molecules such as CO_3^{2-}

This systematic investigation of oxygen functional groups provides a new O1s fitting model and a plausible assignment of single oxygen components in the O1s-XPS spectra to functional groups. This O1s model can be used as a standard reference for the identification of oxygen on carbon materials.

Reference List

[1.] K. P. De Jong, J. W. Geus, *Catalysis Reviews: Science and Engineering* **2000,** *42* 481-510.

[2.] E. Auer, A. Freund, J. Pietsch, T. Tacke, *Applied Catalysis A: General* **1998,** *173* 259-271.

[3.] P. Serp, M. Corrias, P. Kalck, *Applied Catalysis A: General* **2003,** *253* 337-358.

[4.] W. Xia, D. S. Su, A. Birkner, L. Ruppel, Y. Wang, C. Wöll, J. Qian, C. Liang, G. Marginean, W. Brandl, M. Muhler, *Chemistry of Materials* **2005,** *17* 5737-5742.

[5.] A. J. Plomp, D. S. Su, K. P. Jong, J. H. Bitter, *J.Phys.Chem.C* **2009,** *113* 9865-9869.

[6.] J. F. Evans, T. Kuwana, *Analytical Chemistry* **1977,** *49* 1632-1635.

[7.] M. Endo, C. Kim, K. Nishimura, T. Fujino, K. Miyashita, *Carbon* **2000,** *38* 183-197.

[8.] E. Frackowiak, S. Gautier, H. Gaucher, S. Bonnamy, F. Beguin, *Carbon* **1999,** *37* 61-69.

[9.] D. T. Clark, H. R. Thomas, *J.Polym.Sci.Polym.Chem.Ed.* **1976,** *14* 1671-1700.

[10.] D. T. Clark, H. R. Thomas, *J.Polym.Sci.Polym.Chem.Ed.* **1978,** *16* 791-820.

[11.] S. Kundu, Y. Wang, W. Xia, M. Muhler, *J.Phys.Chem.C* **2008,** *112* 16869-16878.

[12.] J. Harvey, C. Kozlowski, P. M. A. Sherwood, *Journal of Materials Science* **1987,** *22* 1585-1596.

[13.] J. H. Bitter, *J.Mater.Chem.* **2010,** *20* 7312-7321.

[14.] M. Zhu, C. J. Weber, Y. Yang, M. Konuma, U. Starke, K. Kern, A. M. Bittner, *Carbon* **2008,** *46* 1829-1840.

[15.] C. Kozlowski, P. M. A. Sherwood, *Carbon* **1986,** *24* 357-363.

[16.] F. Atamny, J. Blöcker, A. Dübotzky, H. Kurt, O. Timpe, G. Loose, W. Mahdi, R. Schlögl, *Molecular Physics* **1992,** *76* 851-886.

[17.] J. L. Hueso, J. P. Espinós, A. Caballero, J. Cotrino, A. R. González-Elipe, *Carbon* **2007,** *45* 89-96.

[18.] L. A. Langley, D. E. Villanueva, D. H. Fairbrother, *Chemistry of Materials* **2006,** *18* 169-178.

[19.] D. Rosenthal, M. Ruta, R. Schlögl, L. Kiwi-Minsker, *Carbon* **2010,** *48* 1835-1843.

[20.] D. S. Su, N. Maksimova, J. J. Delgado, N. Keller, G. Mestl, M. J. Ledoux, R. Schlögl, *Catalysis Today* **2005,** *102* 110-114.

[21.] C. Hontoria-Lucas, A. J. López-Peinado, J. d. López-González, M. L. Rojas-Cervantes, R. M. Martín-Aranda, *Carbon* **1995,** *33* 1585-1592.

[22.] M. T. Martínez, M. A. Callejas, A. M. Benito, M. Cochet, T. Seeger, A. Ansón, J. Schreiber, C. Gordon, C. Marhic, O. Chauvet, J. L. G. Fierro, W. K. Maser, *Carbon* **2003,** *41* 2247-2256.

[23.] M. A. S. Peter, *Journal of Electron Spectroscopy and Related Phenomena* **1996,** *81* 319-342.

[24.] H. Darmstadt, C. Roy, S. Kaliaguine, *Carbon* **1994,** *32* 1399-1406.

[25.] A. Proctor, P. M. A. Sherwood, *Journal of Electron Spectroscopy.and Related.Phenomena.* **1982,** *27* 39-56.

[26.] A. Proctor, P. M. A. Sherwood, *Carbon* **1983,** *21* 53-59.

[27.] E. Desimoni, G. I. Casella, T. R. I. Cataldi, A. M. Salvi, T. Rotunno, E. Di Croce, *Surf.Interface Anal.* **1992,** *18* 623-630.

[28.] C. Kozlowski, P. M. A. Sherwood, *J.Chem.Soc., Faraday Trans.1* **1985,** *81* 2745-2756.

[29.] Y. Xie, P. M. A. Sherwood, *Appl.Spectrosc.* **1989,** *43* 1153-1158.

[30.] Z. R. Yue, W. Jiang, L. Wang, S. D. Gardner, J. Pittman, *Carbon* **1999,** *37* 1785-1796.

[31.] S. Biniak, G. Szymanski, J. Siedlewski, A. Swiatkowski, *Carbon* **1997,** *35* 1799-1810.

[32.] R. Schlögl, G. Loose, M. Wesemann, *Solid State Ionics* **1990,** *43* 183-192.

[33.] P. V. Lakshminarayanan, H. Toghiani, J. Pittman, *Carbon* **2004,** *42* 2433-2442.

[34.] U. Zielke, K. J. Hüttinger, W. P. Hoffman, *Carbon* **1996,** *34* 983-998.

[35.] E. Papirer, R. Lacroix, J. B. Donnet, *Carbon* **1996,** *34* 1521-1529.

[36.] G. Beamson, D. Briggs, *The XPS of Polymers Database*, SurfaceSpectra, Manchester, U.K., **2000**.

[37.] D. T. Clark, A. Dilks, *Journal of Polymer Science: Polymer Chemistry Edition* **1979,** *17* 957-976.

[38.] D. T. Clark, B. J. Cromarty, A. Dilks, *Journal of Polymer Science: Polymer Chemistry Edition* **1978,** *16* 3173-3184.

[39.] C. Kozlowski, P. M. A. Sherwood, *Carbon* **1987,** *25* 751-760.

[40.] B. Marchon, J. Carrazza, H. Heinemann, G. A. Somorjai, *Carbon* **1988,** *26* 507-514.

[41.] B. Stohr, H. P. Boehm, R. Schlögl, *Carbon* **1991,** *29* 707-720.

[42.] K.Siegbahn, C.Nordling, G.Johansson, J.Hedman, P.F.Heden, K.Hamrin, U.Gelius, T.Bergmark, L.O.Werme, R.Manne, Y.Bear, *ESCA applied to free molecules*, North Holland Publishing Company, Amsterdam-London **1969,** pp. 123-127.

[43.] E. Papirer, R. Lacroix, J. B. Donnet, G. Ã. Nanse, P. Fioux, *Carbon* **1994,** *32* 1341-1358.

[44.] G. Beamson, D. Briggs, *J.Chem.Educ.* **1993,** *70* A25.

[45.] H. Ulbricht, R. Zacharia, N. Cindir, T. Hertel, *Carbon* **2006,** *44* 2931-2942.

[46.] Samer Aburous, *Dissertation: HOPG as a model catalyst for the oxidative dehydrogenation of ethylbenzene over carbon materials*, Free University Berlin, **2007**.

[47.] Henan Li, Dirk Rosenthal, Robert Schlögl, *not published* **2011**.

[48.] Henan Li, Dirk Rosenthal, Robert Schlögl, *not published* **2011**.

[49.] J. M. Carlsson, F. Hanke, *not published* **2008**.

[50.] R. Schlögl, *Surface Science* **1987,** *189* 861-872.

[51.] F. R. McFeely, S. P. Kowalczy, L. Ley, R. G. Cavell, R. A. Pollak, D. A. Shirley, *Phys.Rev.B* **1974,** *9* 5268-5278.

[52.] J. Krieg, P. Oelhafen, H. J. Guntherodt, *Solid State Communications* **1982,** *42* 831-833.

[53.] R. F. Willis, B. Fitton, G. S. Painter, *Phys.Rev.B* **1974,** *9* 1926-1937.

[54.] R. Coratger, A. Claverie, F. Ajustron, J. Beauvillain, *Surface Science* **1990,** *227* 7-14.

7. Conclusion

7.1 HOPG structure model after sputtering and its influence

As described in chapter 6.2, there are no absolutely identical HOPG pieces due to their construction defects. HOPG is built from many small crystals oriented the same way. Because of possible stacking faults and displacements of small graphite crystals, there are mainly three kinds of construction defects in HOPG: lattice vacancy, cross-linking between graphene layers and 3d-construction defects. Especially cross linking defects and 3d-construction defects are very sensitive to the sputtering process. During the sputtering process, Ar is irradiated to HOPG surface, Ar ions cross the graphene layers, lose energy and in the end stay somewhere between the graphene layers. When Ar ions irradiate cross-linking and 3d-construction defects, these defects prevent relaxation of the graphene layers, so that Ar ions can work very effectively on these 3d-construction defects for a destruction of the graphitic structure. These construction defects can result in big damages in HOPG during the sputter process. In STM images, the top surface of HOPG stays partly intact only when HOPG was sputtered under very weak conditions. There are not only holes on the HOPG surface, there exist highly mobile particles in the first layer after sputtering. It is supposed, that these mobile surface particles could be small graphite islands generated during the sputter process. Higher sputter dosages leads to a nearly completely amorphous HOPG surface. Ar implants distribute in/under this kind of partly amorphous HOPG surface, but mostly in deeper layers.

7.2 Influence of HOPG original structure on Ar desorption spectra and Ar binding energy

It can be asserted with the help of this HOPG structure model that HOPG possesses three different Ar diffusion barriers after sputtering. These are ordered with decreasing barrier height. Diffusion through hexagonal graphite rings, diffusion along vertical sites in the (a, b)-plane and diffusion through the amorphous carbon. Correlating the diffusion barrier with Ar desorption temperature in TPD spectra, the three desorption states of Ar could be identified in TPD spectra (Ar-α, Ar-β and Ar-γ). Firstly, Ar-α around 300 °C corresponds to the Ar escaped from amorphous carbon or Ar trapped in the first defective layers. Secondly, Ar-β around 500 °C corresponds

to the Ar from deeper layers escaped through vacancies after activation of the diffusion along vertical sites. Thirdly, Ar-γ above 800 °C corresponds to the Ar trapped in nearly defect free (deep) layers escaped from HOPG through hexagonal rings. In other words, the desorption-temperature of Ar-γ can be correlated with the remaining graphitic structure at the surface after sputtering. Therefore, the ratio of desorbed Ar-β to Ar-γ amounts and the desorption-temperature of Ar-γ can mirror the quality of HOPG: The smaller the ratio is or the higher the temperature is, the less construction defects are there and the better is the quality of HOPG. The construction defects in original HOPG have a strong influence on the Ar desorption behavior. In other words, Ar desorption behavior is very sensitive to this minimal structure difference.

A remarkable phenomenon is that after each TPD experiment (heating to 930 °C), the Ar core level position shifts to the high binding energy side of about 0.56 eV. In stepwise heating experiments, when the sample was heated stepwise to higher temperatures (e.g. 100 °C, 200 °C, 300 °C, 500 °C), the Ar binding energy shifted to the higher binding energy in small steps as well. During the heat treatment four factors of the HOPG system changed. Firstly, small parts of the interstitial carbon could change to sp^2 graphitic carbon, this can be observed in C1s-XPS spectra. Secondly, the amount of Ar implants decreased because of Ar-desorption. Thirdly, big amount of interstitial defects (ID) were removed by heating while vacancy defects (VD) survived. Fourthly, the depth profile of Ar position changed. The reasons for the shift are the changes of the depth profile of Ar position in HOPG and change of interstitially trapped Ar and C amounts while heating. The former increase the probability of small electron energy losses, as in graphite. The second together with the partly re-establishment of sp^2 carbon leads to an increase of the electronic interaction (polarization) of trapped Ar atoms with the graphene layers and hence a decrease of the screening of core-electrons. Therefore, the binding energy shifts to the high binding energy site. The Ar binding energy is a function of the interstitial defect amount and the reestablishment of the sp^2 character of the graphene layers.

7.3 Comparison of functionalization methods

As discussed above, Ar desorption spectra are strongly influenced by the available diffusion channels in HOPG. These diffusion ways for Ar apply as well to other desorbing oxygen containing gas as from deeper layers. This means, after having

made a picture of the HOPG structure after sputtering and possible diffusion ways for Ar, it is possible to proceed to analyze and compare the oxygen functionalities introduced by different functionalization procedures correctly.

Two sputter procedures were selected to functionalize HOPGs. One is sputter with Ar and O_2 and the other one is sputter with Ar in O_2 atmosphere (described in chapter 4 and chapter 6.3). For HOPG sputtered with Ar and O_2, both Ar and O_2 go deep into the HOPG bulk. There is dominantly CO and small amounts of CO_2, H_2O and O_2 desorbing from HOPG functionalized with both sputter methods. Big amounts of oxygen containing gases desorb during heat treatment, while the oxygen amount on the surface do not change much. This indicates that the oxygen introduced by this sputter procedure is mainly located in HOPG bulk. This oxygen can be delivered continuously to the surface area while heating, so that the amount of surface oxygen can be held at a constant level. Moreover, the desorption spectra of the oxygen-containing gases have very similar shapes compared to Ar-TPD spectra. The only difference is the intensity. This phenomenon demonstrates that diffusion ways of Ar can be applied to the desorbed oxygen-containing gases. From the high similarity of the TPD shape it can be concluded: Desorption of oxygen-containing gases is strongly influenced by the diffusion ways in HOPG rather than the interaction between oxygen-containing gases and carbon.

For HOPG strongly sputtered with Ar in O_2 atmosphere, dominantly CO desorbs and the amount of CO_2 and H_2O is negligible. Thereby, no O_2 desorption can be observed. The introduced oxygen groups can be removed successively by heating. And the desorbed oxygen amount fits the loss of the oxygen amount on HOPG surface very well. This indicates that mainly surface oxygen was generated by this sputter procedure. The desorption spectra of CO and Ar-TPD are very similar in shape as well. From chapter 7.1 it is known that three desorption states of CO correlated with three diffusion ways in TPD spectra should be observed in CO-TPD spectra, but it is relatively difficult to differentiate the three CO states clearly. The desorption peaks of CO are very broad and not as intense as Ar-desorption peaks. The explanation for that could be: If CO is not formed by interstitial C atoms, firstly CO has to overcome the binding energy to the carbon network and, secondly, CO has much better interaction with carbon atoms, defects and graphene layers than Ar. While Ar gets energy to overcome the diffusion barrier and escape from the diffusion channels without interaction with HOPG, CO gets energy firstly to break the bond

with HOPG. And on the way of diffusion, the diffusion rate of CO could be broken many times by the interaction with other carbon atoms and defects. Therefore, the oxygen-containing gases have very broad desorption peaks. Compared to the oxygen introduced by the first sputter procedure, desorption of CO here is not only strongly influenced by the diffusion ways in HOPG, but also by the interaction between CO and carbon. Moreover, under the same sputter condition, sputter with Ar in O_2 atmosphere introduced much less oxygen to the surface.

Another remarkable phenomenon in all the TPD spectra is, the desorption peak of CO does increase continually in the high temperature range (above 950 °C, depends on the sputter procedure), while desorption peaks of other gases tend to decrease. The reason is the high binding energy of oxygen functional groups leading to the high desorption temperature.

As it has been written in chapter 4, suitable functionalization methods introducing less oxygen groups have to be found, in order to reduce the complexity of the oxygen functionalities. Additionally, oxygen has to be introduced only on HOPG surface and not in the HOPG bulk. This is to simplify the oxygen-carbon model system and to enable the use of surface sensitive techniques to determine the oxygen functionalities. If these two sputter procedures are compared, it is obvious that the sputter procedure of “sputter with Ar in O_2 atmosphere” can serve our purpose. With this sputter method, a suitable model can be built for combining the bulk sensitive methods and surface sensitive methods together to analyze the oxygen functionalities.

It has to be mentioned that the HOPG system sputtered with Ar in O_2 atmosphere is not the best model system to investigate oxygen functionalities, because the HOPG surface is partly or fully amorphous after sputtering. A better system is functionalized HOPG only with point defects as mentioned in chapter 4. To reach this purpose, the sputter energy and sputter intensity were reduced to introduce even less oxygen groups, preventing the further oxidation of point defects. While the introduced oxygen amount was reduced, XPS and TPD cannot be used to determine the oxygen groups on HOPG because of their limited resolution and the limited temperature range. Furthermore, the best system to gain the oxygen information would be a HOPG model with only one oxygen functionality. Unfortunately, we are not able to clarify this purpose due to the same reason mentioned above.

7.4 Nature of oxygen functionalities

As discussed above, a sputter procedure with Ar in O_2 atmosphere was used as the standard functionalization method for HOPG to investigate the oxygen functionalities. In order to investigate the influence of other gases on the oxygen functionalities, HOPG was sputtered with Ar in H_2O and H_2 atmosphere. To obtain information about different oxygen parts on different surface morphologies, sputter conditions such as the sputter energy, sputter intensity and sputter time and the oxygen-containing gas atmosphere (acting as the oxygen source) were varied. To investigate the thermal stability and oxidizability of the different functional groups, functionalized HOPGs were heated in UHV condition and in a high pressure (0.5 mbar) O_2 atmosphere. Thereby, a series of XPS and TPD results were obtained from various experimental series. The successive removal of the functionalities by heating results in different shapes and intensities of the O1s-XPS spectra. According to the statistic appearance of O1s components in all the O1s difference spectra in various experiment series, it can be concluded, that there are at least five fixed O1s components and two flexible components existing on the HOPG surface after sputtering. With these five fixed and two flexible O1s components, we were able to perfectly deconvolute all the measured O1s XPS spectra. This new fitting model for O1s-XPS is a big improvement. With help of this new fitting model, we are gain further insight in the nature of the oxygen functionalities.

Combining the thermal stability and oxidizability of the oxygen groups with the theory of the electron induction effect of various groups, an assignment of the oxygen components in O1s-XPS to the functional groups is proposed as follows:

535 range: positive charged particles such as graphite flakes

534.2 range: -O- in anhydride, pyrone

533.3 range: -O- in hydroxyls, ether, lactone, carboxyls

532.7 range: -O- in H_2O

532.2 range: -O- in hydrogen bridge bond

531 range: =O in carbonyls, lactone, anhydride, carboxyls

530 range: negative charged molecules such as CO_3^{2-}

This systematic investigation of oxygen functional groups gives us a new O1s fitting model and a plausible assignment of single oxygen component in O1s-XPS to functional groups. This O1s model and assignment can be used as a standard reference for the identification of oxygen on carbon material.

8. Acknowledgements

I want to thank all the people who supported me during my stay in Berlin.
First of all I want to express my special gratitude to Prof. Dr. Robert Schlögl, who gave me the opportunity to do this work in the department of Inorganic Chemistry at the Fritz Haber Institute. I want to thank him for his advising and teaching. I appreciate very much, that Prof. Dr. Schlögl always motivated me during my PhD study. His words helped me a lot to go forward.
I want to thank Prof. Dr. Thomas Risse to give valuable feedback about my thesis.
I want to thank the committee members of my doctoral board.
I want to thank Dr. Dirk Rosenthal for his advice and his assistance during the development of my scientific work. I would like to thank him for his help in measuring, as well as for the time he took to discuss with me and correct my work.
I thank all the members of the Surface Analysis group, especially Dr. Axel Knop-Gericke and Dr. Sabine Wrabetz for giving me advices and support during the final stage of my PhD study. I want to thank Dr. Axel Knop-Gericke for giving me the possibility to measure at BESSY and Dr. Raoul Blume for his help in measuring and discussing the XPS data. I am thankful to Manfred Swoboda, Siegfried Engelschalt and Eugen Stolz for helping me to deal with all the possible problems in the ultra-high vacuum chamber and the technical support.
Furthermore, I want to thank Gisela Weinberg for taking the SEM measurement, Dr. Johan Carlsson and Dr. Felix Hanke for the help with the theoretic work. I want to thank Dr. Weiqing Zheng and Dr. Lidong Shao for discussing the data from a catalysts point of view and for sharing their experience of the PhD life.
My thanks also go to all my friends for correcting the English content and the emotional support during my PhD work.
Finally I want to thank my family who supported me along the way.

Curriculum Vitae

For reasons of data protection,

the curriculum vitae is not included in the online version